MAGNETIC LEVITATION OF CELLS FROM BONE MARROW ORIGIN

A Thesis Submitted to
the Graduate School
İzmir Institute of Technology
in Partial Fulfillment of the Requirements for the Degree of

DOCTOR OF PHILOSOPHY

in Bioengineering

by
Müge ANIL İNEVİ

July 2021
İZMİR

ACKNOWLEDMENTS

I would like to express my deep and sincere gratitude to my supervisor Prof. Dr. Engin ÖZÇİVİCİ for his guidance, support, encouragement, patience and understanding throughout my research.

I am also grateful to my esteemed committee members Assoc. Prof. Dr. Hüseyin Cumhur TEKİN, Assoc. Prof. Dr. Serhat TOZBURUN, Assoc. Prof. Dr. Hatice Güneş ÖZHAN, Assoc. Prof. Dr. Özden YALÇIN ÖZUYSAL, Assist. Prof. Dr. Yavuz OKTAY and my dear co-supervisor Assoc. Prof. Dr. Sinan GÜVEN for their mentorships. I am also grateful to Assoc. Prof. Dr. Gülistan MEŞE ÖZÇİVİCİ for her valuable support and guidance.

I would like to thank my teammate and dear friend Öykü SARIGİL for her continuous support and help. I am also thankful my research group members İlayda ÖZKAN, Melike ÇAĞAN, Melike KIZILKAYA, Sinem KAPTAN, previous members Öznur BASKAN and Özge KARADAŞ for their support and motivation. Yağmur Ceren ÜNAL and Kerem DELİKOYUN deserve special thanks for their help.

This study was supported by The Scientific and Technological Research Council of Turkey (TUBITAK) with a scholarship under 2211/C National PhD Scholarship Program in the Priority Fields in Science and Technology, Grant No: 1649B031503358. Financial support by The Scientific and Technological Research Council of Turkey (215S862 and 119M755) is gratefully acknowledged. The Izmir Institute of Technology, Biotechnology and Bioengineering Research Center is also appreciated for instrumental support.

The biggest thanks are for my beloved family. My mom Saniye ANIL, my father Sebahattin ANIL, my little brother Halil Yağız ANIL and my beloved husband Umut İNEVİ were always my biggest supporters in my life. It is my greatest sadness that my precious mother, Saniye ANIL, who passed away last year, is no longer with me. I hope she is watching me from somewhere and we will meet someday. Every good thing and every success in my life is due to her efforts and her love for me.

ABSTRACT

MAGNETIC LEVITATION OF CELLS FROM BONE MARROW ORIGIN

Magnetic levitation via negative magnetophoresis is a new label-free technology that is important in cell- and tissue-level bioengineering applications. Biofabrication applications of the technology is an area that still needs to be developed. In this doctoral thesis, 3D cellular structures with contrable size and cellular arrangement were formed and cultured with magnetic levitation using bone marrow-derived stem cells in both a miniature system that provides levitation between two magnets and a ring magnet-based large-scale system. First, a miniaturized magnetic levitation system that allows real-time imaging was produced and comprehensive protocols were described for its use for both single-cell level analysis and cell culture. With this setup, complex in situ 3D cellular aggregates were formed and their culture was maintained by levitation. Then, a new system that provides levitation on a single ring magnet was produced and used for biofabrication for the first time to overcome the reservoir volume constraint in the existing system and thus to create larger and symmetrical 3D cellular clusters. With the elimination of the upper limit in the system, the volume of the chamber was increased and the medium and biological structure transfer became easily applicable. It has been shown that this ring magnet-based magnetic levitation setup is suitable for cell culture, formation of millimeter-sized cellular structures with various cell types, and that pre-formed cellular structures can be combined by levitation. The low-cost and easy-to-use systems presented in this thesis have the potential to be applied in many areas such as tissue engineering and drug testing.

ÖZET

KEMİK İLİĞİ KÖKENLİ HÜCRELERİN MANYETİK LEVİTASYONU

Negatif manyetoforez aracılığıyla manyetik levitasyon canlı hücrelerin işaretlenmeksizin levitasyonunu sağlayabilen, hücre ve doku seviyesinde biyomühendislik uygulamaları için önem arzeden yeni bir teknolojidir. Bu teknolojinin biyofabrikasyon uygulamaları henüz geliştirilmeye ihtiyaç duyan bir alandır. Bu doktora tezinde, hem iki mıknatıs arasında levitasyon sağlayan minyatür bir sistemde hem de halka mıknatıs tabanlı büyük ölçek bir sistemde manyetik levitasyon ile kemik iliği kökenli kök hücreler kullanılarak boyutu ve hücresel düzeni kontrol edilebilen 3 boyutlu (3B) hücresel yapılar oluşturulmuş ve levitasyon ile kültürlenmiştir. Önce, gerçek zamanlı görüntülemeye izin veren minyatürize manyetik levitasyon sistemi üretilmiş ve hem tek hücre seviyesinde analiz hem de hücre kültürü için kullanımı amacıyla detaylı protokoller tanımlanmıştır. Bu minyatürize manyetik levitasyon düzeneği ile karmaşık in situ 3B hücresel kümelenmeler oluşturulmuş ve kültürleri levitasyon ile sürdürülmüştür. Ardından, mevcut sistemdeki rezervuar hacmi kısıtını aşabilmek ve dolayısıyla daha büyük ve simetrik 3B hücresel kümeler oluşturabilmek için tek bir halka mıknatıs üzerinde levitasyon sağlayan yeni bir mıknatıs düzeneği oluşturulmuş ve bu düzenek ilk kez biyofabrikasyon amacıyla kullanılmıştır. Levitasyon sistemindeki üst sınırın ortadan kaldırılması ile besiyeri haznesinin hacmi arttırılmış ve besiyeri ve biyolojik yapı aktarımı kolaylıkla uygulanabilir hale getirilmiştir. Bu halka mıknatıs tabanlı manyetik levitasyon düzeneğinin hücre kültürü için uygun olduğu, çeşitli hücre tipleri ile milimetre boyutunda hücresel yapılar oluşturulabileceği ve ayrı ayrı oluşturulmuş hücresel yapıların levitasyon aracılığı ile birleştirilebileceği gösterilmiştir. Bu tezde sunulan düşük maliyetli ve kullanımı kolay sistemler doku mühendisliği ve ilaç testi gibi birçok alanda uygulanabilme potansiyeli taşımaktadır.

Dedicated to my mom Saniye ANIL...

TABLE OF CONTENTS

LIST OF FIGURES

CHAPTER 1

INTRODUCTION

1.1. Physics of Magnetic Force-Based Manipulation

Magnetic permeability (μ) of a material which is an intrinsic property of materials determines density of magnetic field lines that can reach a certain value in the material. A closely related property of materials, magnetic susceptibility (χ) is the degree of magnetization of a material in response to an applied external magnetic field and allows classification of the materials according to their magnetic behavior as diamagnetic, paramagnetic and ferromagnetic. An applied external magnetic field cause a response in the medium (e.g., material, vacuum) that is called as magnetic flux density, B (in Tesla or T) and defines the number of field lines passing through a unit area of medium [1, 2]. Magnetic field streght, H (in amperes per meter) and magnetic flux density, which is directly proportional to the applied magnetic field H through permeability of the medium, increase with getting close to a magnet surface (Figure 1.1a). When a material is placed in an applied external magnetic field, local distortions in magnetic field occur according to their magnetic susceptibility and behaviour of the objects under a magnetic field is determined by the magnetization. Diamegnetic objects ($\chi < 0$, from -10^{-6} to -10^{-3}) are composed of atoms that do not have net magnetic dipole moment in the absence of an external magnetic field. Under an external magnetic field, a magnetic dipole moment is directed opposite to the applied magnetic field. Diamagnetic objects repel the magnetic field lines and therefore they are repulsed from maxima of magnetic field strength (Figure 1.1b). Most of the objects exhibit diamagnetic property such as water, proteins and cells. Paramagnetic objects ($\chi > 0$, on the order of 10^{-6} to 10^{-1}) such as oxygen, manganese and gadolinium have dipole moments that are randomly oriented in absence of applied magnetic field [3, 4]. In the magnetized state, magnetic dipoles in such materials align parallel to the applied field until removal of the magnetic field. Paramagnetic objects attract the magnetic field lines and thus they are pulled towards maxima of magnetic field strength (Figure 1.1c). Ferromagnetic objects ($\chi >> 0$) such as iron and nickel exhibit

parallel alignment of moments even in the absence of a magnetic field [5, 6]. Under the influence of a magnetic field, the magnetic dipole moments have a strong tendency to become aligned parallel to each other and unlike the moments in a paramagnetic object, the moments remain parallel to some extent after removal of the field [6, 7]. These objects strongly attract the magnetic field lines and they are moved to the region in which the magnetic field strength is maximum (Figure 1.1d).

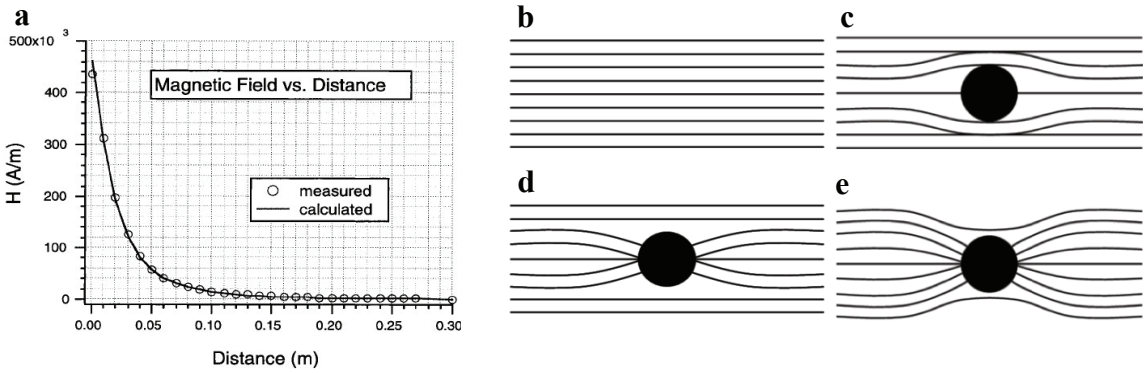

Figure 1.1. (a) The magnetic field strength increases with getting close to a neodymium iron boron (NdFeB) magnet surface [8] Effect of a material on a (b) uniform magnetic field according to their magnetic behavior; (c) diamagnetic, (d) paramagnetic and (e) ferromagnetic [9].

The term magnetophoresis is coined to describe behavior of an object moving under an applied magnetic field [10]. The magnetic force ($\overrightarrow{F_M}$) acting on a particle (or cell) under the influence of an external magnetic field is given by Eq. 1 [11]:

$$\overrightarrow{F_M} = (\vec{m}.\nabla)\vec{B} \tag{1}$$

where B is the magnetic flux density (in Tesla, T), and ∇ is the del operator. $\vec{m}$ is the magnetic dipole that takes the form of Eq. 2 in weak magnetic fields (e.g. 10^3 A/m) [12, 13]:

$$\vec{m} = \frac{V.\Delta\chi}{\mu_o}\vec{B} \tag{2}$$

where μ_o is the permeability of free space which is 1.2566×10^{-6} kg·m·A^{-2}·s^{-2}. Therefore, the magnetic force acting on a particle depends on the volume of the particle (V), the magnetic susceptibility difference ($\Delta\chi$) between the particle (χ_p) and the surrounding

medium (χ_m), together with the gradient and strength of the magnetic flux density. The force equation can be rearranged as:

$$\overrightarrow{F_M} = \frac{V.(\chi_p - \chi_m)}{\mu_0}(\vec{B}.\nabla)\vec{B} \tag{3}$$

For a Cartesian coordinate system, $(\vec{B}.\nabla)\vec{B}$ is expanded into:

$$(\vec{B}.\nabla)\vec{B} = \begin{pmatrix} \mathrm{B_x}\frac{\partial B_X}{\partial x} + B_y\frac{\partial B_X}{\partial y} + B_z\frac{\partial B_X}{\partial z} \\ \mathrm{B_x}\frac{\partial B_Y}{\partial x} + B_y\frac{\partial B_Y}{\partial y} + B_z\frac{\partial B_Y}{\partial z} \\ \mathrm{B_x}\frac{\partial B_Z}{\partial x} + B_y\frac{\partial B_Z}{\partial y} + B_z\frac{\partial B_Z}{\partial z} \end{pmatrix} \tag{4}$$

During magnetic manipulation of particles in the medium, the Stokes' drag force (F_D) appears in the opposite direction of the particle movement which is given for a spherical object as follows [14]:

$$\overrightarrow{F_D} = 6\pi R\eta f_d(\upsilon_p) \tag{5}$$

Here R is the particle radius, η is the dynamic viscosity of the surrounding medium, f_d is the drag coefficient and υ_p is the velocity of the particle. Inertial effects are usually neglected due to small Reynolds numbers in microfluidic magnetophoresis. Therefore, dominant forces for the motion of a particle in medium can be expressed by Eq. 6 [15]:

$$m\frac{\mathrm{d}\overrightarrow{\upsilon_p}}{\mathrm{dt}} = \overrightarrow{F_M} + \overrightarrow{F_D} + \overrightarrow{F_G} + \overrightarrow{F_B} \tag{6}$$

Here m is the mass of the particle; $\overrightarrow{F_G}$ is the gravitational/buoyant force, which is calculated as follows:

$$\overrightarrow{F_G} = V\Delta\rho g \tag{7}$$

with the volumetric density difference ($\Delta\rho$) between the particle (ρ_P) and the medium (ρ_M), and the gravitational acceleration g (9.8 m·s^{-2}).

For the particles with sufficiently small diameters [16] (i.e. down to a few tens of nanometers), the Brownian force, $\overrightarrow{F_B}$, becomes significant in the balance (Eq. 6) and particle diffusion due to Brownian motion influences the magnetic manipulation.

In case of magnetic levitation, the particles placed between two opposing magnets levitate at a unique position where the magnetic force is balanced by the gravitational force [17]:

$$\overrightarrow{F_M} + \overrightarrow{F_G} = 0 \tag{8}$$

$$\frac{V.(\chi_p - \chi_m)}{\mu_0}(\vec{B}.\nabla)\vec{B} = V.(\rho_P - \rho_M)\, g \tag{9}$$

As demonstrated by Eq. 8, equilibrium position of a particle (or cell) is independent from the volume (V) during magnetic levitation.

1.2. Components of Label-Free Magnetic Force-Based Cell Manipulation Systems

Almost all living cells are diamagnetic objects which are repulsed by a weak magnetic force due to magnetization in the opposite direction of the applied magnetic field. Two types of cells exhibit magnetic behavior in nature: magnetotactic bacteria and red blood cells (RBCs). Magnetotactic bacteria synthesize intracellular magnetic iron oxide or iron sulfide crystals to orient themselves according to the Earth's magnetic field [18]. RBCs exhibit paramagnetic behavior in the deoxygenated state of hemoglobin due to four unpaired electrons per iron atom [19]. As white blood cells behave as diamagnetic particles unlike the other blood cells (e.g. white blood cells), RBCs can be separated from whole blood by their native paramagnetic property without magnetic labeling [20].

For magnetic force-based manipulation of diamagnetic cells, two different strategies can be applied: i) manipulation of cells via increasing the repulsive force on these diamagnetic objects (i.e. label-free, negative magnetophoresis), or ii) manipulation of cells via creating an attractive force by labeling them with magnetic particles (i.e.

labeled, positive magnetophoresis). Magnetic field and magnetic medium are the key elements of label-free magnetic force-based cell manipulation techniques.

1.2.1. Magnetic Field

Diamagnetic materials (e.g. almost all cells), which are weakly magnetized proportional to the magnitude of the external magnetic field in the opposite direction to the applied field, can only be manipulated under sufficiently high magnetic fields and steep field gradients [21, 22]. Magnetic fields can be generated by permanent magnets, which are made of magnetic material blocks, or electromagnets, which produce magnetic field via an electric current. Permanent magnets with a simpler structure and lower costs produce only weak or moderate magnetic field (typically <1.5 T). Therefore, permanent magnets can be utilized for manipulation of diamagnetic cells via positive magnetophoresis using magnetic labels or negative magnetophoresis using a magnetic medium.

It is possible to manipulate the diamagnetic cells using superconducting magnets without magnetic labels or magnetic medium. Superconducting magnets, a type of electromagnet, enable to generate high magnetic fields (typically > 10 T) by means of electrical current flow through superconducting wires that are cooled by cryogenic techniques. The magnetic fields generated by superconducting magnets are much higher than other electromagnets owing to the zero resistance features of superconductors and the enhanced current flow [23]. High magnetic field gradient generated through superconducting magnets can be applied to the systems in an attempt to enhance the repulsive force on the diamagnetic materials and manipulate them. Firstly, it was reported that a strong inhomogeneous magnetic field was successfully utilized in levitation of various non-living diamagnetic materials such as wood and plastic (with ≅ 21 T) [24]. Following this, living biological specimens were levitated in the large inhomogeneous magnetic field inside a solenoid such as frogs (with ≅ 16 T) [25], frog embryos (with ≅ 13 T) [26], mice (with ≅ 17 T) [27] and insects (with ≅ 17 T) [28]. Nevertheless, these superconducting magnet systems are not easily accessible and expensive owing to required low temperatures to keep wires at a superconducting state. Besides the use of superconducting magnets, miniaturized systems (i.e. microfluidic devices) incorporated

with magnetic field sources (conventional permanent magnets or electromagnets) can be used to sufficiently enhance magnetic field and field gradient. In this context, the first and simplest approach to enhance magnetic field and field gradient is to bring permanent magnets very close to the microfluidic channel that contains the particle/cells. Several researchers have reported that the particles and cells can be manipulated in a capillary between closely facing two permanent magnets [29-31].

The second approach to produce high magnetic field and field gradients is the use of micro-electromagnets. These magnets are able to generate different magnetic field patterns with varied designs such as single wires [32] and micro-coils [33]. However, the heat produced in such systems can affect both the generated magnetic field and the viability of the cells in the system.

The third approach is embedding ferromagnetic components in the microchannel systems as flux concentrators. These concentrators can concentrate flux produced by a magnetic field source without heat generation. Kim and co-workers used permalloy (nickel−iron) wires, which are placed at an angle to the direction of flow in the bottom of a microchannel and magnetized by an external permanent magnet, to create a patterned magnetic field and separate magnetically labeled cells [34].

Magnetic field, which is an important component of magnetic-based cell manipulation systems, can have different effects on living cells. The impact of the magnetic field on cells depends on magnetic field intensity [35, 36], type (static or dynamic) and spatial distribution of magnetic fields (homogeneous or inhomogeneous) [37], exposure time [38], cell type and density [39], cell status such as infection [40]. Several cellular processes are influenced by the magnetic field, such as membrane properties (e.g. stability, fluidity) [41], cell shape and cytoskeleton organization [42], cell cycle [43], cell viability and proliferation [44, 45], cell orientation [46], cell adhesion, migration [47] and differentiation [36]. Evidence from several studies has shown that biological effects of magnetic field are correlated with magnetic field intensity. Although weak or moderate magnetic fields (<1 T) have only slight effects on cells [35, 48], strong magnetic fields (>20 T) can have drastic effects such as altering mitotic spindle orientations [49].

1.2.2. Magnetic Liquids

Another way to increase repulsive magnetic forces on diamagnetic cells is enhancing medium magnetic susceptibility through the use of magnetic liquid such as ferrofluid [50-52] or a paramagnetic salt solution [53-55]. The use of magnetic fluid eliminates above-mentioned problems arising from the use of high magnetic field exposure.

Paramagnetic salt solutions are usually composed of paramagnetic metals, such as manganese and gadolinium (Gd), and a halide (e.g. chloride) or a chelating agent (e.g. diethylenetriaminepentaacetic acid). Unpaired inner-shell electrons of these metals provide paramagnetic properties to aqueous solutions of paramagnetic ions. Such paramagnetic solutions have been used for various purposes, such as detection [56] or separation [54] of a specific type of cells and formation of 3 dimensional (3D) cell structures [55, 57].

Ferrofluids are colloidal suspensions of nano-sized magnetic particles with a mean diameter of 10 nm [58]. These nano-sized particles, that are commonly magnetite (Fe_3O_4) or maghemite (Fe_2O_3), are kept apart from each other by means of electrostatic or steric surfactants. Similar to that of paramagnetic salt solutions, ferrofluids have been used in a variety of studies in an attempt to manipulate living cells [59-61]. Ferrofluids exhibit about five orders of magnitude stronger magnetic susceptibility than a typical paramagnetic salt solution [61]. Therefore, cell manipulation applications using ferrofluids are generally utilized permanent magnets to generate magnetic fields generated by, while applications using paramagnetic salt solutions may require to use high magnetic fields generated by superconducting magnets [62, 63] or special-fabricated structures to enhance the magnetic field gradient [31]. Besides, ferrofluids are more suitable for continuous flow applications [51, 52, 60] whereas paramagnetic salt solutions are successfully used in static flow conditions [64].

Biocompatibility of magnetic liquids is an important and challenging issue for tissue engineering applications. Gd-based solutions have attracted a greater attention among paramagnetic solutions. Lanthanide ions such as Gd^{3+} have approximately the same size as Ca^{2+}, and can cause competitive inhibition of cellular processes requiring Ca^{2+} and therefore lead to cytotoxicity [65]. Chelation by a ligand mitigates direct toxicity of free Gd^{3+}.

The toxic effect of Gd chelates can be explained by two ways: (i) the dissociation of the complex and transmetallation reaction kinetics [66] and (ii) osmolality of the agent [67, 68], and these events are closely related to the ligand properties. Ligands can be macrocyclic or linear. In general, macrocyclic chelates (Gadobutrol, Gadoterate meglumine and Gadoteridol) have lower dissociation constants and are therefore considered as more stable than linear ones [69]. Thus, macrocyclic chelates tend to be less toxic to living cells. Kauffman et al. reported that the cytotoxic effects of gadoterate meglumine (Gd-DOTA), macrocyclic chelate, on Jurkat cells were weaker than gadobenate dimeglumine (Gd-BOPTA), linear chelate. While Gd-BOPTA (100 mM) caused more than half of the Jurkat cells (lymphocyte cells) to die after 1-day culture, Gd-DOTA resulted in cell viability of more than 80%. [68]. Also, both linear and macrocytic chelates can be ionic or nonionic. Nonionic linear compounds can have decreased stability because of weaker electrostatic interaction between ligand and Gd^{3+}, and therefore they are formulated with excess ligand in an attempt to avoid the release of Gd^{3+} [69]. Furthermore, previous studies have shown that the cytotoxic effect of the same agent may also depend on the type of cell. Winkleman et al. reported that NIH 3T3 fibroblast cells survived and grew in gadopentatic acid (Gd-DTPA) containing solution (40 mM) over 2 days [70], while Rodríguez-Villarreal et al., reported that HaCaT keratinocyte cells survived only a few hours in Gd-DTPA solution with very close concentration [29, 70]. Another study indicated that the toxicity of Gd-DTPA on whole blood cells and white blood cells was negligible at high concentrations (up to 200 mM) over 3 hours [55]. Moreover, commercial gadolinium-based contrast agents may be more biocompatible than paramagnetic salt solutions obtained by dissolving Gd chelate in PBS or cell culture medium. Durmus et al. have reported that JH-EsoAd1 cells (esophageal adenocarcinoma cell line) can be sustained with approximately 100% viability for a long time (5 days) in a commercial Gd solution (gadabutrol, Gadavist®) at a concentration of 100 mM [17]. Tocchio et al. showed that although Gd^{3+} (Gadavist) did not affect NIH 3T3 cell viability up to 100 mM after 3 days of culture, it caused reduction of cell proliferation according to the resazurin-based metabolism assay results [71].

Another magnetic liquid as an alternative to paramagnetic salt solutions is ferrofluid that are not natural media for cells. A number of studies were conducted on investigating the biocompatibility of custom-made or commercial ferrofluids (e.g. EMG 408).

Zhu et al. reported that the viability measures of both *Escherichia coli* and *Saccharomyces cerevisiae* were almost unchanged in EMG 408 (volume fraction of magnetite particles in this ferrofluid: 1.1 %) for up to 2 hours [52]. Moreover, Zeng et al. determined CFU ml^{-1} (Colony Forming Unit) after focusing test with 0.25 x EMG 408 ferrofluid and observed only a 10% decrease in the cell count compared to the original cell suspension prior to ferrofluid exposure for magnetic focusing test [72]. However, the requirements of mammalian cells may differ from prokaryotic cells. Besides maintaining an overall colloidal system of ferrofluids, each component (i.e. materials, blocking agent) and pH value (≅7 for cell culture) of ferrofluids must be biocompatible. For living cell applications, nanoparticles within ferrofluids are made of biocompatible materials (e.g. magnetite or maghemite) [5]. To stabilize these nanoparticles, there are limited numbers of studies reporting the use of different blocking agents. For instance, Krebs et al. used bovine serum albumin (BSA) as a blocking agent and the viability of human umbilical vein endothelial cells (HUVEC) were above 95% after 2 hours of exposure to ferrofluid (BSA coated iron oxide nanoparticles up to 45 mg/ml) [61]. Kose et al. stabilized nanoparticles via citrate and 75% of blood cells remained viable several hours after exposure to the ferrofluid [50]. The nanoparticles can also be functionalized with a graft copolymer as a blocking agent. Zhao et al reported that the viability of 7 cancer cell lines (lung cancer: A549, H1299, cervical cancer: HeLa, breast cancer: MDA-MB-231, HCC1806, MCF-7, prostate cancer: PC3) lines were above 90% after 2 hours exposures to the custom-made biocompatible ferrofluid (graft copolymer functionalized maghemite nanoparticles, 0.26% v/v) [59]. Cell viability of H1299 lung cancer cells was above 80% even after 12 hours incubation with a 0.26% (v/v) concentration ferrofluid [59, 73]. Furthermore, the viability of the whole mouse blood cells were consistently 100% after 2 hours exposure to graft copolymer functionalized maghemite ferrofluids (up to 1.03 v/v) [60].

1.3. Magnetic Force-Based Cell Manipulation

The manipulation of living cells by an external stimulus is an important tool for separation or detection of cells of interest and to guide cells in tissue engineering applications. Together with recent advances in engineering and technology, systems and

designs varying in size, shape, complexity, and cost have been developed for various cell manipulation applications. These applications include blood cell separation [74], rare cell (e.g. circulating tumor cells) isolation in blood [75, 76], detection of pathogens [77, 78], cell counting for disease monitoring (e.g. $CD4^+$ T cell counting for HIV progression) [79, 80], stem cell enrichment [81, 82] and organization of cells into designed spatial arrangements in two or three dimensional cultures [83, 84].

Most cell manipulation techniques are based on physical and/or affinity-based approaches. Physical manipulation techniques are driven by intrinsic cell properties (e.g., deformability, density, electrical capacitance or resistance, size, magnetic susceptibility, mass, morphology) while affinity based-techniques use "labels" (e.g., particle-antibody conjugates specific to a membrane protein) to manipulate cells of interest. Operation principles include electrical [85-87], mechanical [88-90], affinity [91], acoustic [92-94], optical [95-97], and magnetic [12, 98, 99] forces or combined application of these factors [100].

The basic principle of magnetic force-based manipulation relies on a magnetic field strength, field gradient, and a magnetic susceptibility difference between the cell of interest and the surrounding environment, as explained above. This strategy offers several advantages compared to its alternatives. First, the non-contact nature of the technique minimizes potential hazardous effects that could reduce cell viability/integrity [101]. Second, the generation of a magnetic field does not depend on complex or expensive instrumentation as it can be created with an externally located, simple, low-cost rare earth magnet [17, 102]. Third, magnetic manipulation has low sensitivity to internal and external factors such as ionic strength, surface charges, pH and temperature [103].

Positive magnetophoresis is a useful tool in the field of two and three dimensional (2D and 3D) cell culture and can be used to assemble cells into 3D cellular spheroids as building blocks [104, 105], to pattern cells in culture for a suitable cellular microenvironment [106, 107], to guide cells into sheet-like structures for close cellular contact [108, 109] and to enhance the seeding efficiency of cells into scaffolds in tissue engineering applications [110]. However, since positive magnetophoresis heavily rely on the labeling of cells with magnetic particles, problems related to adequate and standard cellular internalization [111, 112], time consuming experimental steps [113, 114] and possible biological interference of magnetic labels [30, 115, 116] stand out as the most common limiting factors.

In recent years, a label-free magnetic manipulation alternative based on negative magnetophoresis has been developed to eliminate the adverse effects of cell labeling. In this method, cells are placed in a medium containing either a paramagnetic salt solution[30]

or a ferrofluid [51]. Since cells magnetize less than the medium, cells are focused in the lower magnetic field regions when placed under a magnetic field [54]. Thereby cells can be manipulated based on the arranged magnetic field pattern. This method was successfully used to trap bacteria [117], to separate tumor cells [59, 73], and to detect lipid-accumulating bone marrow cells [118], and cells with impaired function (e.g. sickle cells) [56]. Moreover, there are successful applications of this technique to create ordered cellular structures such as the assembly of cells into linear arrangements [61] or spheroids [119] and levitation of cell encapsulated polymers [120]. Besides these applications, since label-free magnetic levitation is able to balance the gravitational force by a homogeneous magnetic force on entire structures of the cell, it offers the opportunity to simulate microgravity condition on the Earth and to study biological effects of microgravity [121].

A protocol for label-free magnetic levitation of living cells was comprehensively described in Chapter 2. This protocol enables density-based detection of cells in a heterogeneous population, self-assembly of cells for biofabrication of 3D living structures and culture of cells under simulated microgravity condition.

1.4. Biofabrication by Label-free Magnetic Levitation

To meet functional requirements, organs arrange one or more cell types in specific forms [122]. Manipulation of cells in 2D and 3D cell culture that aims biomimicry is therefore crucial to reflect appropriate form and function. Thus, development of techniques to organize cells in targeted arrangements in convenient microenvironments is one of the most important trends in cell culture technologies. Magnetic cell manipulation techniques have been used for various purposes in 2D and 3D cell culture (Figure 1.2) such as; to form 3D cellular assembly as building blocks [104], to organize cells or spheroids into a targeted pattern [106, 107], to create cell sheets for a tight and close cellular contact [109] and to increase cell seeding efficiency into scaffolds [110].

Here, we focused on utilization of label-free magnetic levitation on the application of the label-free magnetic levitation technique for the biofabrication of various 3D structures.

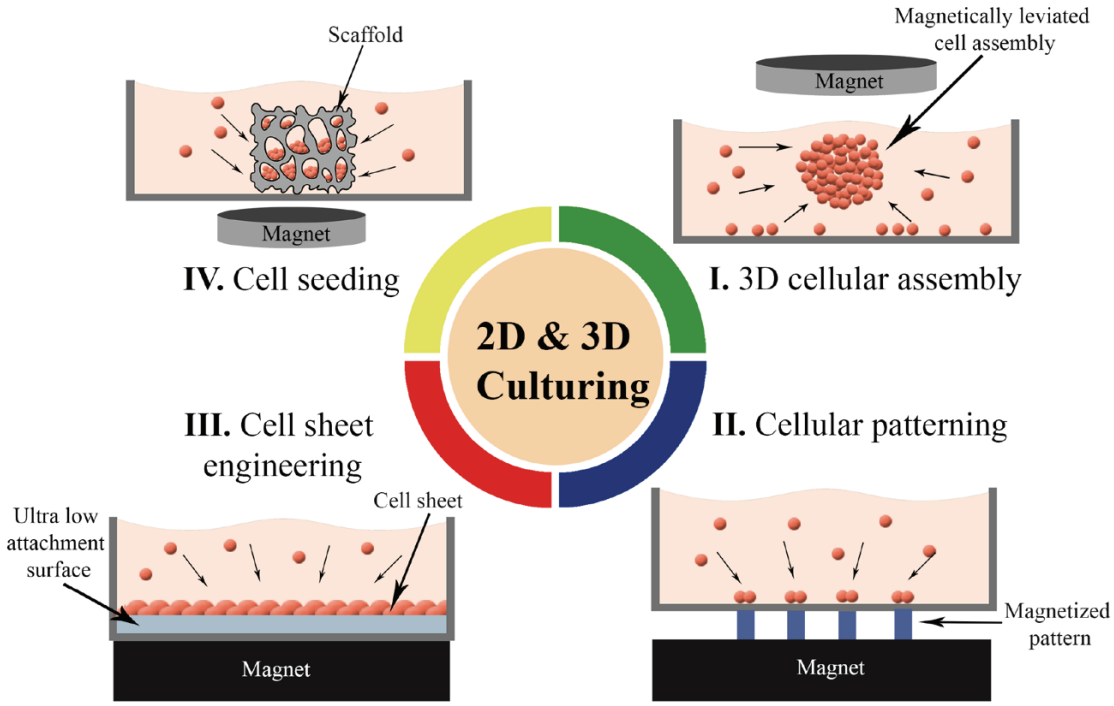

Figure 1.2. Magnetic force-based 2D and 3D cell culture techniques. (I) Formation of 3D cellular assembly as building blocks, (II) Organizing cells or spheroids into a targeted pattern, (III) Guiding cells into sheet-like structures for a close cellular contact, and (IV) Enhancing the seeding efficiency of the cells into scaffolds [123].

Positive magnetophoresis techniques based on magnetic labeling have been successfully applied for the biofabrication of 3D structures of various shapes (Figure 1.3a-e). Label-free principle based on negative magnetophoresis (Figure 1.3f-i) provides a powerful alternative to eliminate acute and long-term cytotoxicity concerns due to cell binding or uptake of magnetic particles. Firstly, 3D cellular aggregates were formed by negative magnetophoresis using a paramagnetic medium [119]. The experimental setup consisted of a culture chamber on four cubic NdFeB magnets (side dimension of 10 mm), placed with opposite poles next to each other. For cellular assembly, cells were suspended in a Gd-DTPA containing culture medium (34.6 mM) to enhance the diamagnetic property of the cells and poured into the chamber. Cells were aggregated into an egg-shaped structure in the center of the magnets, the area of lowest magnetic flux density, in 20 min. They also demonstrated another device for spheroid array formation that was able to form larger numbers of spheroids using the same principle [124]. In this system, a cell culture chamber was set on a magnet array composed of 6 × 6 NdFeB magnets (3 × 3 × 10 mm), corresponding to 25 array spots with low magnetic flux densities at equal

distance from each other. Furthermore, this magnetic cell manipulation principle was combined with microfluidic technology to generate rapid and high throughput systems for spheroid formation [57]. This microfluidic chip was composed of a cell aggregation chamber (8 mm in wide and 0.5 mm in deep) on a similar magnet array with 2 × 3 aggregation spots and a syringe pump for medium perfusion after aggregation. Cells assembled into spheroids within one minute in the chip and most of the cells were alive in spheroids after 12 hours of culture with medium perfusion. It is also possible to control the shape and size of cellular assemblies with the negative magnetophoresis principle. Abdel Fattah et al. placed two magnets, facing the same poles, on both sides of the cell culture chamber to form a rectangular bar-shaped cellular assembly and used an arrangement of three magnets with 120° pole angles placed next to each other to form a three-pointed star-shaped cellular assembly [55]. Besides organizing cells into these different shapes, a strategy was developed that could control the size of spheroids generated by placing magnets under the cell culture chamber. This strategy involved the formation of larger spheroids by increasing the distance between the cell culture chamber and the magnet under the chamber, and consequently lowering the magnetic field strength [55].

Negative magnetophoresis is also a convenient technology for assembly of cells by complete levitation of cells, this application is also depicted as diamagnetic levitation. A system, composed of two permanent NdFeB magnets with the same poles facing each other and a container filled with a solution of paramagnetic ions between these magnets, was described for levitation of nonliving materials [64, 125, 126]. Durmus et al. used a miniaturized magnetic levitation system, consisting of a glass capillary (with 1 mm inner diameter) between two NdFeB magnets to load cells in a paramagnetic medium, and two 45° tilted mirrors added to the sides to observe cells in real time, as a cell densitometry platform [17, 127]. Following the study showing that the magnetic levitation system was suitable for the levitation of living cells, several studies aiming at manipulation of 3D living building blocks were conducted using this strategy. Cellular clusters of varying sizes were formed by changing the number of cells loaded into the capillaries within this system and fabricated tissue strings with patterning spheroids, already assembled with ultra-low attachment microplates [71].

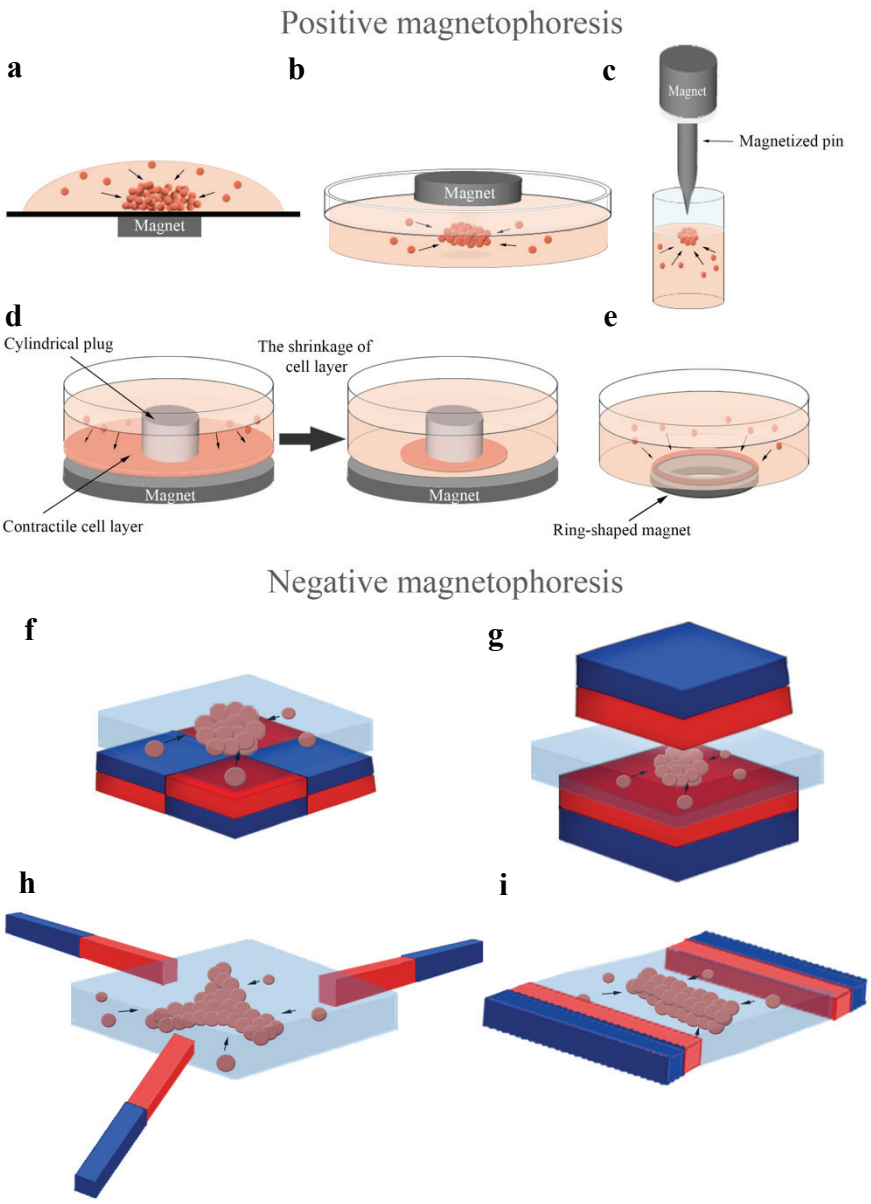

Figure 1.3. Magnetic force-based manipulation of magnetically labeled cells (positive magnetophoresis) and label-free diamagnetic cells (negative magnetophoresis). 3D assembly of magnetically labeled cells into a spheroid by a magnet (a) under the culture chamber, (b) on the top of the culture chamber and (c) by a magnetized pin beneath the magnet to concentrate the magnetic field for attracting cells in a focused direction. 3D assembly of magnetically labeled cells into a ring-shaped structure (d) using a cylindrical plug and a magnet under it to accumulate contractile cells around the plug and (e) using a ring-shaped magnet. 3D assembly of label-free diamagnetic cells into (f, g) spheroid, (h) three-pointed star and (i) rectangular bar in a magnetic liquid with different configurations of magnets to produce a spatially varying field along the culture chamber (The north poles: red, the south poles: blue) [123].

They also described a droplet-based magnetic levitation assembly design to form a larger number of 3D cellular structures. In this design, cells were compartmentalized in water-in-oil droplets generated by alternate aspiration of mineral oil and cell suspension, in the magnetic levitation device and assembled into individual 3D architecture within 24 h. This cellular assembly process resulted in faster cellular aggregation and enhanced shape uniformity of biological structures. As an alternative, Parfenov et al. designed a new installation consisting of 2 ring-shape NdFeB magnets (external diameter: 85 mm, internal diameter: 20 mm, thickness: 24 mm), oriented to each other with the same poles, a glass container (12 × 12 × 50 mm), inserted into the hole of the magnets and a camera system for label-free magnetic levitation of tissue spheroids [105]. These studies presented the manipulation and fusion of the pre-formed 3D living structures. In this thesis, we achieved manipulation of individual cells and formation of *in situ* 3D aggregates with controllable structures both in a microfluidic [128] and a ring-magnet based large scale magnetic levitation system [129]. A deeper information about these label-free magnetic levitation applications will be given in Chapters 3 and 4.

1.5. Weightlessness Simulation by Magnetic Levitation

Space missions induce many biological changes, and gravitational loading is one of the major contributors to these changes [130]. Alterations in gravitational loading act as regulatory physical signals that affect structure and function at both the cell [131, 132] and tissue level [133-135]. It is known that microgravity causes several health problems such as muscle atrophy [136], bone loss [137], immune system dysregulation [138] and cardiovascular deconditioning [139]. Understanding the biological effects of gravitational alterations is crucial in terms of extending the duration of spaceflights and potential future colonization efforts in space bodies.

Spaceflight technologies allows both in vitro [140] and in vivo [141] tests providing an understanding of the effects of gravitational changes on living systems. However, microgravity research conducted with such technologies are expensive and rare [142], which underscores the importance of earth-based microgravity simulation systems. Microgravity that is also depicted as weightlessness to describe the condition where a net sum of all forces is zero (e.g. hydrostatic pressure, cell surface binding) [143], can be

simulated with several ground-based technologies. Experiments in rodents provides simulation of both of partial weight-bearing [144] and complete lack of weight-bearing [145-149] on Earth. However, such animal models are generally applied to test hypotheses at tissue level especially on the musculoskeletal tissues, cause high variation at the molecular/cellular level and requires expensive setups [150]. Alternatively, in order to examine molecular and cellular level *in vitro* adaptations a few microgravity simulation devices are available. These microgravity simulation techniques, including (i) clinostat, (ii) random positioning machine (RPM), (iii) rotating wall vessel (RWV) and (iv) magnetic levitation-based systems, offer the opportunity to be used in experimentations to test the biological effects of microgravity on Earth. Unlike other microgravity simulation devices [151-153] that cause fluid shear stress on the living cells as a result of rotation of culture chamber [154, 155], magnetic levitation-based systems do not generate such additional forces interrupting the cellular response. Therefore, one of the important application areas of magnetic levitation technology is microgravity simulation to enhance our understanding of microgravity effects on the living systems as an alternative to spaceflight experiments and other ground-based facilities. However, not all magnetic levitation strategies are convenient to create simulated microgravity. Magnetic levitation by magnetic labeling of diamagnetic cells is not able to generate microgravity since it cannot create a homogeneous magnetic force on all cellular structures [156, 157]. In contrast, the diamagnetic levitation principle balances gravitational force with magnetic force on all cellular structures since water is the main component of the cellular mass and the cellular constituents have a density and magnetic susceptibility value similar to that of water [158]. Diamagnetic levitation is a powerful technology to simulate microgravity with several advantages such as rotation free application and real time monitoring. In our studies, diamagnetic levitation system composed of two permanent magnets with the same poles facing each other that was initially designed for single cell levitation [118, 159-161], then were implemented to create a microgravity condition and to perform biofabrication [128, 162-166]. Here, in Chapter 2, magnetic levitation protocols for both analysis and cellular self-assembly under microgravity were defined [167]. In Chapters 3 [128] and 4 [129], biofabrication was performed at different scales using different magnet configurations under microgravity condition.

CHAPTER 2

SINGLE CELL DENSITOMETRY AND WEIGHTLESSNESS CULTURE OF MESENCHYMAL STEM CELLS USING MAGNETIC LEVITATION

2.1. Background

2.1.1. Single Cell Density Detection with Magnetic Levitation

Mass density of cells is a critical biophysical property indicating parameters such as cell differentiation or state [118, 168]. It is possible to measure cellular density with several techniques such as Ficoll gradient centrifugation, optically induced electrokinetics [169] and suspended microchannel resonator [170]. However, such systems either provide density measurement of bulk cell population rather than single cell-level measurement, or their application is challenging due to complex and expensive operation requirements [118]. Diamagnetic levitation is a novel, simple and cost-effective technique to detect cell density at single cell-level and to separate cell populations based on their densities.

Magnetic levitation by negative magnetophoresis allows cells suspended in a magnetic medium (i.e. paramagnetic salt solution and ferrofluid) to be moved towards the lower magnetic field region and to be equilibrated at different positions of the magnetic field gradient depending on cell densities. Magnetic levitation technique, that was initially described for the manipulation of non-living objects [64, 126, 171, 172], was adapted for levitation of biological components with the intent of density measurement and density-based separation of them. This technology has been applied for label-free separation of many types of cells including adipocytes, cancer cells, blood cells and circulating cells [17, 118, 127].

2.1.2. Cell Culture with Magnetic Levitation

Magnetic levitation technology has the potential to be applied for culturing cells with a suitable experimental setup. The levitation process applied at a label-free manner is able to simulate a weightlessness environment on the cells. Weightlessness research is crucial for space biology applications to demonstrate adaptive alternations in physiology and function caused by the space environment. However, traditional weightlessness simulation techniques as an alternative to rare space experiments include *in vivo* tissue-level studies that are relatively challenging and costly [146, 149] and *in vitro* bioreactor-based systems (e.g. random positioning machine, clinostat and rotating wall vessel) that generate shear forces on cells due to rotation of the chamber [173, 174]. Magnetic levitation, that provides absence of net force on the cells by balancing gravitational force with magnetic force and cancels out individual weight of them, has emerged as an alternative to these weightlessness simulation techniques. The technique shows superiority over other methods due to its real-time imaging capability, its potential to allow operation at the single cell level, its low cost and ease of application. This weightlessness environment results in the self-assembly of living cells when the cell levitation process is extended and can therefore also be applied for the biofabrication of 3D living structures [175].

The diamagnetic levitation technique offers the opportunity to be used both as a diagnostic tool due to its ability to distinguish cells based on their density [176, 177], and as a weightlessness environment simulation instrument since it cancels out the gravitational force on the cell during levitation [128, 178]. In this chapter, a standardized protocol for cell levitation using a miniaturized magnetic levitation device is described step-by-step.

2.2. Magnetic Levitation Procedure

Cells are harvested from the culture shortly before levitation in order to preserve health and the physical properties of the cells in culture. All steps are performed at room temperature.

2.2.1. Installation of the Magnetic Levitation Device

1. N52-grade neodymium (NdFeB) magnets (50 mm in length, 2 mm in width, and 5 mm in height), that are magnetized through their heights, are positioned at 1.5 mm distance with facing the same poles together. With this positioning, a magnetic field gradient perpendicular to gravity vector is formed in the area between the magnets, which increases with getting closer to the magnet surfaces and decreases with getting closer to the middle of the area between the magnets. (*see* **Note 1**).
2. A glass micro-capillary channel (1 × 1 mm square cross-section, 50 mm length) is placed between magnets to serve as a levitation chamber.
3. Two mirrors are positioned on both sides of the transparent capillary channel at 45° for real-time observation and imaging of levitation under an inverted microscope (*see* **Note 2**). The light coming from the light source of the microscope is reflected from a mirror and transmitted through the capillary channel to the microscope objective and thus the inside of the levitation chamber can be observed at real-time. (Figure 2.1).

2.2.2. Preparation of Living Cell Sample

1. Cells are cultured and proliferated considering routine cell-specific culture conditions. (*see* **Note 3 and 4**).
2. If the cells to be levitated are adherent cells, the cells on the culture surface are harvested by applying appropriate physical or chemical detachment protocol considering the cell type, and the cell suspension is transferred to a centrifuge tube.
3. If the cells to be levitated are grown in suspension culture, the cell suspension is directly transferred to a centrifuge tube.
4. Cells are centrifuged and the pellet is resuspended in a proper solution (*see* **Note 5**).
5. Count the cell number in suspension using either cell counter or a hemocytometer.

6. Following counting of the cell number in suspension, the cell suspension at the desired final concentration is prepared with the selected solution (*see* **Note 6** and **Note 7**).

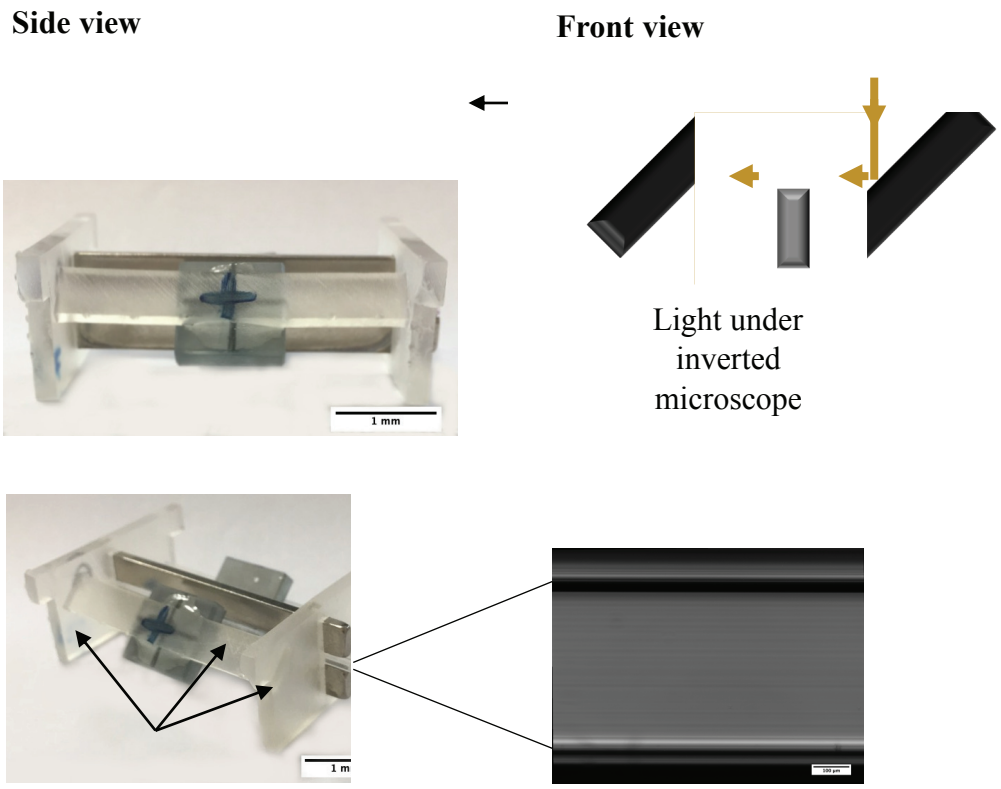

Figure 2.1. Magnetic levitation device. (a) Side and front view of the device: (1) NdFeB magnets, (2) mirrors, and (3) glass capillary channel. Scale bar, 1 mm. (b) Perspective view of the device (scale bar, 1 mm) and micrograph of a magnetic levitation channel under an inverted microscope. The components for this specific magnetic levitation setup are held together with 3D-printed frames. (Scale bar, 100 µm) The components are assembled using connecting pieces that are printed by a 3D printer in this magnetic levitation device.

2.2.3. Magnetic Levitation of Cells

1. The surface of the glass channel is cleaned with an ethanol (70%) moistened napkin before the levitation for a spotless observation and imaging. (see **Note 8**).
2. Gadolinium-based agent (Gadavist®, Bayer) is added at the preferred final concentration shortly before the operation to paramagnetize the solution surrounding the cells. (*see* **Note 9-12**) (Figure 2.2).

3. The cell suspension rendered as paramagnetic is loaded into the capillary levitation chamber.
4. Both to protect the user and peripheral equipment from sample contamination and to protect the sample from contamination, the levitation chamber is sealed with Critoseal before the chamber is placed in the slot between the permanent magnets.
5. For the determination of density at the single cell level, it is waited by real-time observation under the microscope for the cells to reach the equilibrium position. After reaching equilibrium, it is recommended not to wait too long so that cellular gathering does not start. (see Subheading 2.2.4) (see **Note 13**).
6. To perform cell culture by levitation, magnetic levitation culture is placed in a petri dish containing sterile water (~5 mL) under sterile conditions to prevent evaporation from the suspension. Then, the culture is maintained in an incubator that provides the gas, temperature and humidity conditions that the cell needs during culture.

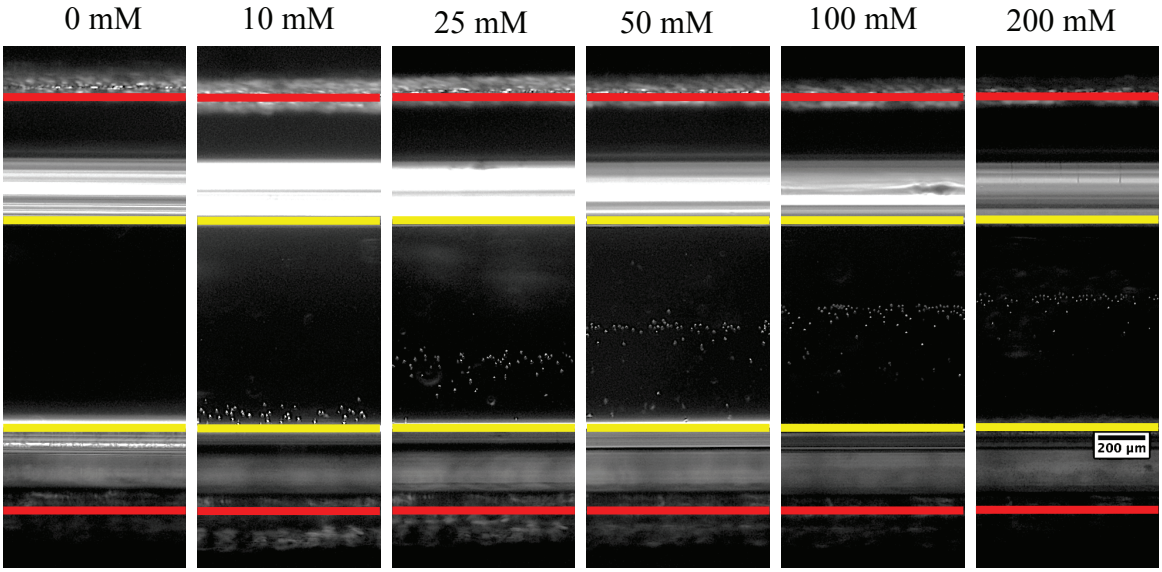

Figure 2.2. Micrographs of D1 ORL UVA cells (mouse bone marrow cell line) levitated and reached equilibrium position (approximately 10 min) in growth medium containing different concentrations of Gd^{3+} (Gadavist®; 0, 10, 25, 50, 100, and 200 mM). Red lines indicate the lower limit of the upper magnet and the upper limit of the lower magnet, and yellow lines indicate top and bottom levels of the inside of the levitation chamber. Scale bar, 200 µm.

2.2.4. Imaging and Analysis

1. The magnetic levitation device is positioned on sample stage of an inverted microscope with an adaptor piece that provide the device to be positioned close enough to the objective for visualization.
2. Levitated cells in the device is focused with focus knob of the microscope (*see* **Note 14**).
3. In order to obtain a clear image of levitated cells, exposure time, arrangement of optical element engaged in the light path and condenser height are adjusted (*see* **Note 15** and **16**).
4. The area where the image of the levitated cells is recorded should also be recorded by focusing the magnets so that the magnet surfaces can be used as a reference level in determining the levitation height of the cells.
5. Images separately focused on levitated cells and magnets are opened in ImageJ Fiji software.
6. The area between the two magnets is selected with the rectangular selection tool on the image on which the magnets are focused as reference, and the image belonging the same sample on which the cells are focused is cropped by applying this region of interest.
7. In order to fix uneven backgrounds, the command "subtract background" is used.
8. To properly find edges of the levitated cells and to turn them into analyzable particles, the threshold is set (*see* **Note 17**).
9. Measurements are set to include at least area and center of mass for determination of size and levitation height, respectively.
10. The region where the levitated cells or 3D structures are positioned is selected with the rectangle selection tool and these particles are analyzed (*see* **Note 18** and **19**).
11. Measurements are recorded in the analysis window, which includes at least the size of the particles and the distance between the mass centers of the particles and the upper level of the lower magnet. (*see* **Note 20**).

2.2.5. Calibration of Setup

When the magnetic levitation technique is used to measure the density of cells or cellular structures, the system is calibrated with beads of known density and the density-levitation height relationship is determined. (*see* **Note 21**).

1. PBS-Tween solution (200 µL) by diluting 2% (volume/volume) Tween-20 in PBS is prepared for properly dispersing particles.
2. For each micro-bead, a stock solution is prepared by suspending the beads in PBS-Tween solution.
3. The bead concentration of the prepared suspension is determined with the aid of a hemocytometer.
4. Bead suspensions are prepared with a final concentration of 10^4-10^5 beads/mL in the solution used for the levitation of cells. Each sample is prepared to be at least 50 µL with paramagnetic agent, considering the volume of the capillary channel.
5. Gadobultrol is added to the bead suspension to provide the Gd^{3+} concentration at which the levitation height of the cells is recorded, and magnetic levitation is immediately applied (see Subheading 2.2.3).
6. When the beads come to the equilibrium position, their levitations are imaged and their levitation heights are analyzed (see Subheading 3.4).
7. The graph showing levitation height of beads versus density of beads is plotted and linear regression is performed over the data to obtain equation providing the density corresponding to the measured levitation height.
8. The measured levitation heights of cells are converted to density of cells using the resulting equation.

2.3. Notes

1. The magnetic field gradient can be controlled by changing the distance between magnets. The expected magnetic field distribution in the magnetic levitation setup can be simulated with finite element method. So far, studies in which the expected magnetic field distribution in the magnetic levitation device [17, 123, 128] and the

balancing positions of the cells in the device [118] have been theoretically presented and experimentally supported have been reported.

2. Connecting parts to be used to hold magnets and mirrors together and to form the slot where the levitation chamber will be placed can be cut by laser system [17, 179] or printed with a 3D printer [128].
3. The protocol described in this chapter has been implemented using stem cells from bone marrow origin that are able to differentiate into adipogenic and osteogenic lineages [180]. If cells are obtained from a different source other than 2D culture of stable cell lines, such as cells cultured in a support material, the cells should be harvested by applying appropriate additional preliminary steps.
4. If frozen cells are to be used directly without culturing, the cells are thawed quickly (< 1 minute) and then step four is followed.
5. Depending on the purpose of the operation, cells can be suspended in different solutions. If the cells are to be cultured during levitation, growth medium must be used for the maintenance of the cells [128]. On the other hand, if the purpose of cell levitation is density-based cell separation, FBS may be more appropriate [17].
6. The concentration of cells to be levitated should be chosen according to the purpose of the operation (Figure 2.3). For example, for medium-sized cells such as stem cells, it is proper to use a concentration of 10^5 cells/mL or less if the cells are to be imaged individually for density determination [118]. For larger cells it may be necessary to further reduce this concentration. This concentration can be increased when it is aimed to form large cellular structures by self-assembly of cells under magnetic levitation [128, 179].
7. The volume of the aforementioned levitation chamber is approximately 50 µL. If the entire capacity of the chamber will be used, the sample should be prepared at least this volume considering the paramagnetic agent to be added.
8. If the magnetic levitation process is to be used for cell culture, all magnetic levitation device components must be sterile and their sterility must be maintained throughout the procedure. That is to say, the "magnetic levitation of cells" step following the "preparation of living cell sample" step should also be continued under sterile conditions. The components of the magnetic levitation device should be used after sterilization by exposure to UV (30 minutes). Especially, the capillary channel, where the cell suspension will be loaded, should be washed with ethanol (70%) before UV exposure, and the ethanol should be completely

removed and its sterility should be ensured. Alternatively, this glass components can be sterilized by autoclave or dry heat treatment using hot air oven.

9. Lanthanide ions, especially Gd^{3+} that are one of trivalent lanthanide ions, have similar cationic radii to that of calcium ions and thus competitively inhibit calcium channels, affect several calcium-mediated biochemical pathways in animal cells. These biological interference cause Gd^{3+} to be cytotoxic [181]. In order to reduce this high cytotoxicity, free gadolinium ion is chelated by some sort of ligand. There are several chelate forms of gadolinium that are commercially available to provide an appropriate biocompatibility. Gadobutrol (Gadavist®, Bayer) is an effective contrast agent in the use of magnetic levitation for both cell separation and cell culture, as it does not reduce cell viability even at high concentrations (100 mM) and provides higher levitation at the same concentrations compared to most of its competitors [17, 128, 175, 179].
10. Gd-containing magnetic resonance imaging contrast agents contain either linear or macrocyclic ligand, and the agents can be ionic or nonionic. Agents with these structural differences can also be used in magnetic levitation of cells as an alternative. Structural differences of agents can affect the application. That is, nonionic agents, such as gadobutrol (Gadavist®) and gadodiamide (Omniscan™), provide higher levitation heights than ionic agents; such as gadopentetate dimeglumine (Magnevist®), gadoterate meglumine (Dotarem®) and gadobenate dimeglumine (Multihance®). Macrocyclic agents (gadobutrol and gadoterate meglumine) provides better cell viability than linear agents (gadopentetate dimeglumine, gadodiamide and gadobenate dimeglumine) [128].
11. Aqueous solution of several paramagnetic species such as $MnCl_2$ and $MnBr_2$, may be used to levitate diamagnetic objects. Similar to Gd-containing substances, they form transparent solutions, which allows for straightforward imaging of samples [64, 182, 183]. However, when the object to be levitated is cells rather than nonliving objects, the short- and long-term effect on viability, specific to the cell type, must be considered before use. [184].
12. If the aim is to determine density differences between objects, low Gd^{3+} concentrations (~20-50 mM) are more suitable. As the concentration is reduced, the change in unit density can be observed with a larger levitation height difference [17, 118]. On the other hand, if the goal is to form and culture 3D living

structures, higher concentrations are more effective to preserve complete levitation and prevent the cellular structure from contacting the ground [128, 175, 179].

13. Studies on bone marrow-derived stem cells show that 10-15 minutes is sufficient for these cells to reach equilibrium [118, 128]. Since this period may vary depending on the cell type and the physical and chemical properties of the solution surrounding the cells, the length of this process should be determined before starting the main experiments.
14. The default stage limit on the z-axis to protect the microscope parts may in some cases not allow to properly focus cells in the device. In such a case, it is necessary to manipulate this limit considering dimensional specifications of the microscope.
15. A strong illumination is required as the visualization of the cells is provided by parallel mirrors placed on both sides of the levitation chamber.
16. In order to obtain reproducible and comparable results, it is recommended to record the hardware and software settings and continue using the same.
17. For the accurate determination of the size and position of individual cells or 3D structures, objects that are close to each other and appear to be single should also be carefully analyzed as separate particles. If the separate objects are displayed as a single particle when the threshold value correctly find the edges of the objects, the converging objects are divided by using the “watershed” tool.
18. If the region where the levitated cells are collected during the analysis is not selected appropriately, cells whose membrane integrity has been lost and therefore levitated at a different level or settled on the culture surface may also be included in the analysis. In addition, regions close to the surface of the capillary reflect light, making analysis difficult if included in the area of interest.
19. The size and circularity limits in the "analyze particle" window are helpful to exclude impurities that should not be included in the analysis in ImageJ Fiji software. Although proper values may vary according to the size of the cell and the cleanliness and resolution of the image, it has been showed that size limits between 1-300 and circularity limits between 0.01-1 are proper in the analysis of bone marrow-derived stem cells imaged under 4× magnification in a 1600×1200-pixel image where 1 pixel is equal to 1.724 µm.
20. In order to obtain the levitation height results in µm, either the scale of the picture is set with using the scale bar in ImageJ Fiji software before the analysis or the

pixel values obtained from the analysis are converted into μm with using the known pixel-μm conversion.

21. In order to obtain an equation, preferably by interpolation, at least three different beads with known density should be selected, covering the expected density distribution of living cells (e.g. 1.01-1.10 g/mL) for determining the density-levitation height relationship of cells.

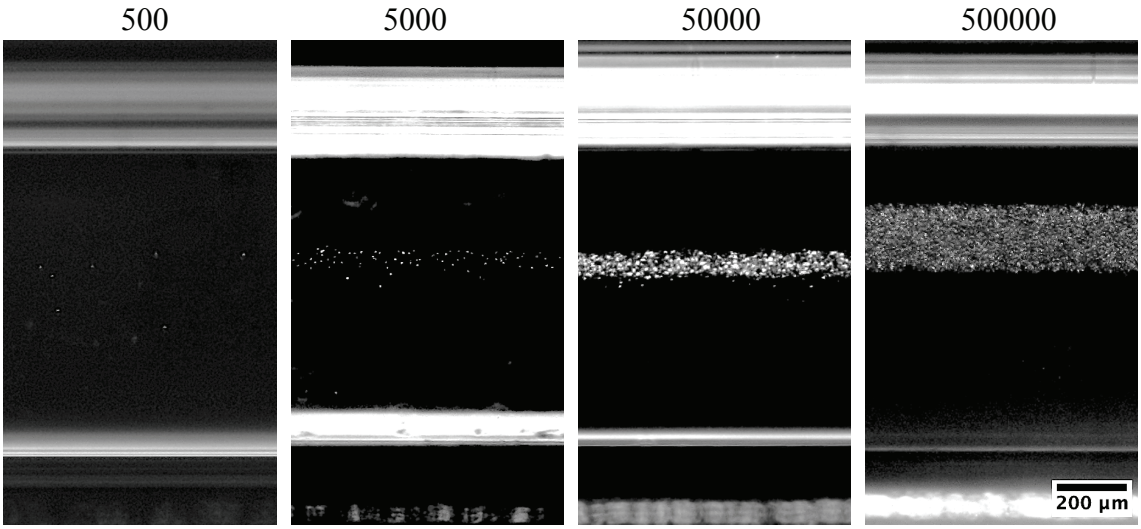

Figure 2.3. Micrographs of D1 ORL UVA cells that are levitated using different cell numbers (total 500, 5000, 50000, and 500000 cells in the levitation chamber) after 10 min of levitation (100 mM gadobutrol). Scale bar, 200 μm

CHAPTER 3

BIOFABRICATION OF IN SITU SELF ASSEMBLED 3D CELL CULTURES IN A WEIGHTLESSNESS ENVIRONMENT GENERATED USING MAGNETIC LEVITATION

3.1. Background

3.1.1. Lack of Mechanical Stimuli for Cells

Cells in organisms are constantly exposed to varying degrees of mechanical forces, that serve as important stimuli and effect cellular fate [185-188]. These physical signals are critical regulators for biological system maintenance, repair and renewal at the cell and tissue level in mammals [189, 190]. Permanent or temporary reduction of mechanical stimulations, as experienced during spaceflight, immobilization, paralysis and bed rest, cause deteriorations in the human body [191], especially in the musculoskeletal system such as demineralization of bones and mass loss of skeletal muscle [192-196].

Gravity is a critical mechanical signal that constantly acts on living organisms on Earth. Gravitational force is converted into biochemical stimuli by cells, causing cellular and molecular changes [197]. Such changes cause physiopathological effects on various biological systems, especially on bone tissue mainly consisting of osteoblast osteocytes, osteoclast and mesenchymal stem cells. Several studies have showed that weightlessness environment induces adipogenesis and inhibits osteogenic differentiation of mesenchymal stem cells that can differentiate into various tissues such as bone, fat, cartilage and muscle [198, 199]. Conversely, mechanical stimulation promotes differentiation of these cells into osteogenic lineage [200]. These responses of mesenchymal stem cells to mechanical stimuli or stimulus deprivation have made mesenchymal stem cells one of the most critical cell types for weightlessness research.

Spaceflight experiments offer great opportunities to improve our understanding on short term and long duration biological effects of weightlessness [201-203]. Nevertheless, such experiments are rare, expensive to operate and hard to secure, and alternative ground-based techniques have hence been developed to simulate the weightlessness environment [204]. The most commonly used devices to study simulated weightlessness are the rotating-wall vessel (RWV) platform [151, 205, 206], 2D clinostats [152, 207, 208] and Random Positioning Machines (RPM) [153, 207, 209]. However, these devices create fluid shear stress on the cells due to rotation and this can interrupt the response of cells to a randomized gravity vector [154, 155]. Furthermore, both the clinostat and the RPM requires time for randomization of gravity vector and therefore they are not convenient for relatively rapidly occurring cellular processes.

3.1.2. Magnetic Levitation to Simulate Weightlessness

One of the most recent ground based technology to mimic the biological effects of weightlessness is magnetic levitation technique [121]. Magnetic levitation can be applied via positive or negative magnetophoresis, however positive magnetophoresis (i.e. magnetic bead labeling technique) cannot simulate weightlessness because acting forces that levitate the subject of interest only act on the surface of the subject and any internal structures are free of those forces [156, 157]. In contrast, levitation through negative magnetophoresis (also referred to as diamagnetophoresis) can exactly mimic weightlessness. During negative magnetophoresis, gravitational force on the subject is compensated by a counteracting force that induces weightlessness. In contrast to other ground-based methods, magnetic levitation allows the investigation of relatively fast cellular processes.

In magnetic levitation technique, diamagnetic objects (i.e. almost all cells) are guided towards regions of low magnetic field in a magnetic field gradient and the process is resulted in stable magnetic levitation and the simulation of weightlessness environment as long as the gradient is intact [24, 25, 210]. Such a strategy requires high magnitude magnetic fields that can be detrimental to biological subjects [37]. In order to reduce the magnitude of magnetic fields, it is possible to increase the magnetic susceptibility of medium by using paramagnetic solutions [64, 125, 126] or ferrofluids [52]. Recently an inexpensive strategy

has been demonstrated for label-free cell levitation in gadolinium (Gd^{3+}) based solution [127] and successfully applied for detection of differences in cell densities at the single-cell level [17] and guided assembly of *ex situ* generated spheroids [211]. However, self-guided assembly of cells *in situ* during levitation and appropriate Gd^{3+} based solution for longer term culturing is largely unknown.

In this research, we used a magnetic levitation system for *in situ* cell culture in simulated microgravity. First, we investigated the most appropriate composition and concentration for Gd^{3+} based solution for weightlessness culturing. Further, we documented the self-assembly pattern of cells and controlling of cluster size with initial cell number. Finally, we applied our previous findings to determine the possibility of coculture and biofabrication of novel cellular patterns. Our study established the possibility of levitation through diamagnetophoresis as a powerful biomedical tool that will allow testing of molecular and cellular level hypotheses on biological effects of weightlessness in a single cell level that is not possible with current methods simulating weightlessness.

3.2. Methods

3.2.1. Experimental Setup

Cells suspended in the paramagnetic medium (i.e., Gd-based solution) move away from high magnetic field (i.e. regions close to the magnets) to low magnetic field due to the difference between the magnetic susceptibility of cells and surrounding paramagnetic medium. Until cells reach equilibrium position, fluidic drag (F_d), inertial (F_i), buoyancy (F_b), and magnetic forces (F_{mag}) act on them. When cells get closer the equilibrium position, velocity of the cells and thus F_d and F_i become smaller and cells are levitated at the position where, F_{mag} and F_b equilibrate in opposite directions [127].

In this context, our magnetic levitation platform consists of two high grade (N52) neodymium (NdFeB) magnet (50 mm length, 2 mm width, and 5 mm height, Supermagnete) positioned at 1,5 mm distance with same poles facing each other, a micro-capillary channel (1 mm × 1 mm square cross-section, 50-mm length, Vitrocom) between two magnets and mirrors (12,7 x 12,7 x 3,2 mm, Thorlabs) at 45° for real-time inverted

microscope imaging (Figure 3.1a). The components of the magnetic levitation device are held together with photoreactive resin (Clear v2 FLGPCL02) printed using 3D printer (Formlabs Form 2).

3.2.2. Cell Culture

D1 ORL UVA, D1 ORL UVA^{eGFP} (bone marrow stem cell line) [212] and MDA-MB-231^{dsRed} cells (human breast cancer cell line) were cultured in Dulbecco's Modified Eagle's medium (DMEM, Gibco) supplemented with 10% fetal bovine serum (FBS) and 1% penicillin/streptomycin. The cells were grown in a humidified 37 °C incubator with 5% CO_2. The growth medium was changed every other day and the cells were passaged every four to six days.

3.2.3. Short-Term Levitation of Cells

D1 ORL UVA cells were thawed and centrifuged at 125 × g for 5 min and supernatant was discarded. The cells were resuspended to 10^5 cells/ml in the culture medium with different Gd-based solutions; Gd-BT-DO3A (Gadavist®, Bayer), Gd-DTPA (Magnevist®, Bayer), Gd-DTPA-BMA (Omniscan™, GE Healthcare), Gd-DOTA (Dotarem®,Guerbet) and Gd-BOPTA (Multihance®, Bracco) at variable concentrations of Gd^{3+} (0, 10, 25, 50, 100 and 200 mM), approximately 50 µL of cell suspension was loaded into the micro-capillary channel and the channel was sealed with Critoseal. The cells were levitated in the magnetic levitation device for 10 min and imaged every 1 min under the inverted microscope (Olympus IX-83).

Levitation heights of cells (distance of cells from the bottom surface of micro-capillary channel) were measured with ImageJ Fiji software by performing threshold and particle analysis. In order to determine when cells reached to the equilibrium at a specific levitation height in different paramagnetic solutions, the time point that cells were approaching ± 5% of the levitation height reached at 10 min was considered as equilibrium time. The levitation heights of D1 ORL UVA^{eGFP} and MDA-MB-231^{dsRed}

cells in the medium containing 100 mM Gd-BT-DO3A were also measured by the same method.

3.2.4. Cell Viability Assay

D1 ORL UVA cells were seeded at a starting concentration of 10^4 cells/well in a 96-well plate and cultured for 48 h. The cells were exposed to different Gd-based solutions (Gd-BT-DO3A, Gd-DTPA, Gd-DTPA-BMA, Gd-DOTA and Gd-BOPTA) at variable concentrations of Gd^{3+} (0, 10, 25, 50, 100 and 200 mM) and cell viability was measured every 24 h for 3 d with thiazolyl blue tetrazolium bromide (MTT) assay. 0.5 mg/ml of MTT reagent (Amresco) was added to each well and the plates were incubated at 37 °C for 3 h in the dark. The media was removed, 100 µl of DMSO was subsequently added to each well and colorimetric measurements were performed at 570 nm with a reference wavelength of 690 nm (Thermo Scientific Multiskan Go). Furthermore, to evaluate whether stock concentration differences between commercial products (Gadavist®: 1000 mM; Magnevist®, Omniscan®, Dotarem® and Multihance®: 500 mM) had an effect on cell viability, D1 ORL UVA cells were exposed to the medium containing phosphate buffer solution (PBS), instead of the contrast agent, (0, 10, 20, 30, 40 and 50%; v/v) for 24, 48 and 72 h and cell viability was measured by MTT assay. 20% and 40% PBS containing medium represent the dilution at the highest tested agent concentration (200 mM) of Gd-BT-DO3A and other contrast agents, respectively.

3.2.5. Live/Dead Assay

D1 ORL UVA cells were seeded at a starting concentration of $4x10^4$ cells/well in a 24-well plate and cultured for 48 h. The cells were exposed for 72 h to Gd-BT-DO3A and Gd-DTPA-BMA at variable concentrations of Gd^{3+} (0, 10, 25, 50, 100 and 200 mM). Cell viability was assessed by live/dead assay (calcein-AM/propidium iodide, Sigma Aldrich).

The cells were stained for 15 min and imaged under the fluorescence microscope (Olympus IX-83). For the assessment of longer-term effect, the viability of cells exposed

to 100 mM Gd-BT-DO3A for 120 hours in 2D monolayer culture and 3D magnetic levitation cultures (5000 cells/channel) were also analyzed by the same method. For 3D clusters assembled during weightlessness, cells were both investigated as clusters and as dissociated single cells.

3.2.6. Levitation of Cells at Various Temperatures

D1 ORL UVA cells were centrifuged at 125 × g for 5 min and supernatant was discarded. The cells were resuspended to 10^5 cells/ml in the culture medium containing Gd-BT-DO3A (50, 100 and 200 mM concentrations of Gd^{3+}). The sample (≈ 50 µL) was loaded into the micro-capillary channel and the channel was sealed. The magnetic levitation system was then placed within a microscope observation chamber in which temperature could be adjusted. The cells were levitated at 28, 32 and 36 °C, allowed to reach equilibrium (≈ 3 min) at each temperature and imaged under the inverted microscope (Observer Z1, Zeiss). Levitation heights of cells (distance of cells from the bottom surface of channel) were measured with ImageJ Fiji software and normalized to levitation heights of cells with magnetic levitation with 50 mM Gd^{3+} at 28 °C.

3.2.7. Real-Time Assembly of Cells with Magnetic Levitation

D1 ORL UVA cells were detached by 0.25% trypsin, centrifuged at 125 × g for 5 min and medium was removed. The cells were resuspended to 10^5 cells/ml in the culture medium with 100 mM Gd-BT-DO3A, cell suspension (≈50 µL) was loaded into the channel and the channel was sealed. The cells were levitated in the magnetic levitation device for 10 h and imaged every 15 min under the inverted microscope (Olympus IX-83) in a tiled acquisition manner to obtain images of the entire viewable area of the channel.

3.2.8. Formation of 3D Cellular Clusters with Magnetic Levitation

D1 ORL UVA cells (10^5 cells/ml) were firstly levitated with 50 mM Gd-BT-DO3A, which appeared to be advantageous in terms of cell viability and sufficient levitation height of cells, and cultured in a humidified 37 °C incubator with 5% CO_2 over 72 h. However, due to the fact that some cell spheres collapsed and proliferated on the ground of the micro-capillary channel, the concentration of Gd^{3+} was increased to 100 mM for long-term culture of cells with magnetic levitation. Briefly, after trypsinization, D1 ORL UVA^{eGFP} cells were harvested and resuspended to 10^5 cells/ml (5000 cells/capillary), 10^6 cells/ml (50000 cells/capillary) and 10^7 cells/ml (500000 cells/capillary) in the culture medium with 100 mM Gd-BT-DO3A. The samples (≈50 µL) were loaded into the channel and the channel was sealed. The cells were cultured with magnetic levitation for 48 h at 37 °C and 5% CO_2 in a humidified atmosphere and imaged every 24 h under the inverted microscope (Olympus IX-83). The long self-assembled clusters (>2.07 mm) were imaged in a tiled manner to obtain images of the whole cluster. When the reflection was distorting the image on the channel, these were removed manually.

All geometric features of the self-assembled clusters were quantified with ImageJ Fiji. Threshold and particle analysis were performed to measure total area (A), perimeter (P) and position of the center of mass. Elongation was calculated the following equation: Elongation= $P^2 / (4\pi \times A)$. To quantitate positions of the clusters, the image of the same area, where the cluster was imaged, was captured by focusing on the magnets for each cluster and the position of the center of mass between magnets was determined by considering the top point of the bottom magnet=0, the bottom point of the top magnet=1. To calculate average thickness of the clusters, grid lines were added on the image to sample 5 points along the cluster (on the x-axis) at equal distance, the thickness values corresponding to these lines were measured ImageJ Fiji software using the “straight line” tool and averaged. The lengths of the clusters were measured as cluster's distance of the starting and ending points on the x-axis. The geometric features of MDA-MB-231^{dsRed} clusters (5000 cells/channel) were also measured by the same method.

3.2.9. Coculture Assembly with Magnetic Levitation

Coculture assembly of D1 ORL UVA^{eGFP} and MDA-MB-231^{dsRed} cells with magnetic levitation (100 mM Gd-BT-DO3A) was performed using different cell loading strategies; L1, L2 and L3.

In the strategy of L1, cell suspension containing both of D1 ORL UVA^{eGFP} and MDA-MB-231^{dsRed} cells (total ≈5000 or 50000 cells in ≈50 μL with 1:1 cell ratio) was loaded into the magnetic levitation system and these cells were cocultured with magnetic levitation for 28 h.

In L2, D1 ORL UVA^{eGFP} cells (total ≈2500 or 25000 cells in ≈25 μL) were cultured with magnetic for 24 h for single type cellular assembly. For coculture assembly, MDA-MB-231^{dsRed} cells (total ≈2500 or 25000 cells in ≈25 μL) were then added into the system and cultured for 4 h.

In L3, MDA-MB-231^{dsRed} cells were cultured with magnetic levitation for 24 h, D1 ORL UVA^{eGFP} cells were added into the system and cultured for 4 h using the same cell numbers and medium volumes as the L2 experiment. The cells in the magnetic levitation system were cultured in a humidified 37 °C incubator with 5% CO_2. The cellular clusters were imaged with the confocal (Leica DMi8) and fluorescence microscopy (Olympus IX-83).

3.2.10. Statistical Analysis

All experiments were repeated at least three times. Data are presented as mean ± standard deviation (SD). Coefficient of variation (CV%) was used as standard deviation / mean to reflect variability within and between experiments. Statistical significance was determined by Student's t-test (two-tail) or two-way analysis of variance (ANOVA) with Sidak post hoc correction, through GraphPad Prism version 6.0 (GraphPad Software). $P < 0.05$ was considered statistically significant.

3.3. Results

3.3.1. Short-Term Levitation of Cells with Different Gd-Based Solutions

In order to select the most appropriate media for cell culture during magnetic levitation, we used a custom made microfluidic levitation device (Figure 3.1a, Figure 3.2) to levitate D1 ORL UVA bone marrow mesenchymal stem cells with different Gd-based contrast agents; gadobutrol (Gd-BT-DO3A), gadopentetate dimeglumine (Gd-DTPA), gadodiamide (Gd-DTPA-BMA), gadoterate meglumine (Gd-DOTA) and gadobenate dimeglumine (Gd-BOPTA) at increasing concentrations (0, 10, 25, 50, 100 and 200 mM) and measured location of cells from bottom surface of capillary after 10 min of levitation to allow cells levitated at lower concentrations of Gd^{3+} to reach steady state (Figure 3.1a, b, d and Figure 3.3). Irrespective of the chemical composition of the Gd-based agent, increasing concentrations resulted in increased levitation height of cells. Levitation heights of cells at concentration of 100 mM solutions reached more than 80% of the cell heights observed at 200mM concentrations (86.4, 84.1, 87.1, 88.1 and 88.1% for Gd-BT-DO3A, Gd-DTPA, Gd-DTPA-BMA, Gd-DOTA and Gd-BOPTA, respectively). Furthermore, nonionic structure containing Gd-BT-DO3A and Gd-DTPA-BMA, provided higher levitation heights at Gd^{3+} concentrations of 100 and 200 mM than ionic structure containing ones (Gd-DTPA, Gd-DOTA and Gd-BOPTA). Levitation heights for non-ionic structure containing solutions were 15.87% ($p<0.0001$) and 15.95% ($p<0.0001$) higher compared to ionic structure containing solutions at 100mM and 200mM concentrations (Figure 3.1b). According to the coefficient of variation (CV%) of calculated cellular levitation (Figure 3.1c), increasing concentrations not only reduced CV% values, but also standard deviation of CV% values as well, showing a reduction in variability within- and between-experiments with increased concentrations. Furthermore, increased Gd concentrations allowed the cells to equilibrate faster in the levitation platform for all agents. All contrast agents, except for Gd-DOTA (equilibrium time: 3 min), immediately provided equilibrium of levitated cells at 200 mM. However, time of equilibrium was higher than 4 min at the concentration of 10 mM Gd^{3+} for all agents (Figure 3.4a-e).

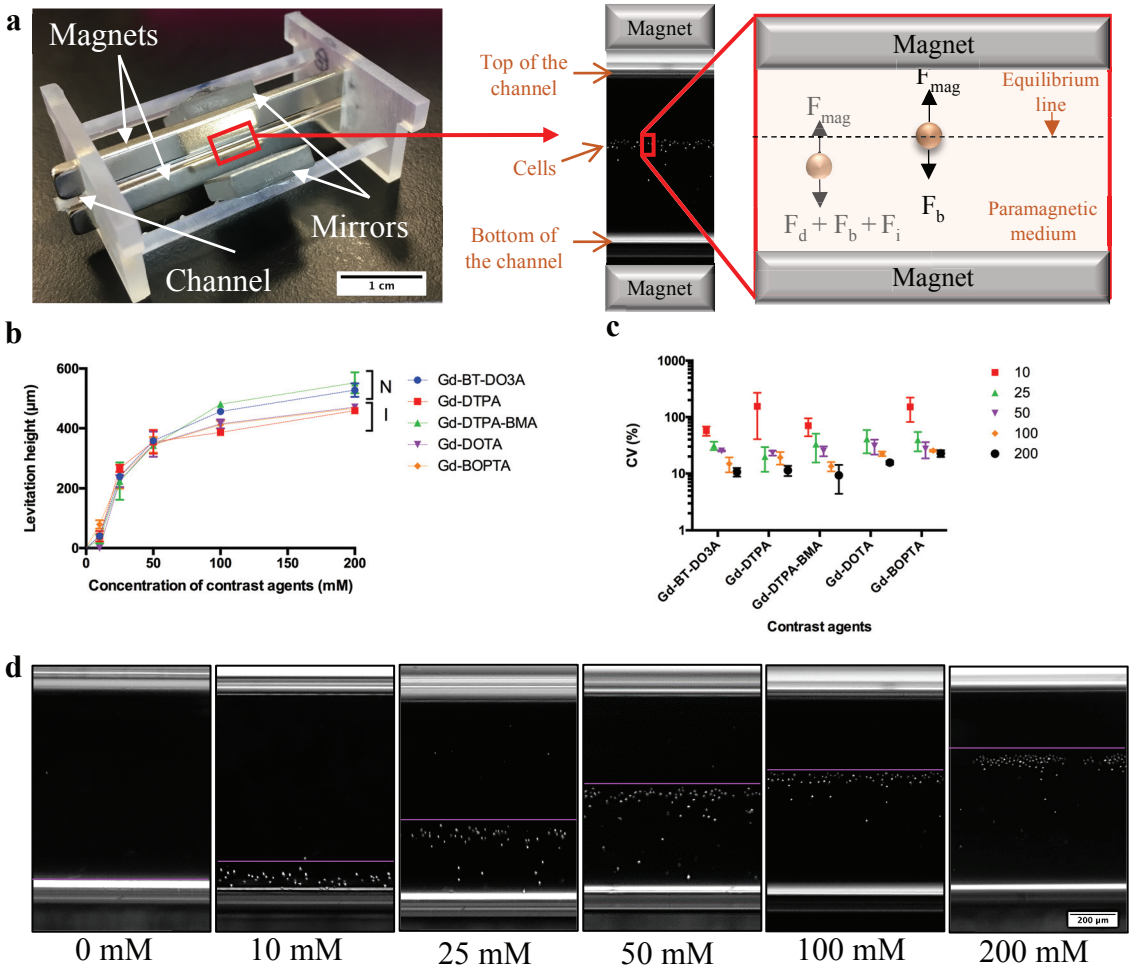

Figure 3.1. Photograph of magnetic levitation platform and forces which act on cells in it until equilibrium; fluidic drag force (F_d), inertial force (F_i), buoyancy force (F_b) and magnetic force, F_{mag}, and at the equilibrium position; F_{mag} and F_b. Microcapillary channel, in which cells are levitated and cultured, is placed between two permanent neodymium magnets whose same negative poles are facing each other. Mirrors are placed at each open side of the channel at 45° and used to visualize cells in the channel with conventional microscopy systems. (b,c) The relationship between Gd concentrations and, levitation heights of cells (from bottom surface of capillary) (b) and CV (%) of levitation heights (c) after 10 min of levitation in different Gd-based solutions (Gd-BT-DO3A, Gd-DTPA, Gd-DTPA-BMA, Gd-DOTA and Gd-BOPTA). Data are plotted as mean of replicates with error bars (±SD). N: nonionic agents, I: ionic agents. (d) Micrographs of levitated cells after 10 min of levitation in the medium containing Gd-BT-DO3A at variable concentrations (0, 10, 25, 50, 100 and 200 mM). The lines show the upper level of the levitated cell population. Scale bar: 200 μm.

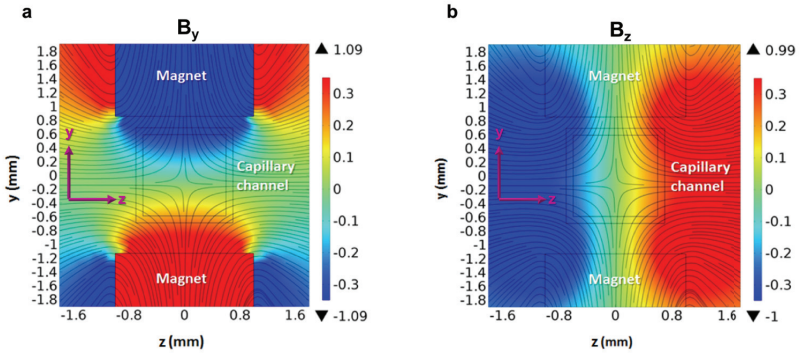

Figure 3.2. Simulation of (a) y component (B_y) and (b) z component (B_z) of magnetic induction (B) between two opposing magnets via Finite Element Methodology. Streamlines on the images represent total magnetic induction (B_y+B_z).

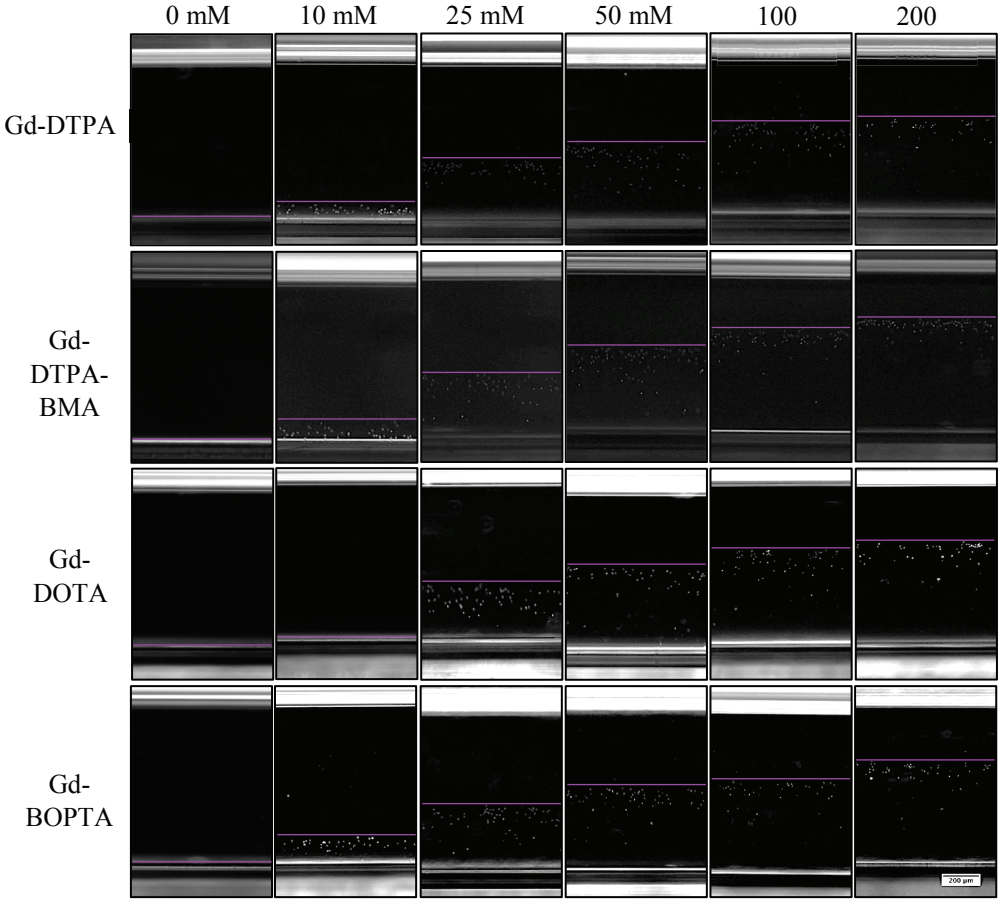

Figure 3.3. Micrographs of levitated D1 ORL UVA cells after 10 min of levitation in different Gd-based solutions (Gd-DTPA, Gd-DTPA-BMA, Gd-DOTA and Gd-BOPTA) at variable concentrations (0, 10, 25, 50, 100 and 200 mM). The lines show the upper level of the levitated cell population. Scale bar: 200 µm.

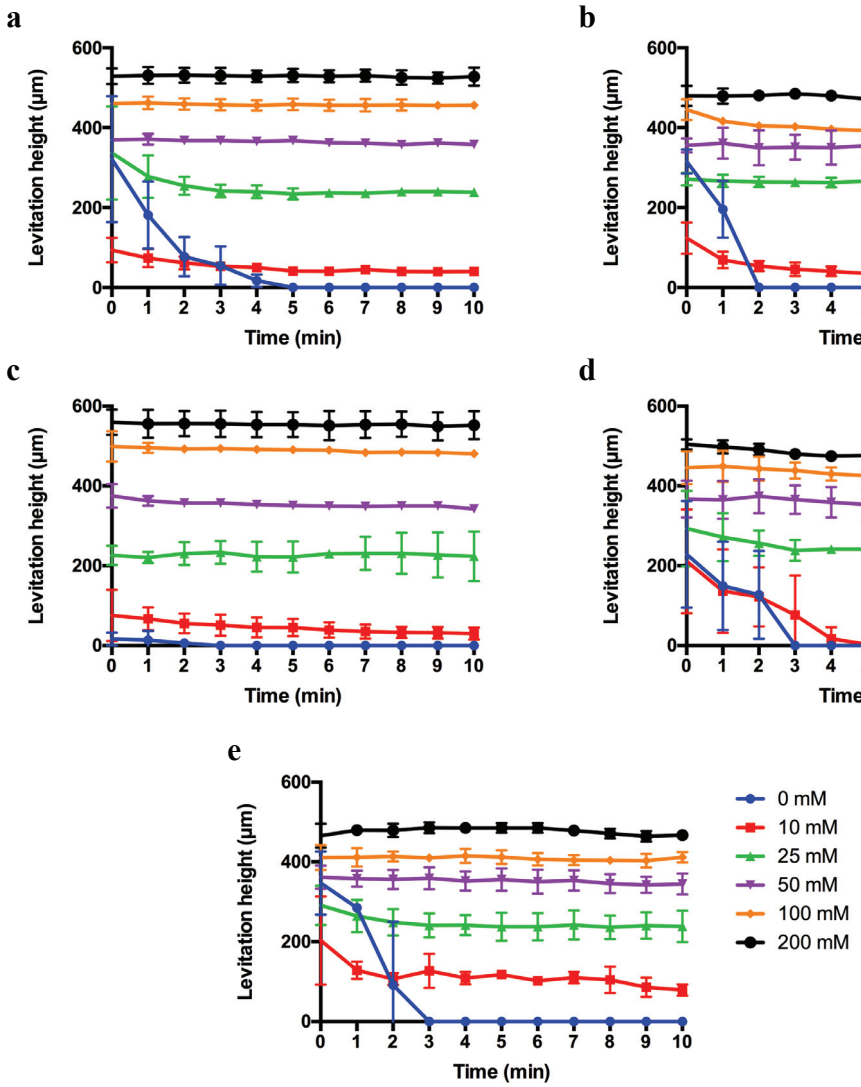

Figure 3.4. Time-dependent levitation heights of D1 ORL UVA cells (from bottom surface of capillary) levitated in different Gd-based solutions; (a) Gd-BT-DO3A, (b) Gd-DTPA, (c) Gd-DTPA-BMA, (d) Gd-DOTA and (e) Gd-BOPTA, at variable concentrations (0, 10, 25, 50, 100 and 200 mM) toward their equilibration point. Data are plotted as mean of replicates with error bars (± SD).

3.3.2. Long-Term Culture of Cells in Gd-based solutions

To quantify the impact of Gd-based solutions on cell viability for long-term culturing, we cultured D1 ORL UVA cells on plate with different paramagnetic medium at increasing concentrations (0, 10, 25, 50, 100 and 200 mM) and measured cell viability

by MTT assay (Figure 3.5a, b and Figure 3.6). Gd-DTPA, Gd-DTPA-BMA, Gd-DOTA and Gd-BOPTA led to massive cell death after 72 h of incubation at 200 mM concentration, whereas, Gd-BT-DO3A only prevented cell growth. For other concentrations, macrocyclic ligand containing Gd-BT-DO3A and Gd-DOTA provided higher cell viability compared to linear ligand containing solutions (Gd-DTPA, Gd-DTPA-BMA and Gd-BOPTA). Cells cultured with macrocyclic ligand containing solutions during 72 h had 70.3% ($p<0.0001$), 125.39% ($p<0.0001$), 160.25% ($p<0.0001$) and 219.94% ($p<0.0001$) higher cell viability than cells cultured with linear ligand containing solutions at 10 mM, 25 mM, 50 mM and 100 mM concentrations, respectively. Gd-DTPA-BMA, one of the two contrast agents providing high levels of levitation, inhibited cell growth even at low concentrations (25 mM), while Gd-BT-DO3A, showed a 27.92% increase in cell viability after 72 h of culture even at high concentration (100 mM).

The effects of these two contrast agents on cell viability were also assessed by live/dead assay (Figure 3.5c). Cells cultured with Gd-BT-DO3A including 100 mM for 72 h exhibited similar viability and confluency compared to the control group. For better display of dead cells, micrographs presented in Figure 3.5c were zoomed-in (Figure 3.7) showing that the ratio of dead cells in these concentrations were comparable with control culture. Consistent with MTT results, at the concentration of 200 mM Gd-BT-DO3A, non-uniform gaps began to form in the culture indicating cell loss. Culture with Gd-DTPA-BMA agent at concentrations of 50 mM and above resulted in almost complete cell loss, and the culture at 25 mM did not only lead to a decrease in cell confluency but also to increase in the size of the cells.

Commercial contrast agents added to the culture medium (Gd-BT-DO3A, Gd-DTPA, Gd-DTPA-BMA, Gd-DOTA and Gd-BOPTA) dilute the cell culture medium in varying proportions depending on stock concentrations of the commercial agents. Stock concentrations of the agents used in the study were 1000 mM (Gd-BT-DO3A) and 500 mM (Gd-DTPA, Gd-DTPA-BMA, Gd-DOTA and Gd-BOPTA) and for the highest concentration (200 mM), agents constituted 20% and 40% of the medium, respectively. In order to assess whether this product-related difference in dilution rate had an effect on cell viability, D1 ORL UVA cells were cultured in the medium containing PBS, instead of the contrast agent (0, 10, 20, 30, 40 and 50%; v/v) for 24, 48 and 72 h and cell viability was tested by MTT assay (Figure 3.8). There was no statistically significant difference between the viability of cells grown in 20% and 40% PBS containing medium, which

mimics the 200 mM agent concentrations, for 24 (P=0.27), 48 (0.14) and 72 h (P=0.08). Taken together, Gd-BT-DO3A was chosen for following magnetic levitation experiments due to providing both higher levitation height of cells and at least 43.9% higher cell viability than the other agents after 72 h of culture at all concentrations (except for Gd-DOTA).

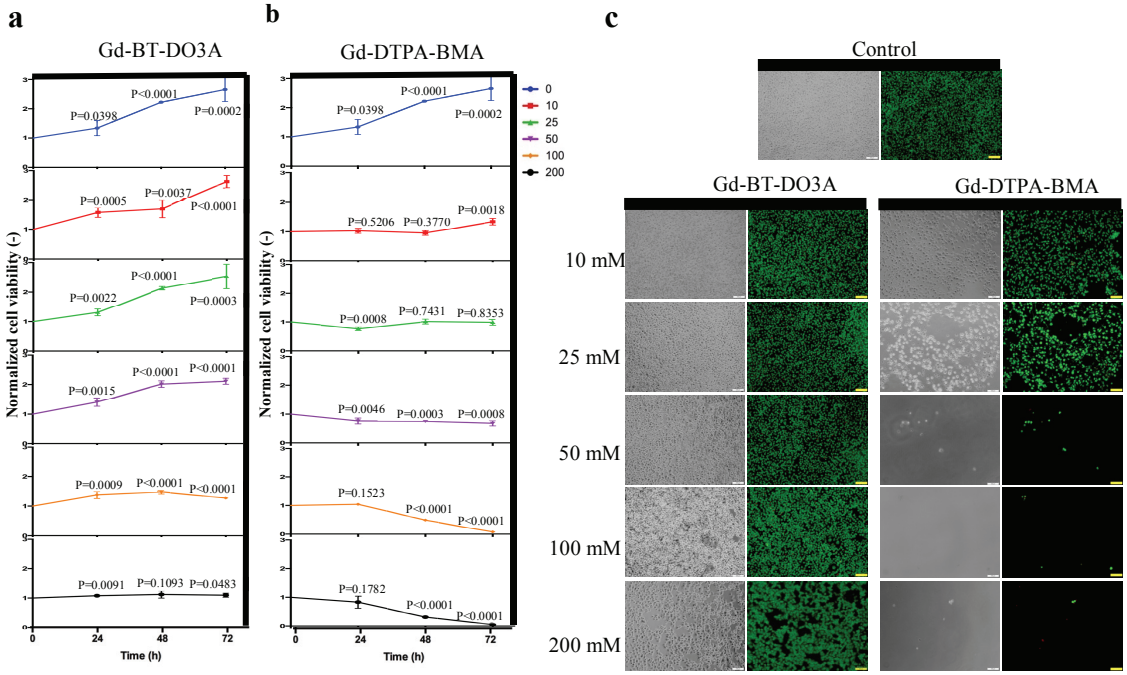

Figure 3.5. Long-term culture viability results of D1 ORL UVA cells. (a,b) Cell viability for long-term culturing with Gd-BT-DO3A and Gd-DTPA-BMA at increasing concentrations (0, 10, 25, 50, 100 and 200 mM), respectively. Cell viability was determined with MTT assay. Data are plotted as mean of replicates with error bars (±SD). Groups were evaluated using the unpaired Student's t-test. Statistical significance was defined as $P < 0.05$. (c) Fluorescent and phase-contrast microscopy images of D1 ORL UVA cells cultured for 72 h with 0, 10, 25, 50, 100 and 200 mM Gd-BT-DO3A and Gd-DTPA-BMA (live: green, dead: red). Cell viability was visualized by live-dead staining (Calcein/PI). Cells were cultured in the standard culture medium, as a control. Scale bars: 100 µm.

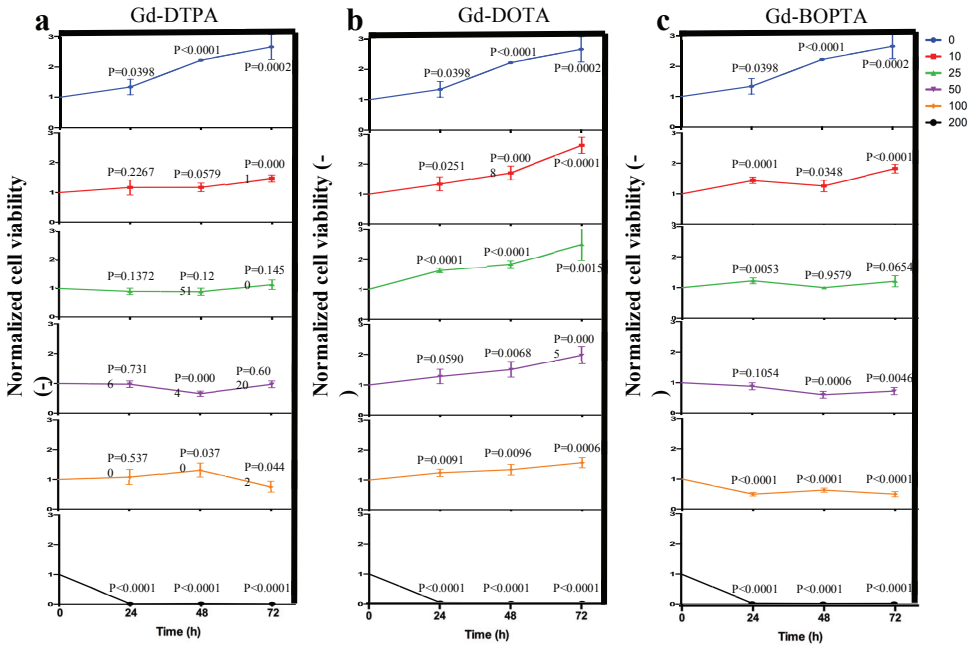

Figure 3.6. Cell viability was visualized by live-dead staining (Calcein/PI). Cells were cultured in the standard culture medium, as a control. Scale bars: 100 µm. Cell viability for long-term culturing with (a) Gd-DTPA, (b) Gd-DOTA and (c) Gd- BOPTA at increasing concentrations (0, 10, 25, 50, 100 and 200 mM). Cell viability was determined with MTT assay. Data are plotted as mean of replicates with error bars (± SD). Groups were evaluated using the unpaired Student's t-test. Statistical significance was defined as P<0.05.

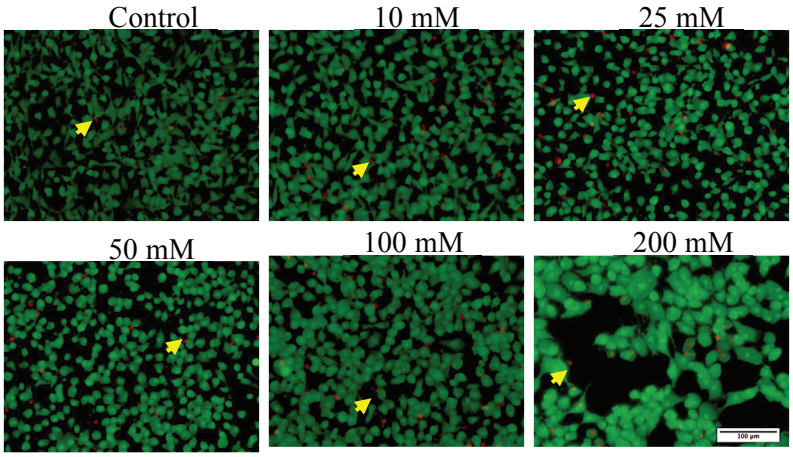

Figure 3.7. Zoomed-in depictions of the micrographs presented in Fig. 2c; D1 ORL UVA cells cultured for 72 h with 0, 10, 25, 50, 100 and 200 mM Gd-BT-DO3A (live: green, dead: red). The arrows indicate some of dead cells. Scale bar: 100 µm.

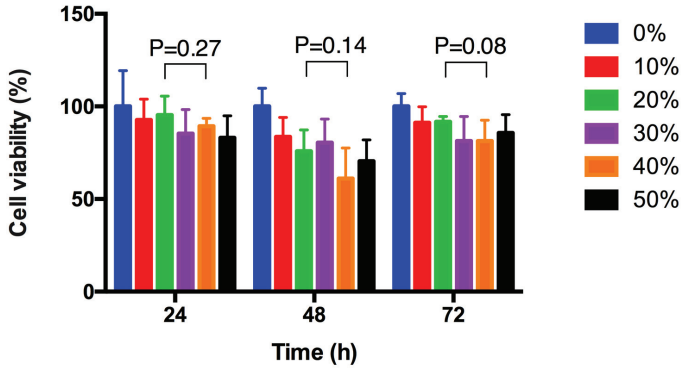

Figure 3.8. Cell viability of D1 ORL UVA cells cultured in 0, 10, 20, 30, 40 and 50% PBS (v/v) containing medium for 24, 48 and 72 h. Cell viability was determined with MTT assay. Data are plotted as mean of replicates with error bars (± SD). Groups were evaluated using the unpaired Student's t-test. Statistical significance was defined as $P<0.05$.

3.3.3. Self-guided 3D Cellular Assembly during Weightlessness

Before levitation of cells at the standard culture conditions (37 °C), D1 ORL UVA^{eGFP} cells were levitated at varying temperatures (28, 32 or 36 °C) with 50, 100, and 200 mM Gd-BT-DO3A solution and the levitation was examined after time of equilibrium (Figure 3.9). The results showed that cells reached similar equilibrium levels at all tested temperatures and Gd-BT-DO3A concentrations. Following the observation that slight temperature changes had no effect on cell levitation heights, cell culture studies were performed in the levitation device. Cells were first levitated and cultured for 72 h in the levitation system using 50 mM Gd-BT-DO3A concentration, which appeared to be advantageous in terms of cell viability and provided sufficient levitation height. Although the levitated cell spheres were observed after assembly, some cellular clusters collapsed and attached on the ground of the capillaries during culture time (Figure 3.10). We therefore increased Gd-BT-DO3A concentration to 100 mM for culturing, which was also suitable for cell viability and adequate cell levitation height.

First, to investigate whether 100 mM Gd-BT-DO3A exposure is suitable for longer-term cell culture with regard to cell viability, we exposed D1 ORL UVA cells to 100 mM Gd-BT-DO3A for 120 h in 2D culture (Figure 3.11a-d) and in 3D magnetic levitation (Figure 3.11e-j). In 2D culture, cells showed healthy morphology at 24th, 72nd

and 120th h of exposure (Figure 3.11a-c) and limited number of dead cells were observed after 120 h (Figure 3.11d). In 3D magnetic levitation, cells maintained their cluster shape at 24th, 72nd and 120th h of magnetic levitation (Figure 3.11e-g) and the clustered cells were viable after 120 h (Figure 3.11h, i). For a better observation of dead cells within the clusters, we dissociated clusters into single cell suspension with gentle pipetting for live/dead staining and consistently large majority of the cells were found to be viable (Figure 3.11j).

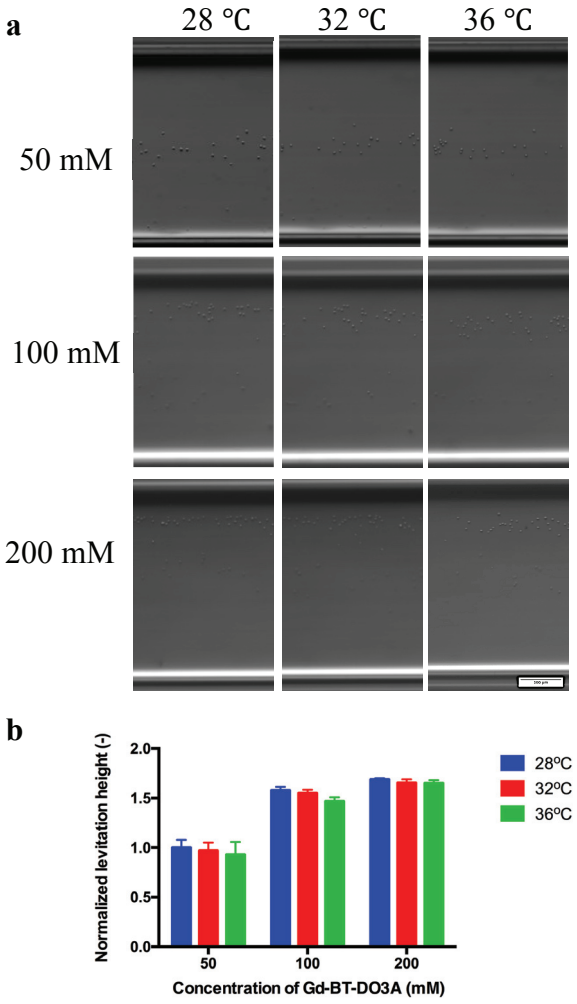

Figure 3.9. (a) Micrographs and (b) normalized levitation heights of levitated D1 ORL UVA cells at different Gd-BT-DO3A concentrations (50, 100 and 200 mM) after 3 min of levitation at 28, 32 or 36 °C. Data are plotted as mean of replicates with error bars (± SD) and statistically analyzed using a two-way ANOVA and Sidak posthoc test. Statistical significance was defined as $P<0.05$. Scale bar: 100 µm.

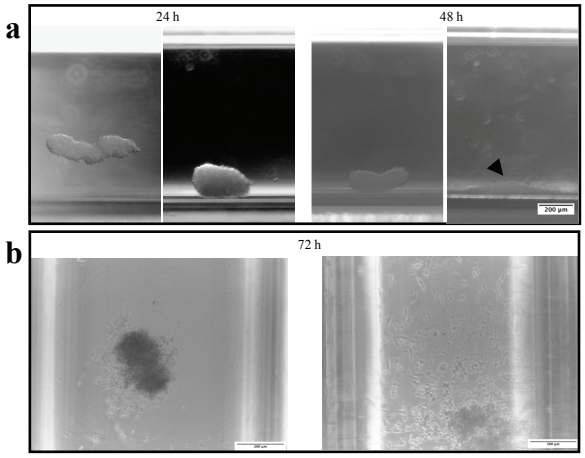

Figure 3. 10. Micrographs of levitated D1 ORL UVA cells at 50 mM concentration of Gd-BT- DO3A after (a) 24 and 48 h of levitation in horizontal direction (across the capillary height) and (b) after 72 h in vertical direction (on the bottom of the capillary) (Scale bars: 200 µm). The arrow indicates a collapsed cellular cluster.

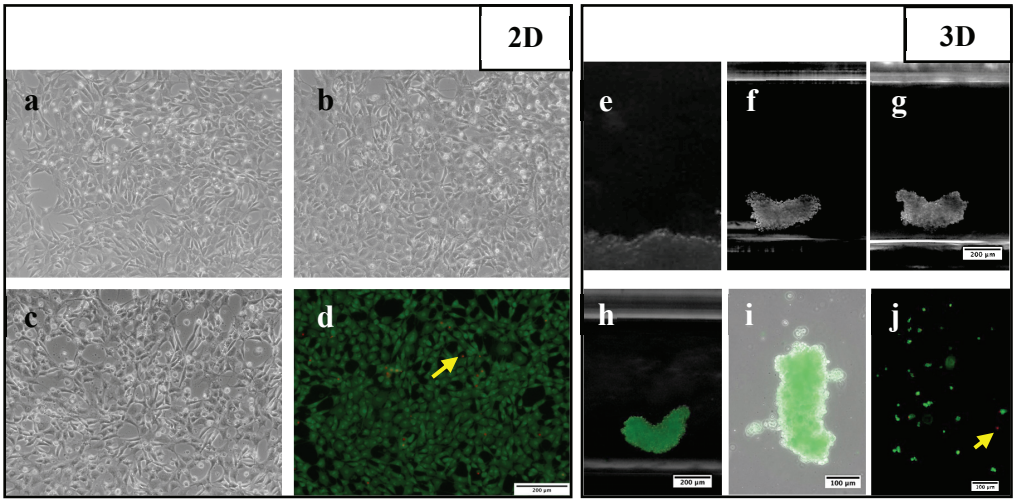

Figure 3.11. Micrographs of D1 ORL UVA cells exposed to 100 mM Gd-BT-DO3A in 2D culture for (a) 24, (b) 72 and (c) 120 h and live-dead image of cells after (d) 120 h. (Scale bar: 200 µm). Micrographs of levitated D1 ORL UVA cells at 100 mM Gd-BT-DO3A after (e) 24, (f) 72 and (g) 120 h (Scale bar: 200 µm). Calcein-AM staining of the D1 ORL UVA cluster assembled with magnetic levitation (100 mM, 120 h); (h) inside (Scale bar: 200 µm) and (i) outside the magnetic levitation device (Scale bar: 100 µm). j, Live/dead image of single cell suspension obtained from a cellular cluster assembled by magnetic levitation (100 mM, 120 h) (Scale bar: 100 µm). Cell viability was visualized by live-dead staining (Calcein/PI; live: green, dead: red). The arrows indicate dead cells.

Second, to investigate the effect of cell number increase on the morphology of cell clusters forming under microgravity condition; 5000, 50000 or 50000 D1 ORL UVA cells were levitated at 100 mM Gd-BT-DO3A, cultured in the levitation device for 48 h and resultant cluster morphologies were analyzed and all clusters in each experiment were averaged (Figure 3.12).

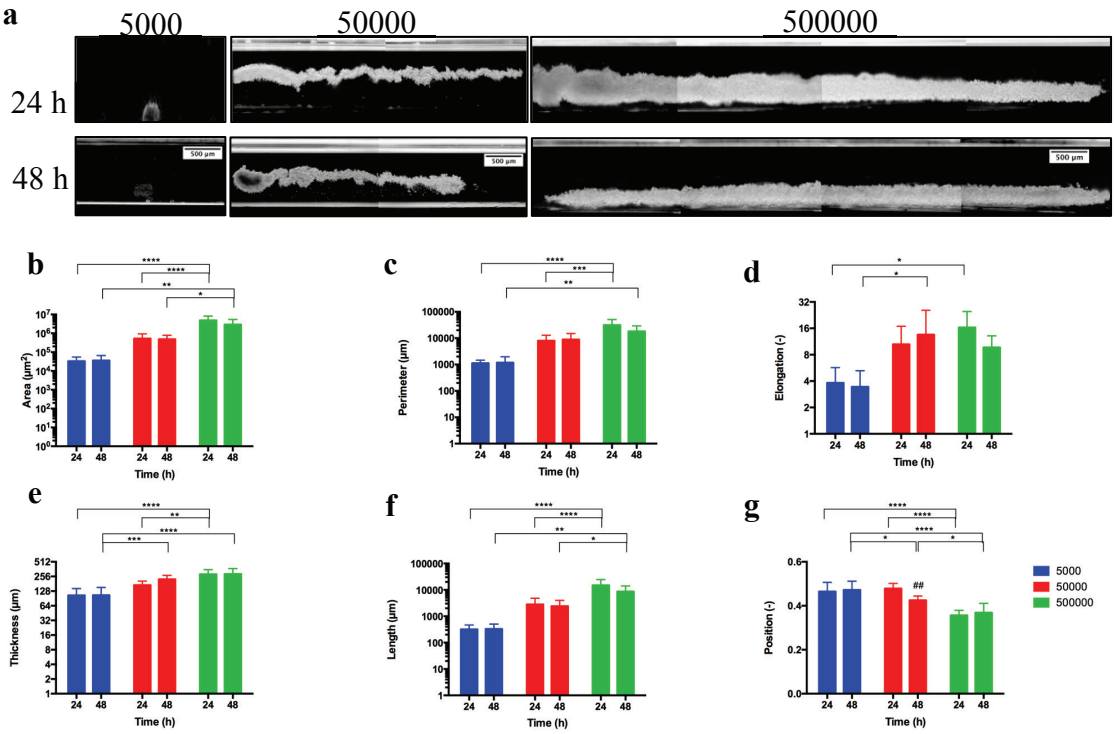

Figure 3.12. 3D cellular organization of D1 ORL UVA cells under microgravity. (a) Micrographs of cells levitated and assembled for 24 and 48 h (with 100 mM Gd-BT-DO3A) at different cell numbers (total 5000, 50000 and 500000 cells). Scale bars: 500 µm. (b–f) Quantitative description of the cellular clusters formed for 24 or 48 h with magnetic levitation (100 mM Gd-BT-DO3A) at different cell numbers (total 5000, 50000 and 500000 cells); (b) area, (c) perimeter, (d) elongation, (e) thickness and (f) length, and (g) position of the clusters between magnets (the top point of the bottom magnet:0, the bottom point of the top magnet: 1). Data are plotted as mean of replicates with error bars (±SD) and statistically analyzed using a two-way ANOVA and Sidak posthoc test. Statistical significance was defined as $P < 0.05$.

There was no statistical difference between the area, perimeter, elongation, thickness and length of the cellular constructs formed at the 24th hour of the culture, and at the 48th hour of the culture. However, as expected, the increase in the number of cells

led to an increase in these shape parameters (Figure 3.12a-f). The results showed that, when 500000 cells were seeded, the morphological parameters of cellular constructs at 24th hour increased by 87.6, 16.1, 2.5, 2.8 and 21.1-fold compared to 5000 cells for area, perimeter, elongation, thickness and length, respectively. This increase in the size of the structures occurred in the direction of the length rather than the thickness (9.9-fold higher increase), owing to the tendency of the cells to remain in the low magnetic field. The center of mass of the formed clusters was lowered as the number of cells increased, possibly due to the tighter clusters formed by cells (Figure 3.12g). Besides, to understand the formation of the stabilized cell clusters, which were observed after 24 h of the culture, the cultured cells were visualized during 10 h in the levitation device (Figure 3.13). In the first 5 h of the culture, cells apparently assemble into an unstable thin and long cluster and between 5-10 h they stabilize the structure by the shortening of cluster.

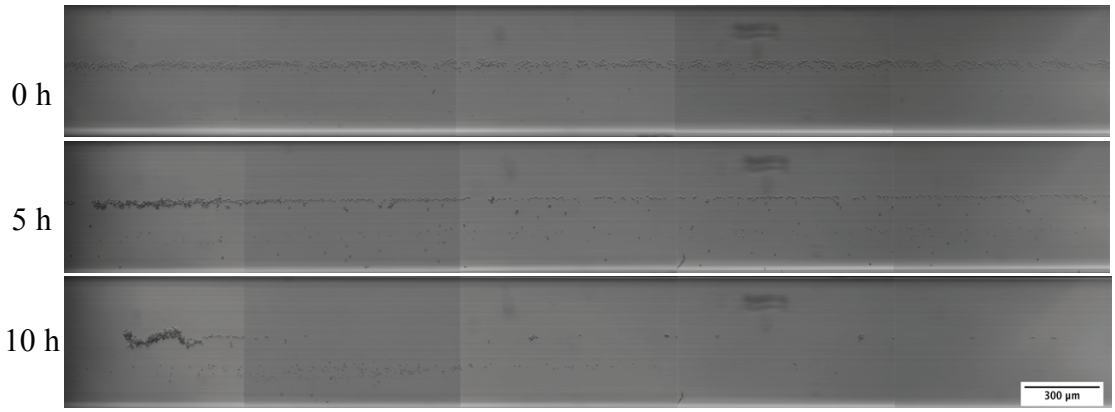

Figure 3.13. D1 ORL UVA cells (total 5000 cell) levitated for 5 and 10 h (with 100 mM Gd-BT-DO3A). Scale bar: 300 µm.

3.3.4. Biofabrication of Biphasic Assemblies during Weightlessness

To examine self-assembly of different cell types with different cell to cell adhesion characteristics during weightlessness and to form multiple assembly models with magnetic levitation, D1 ORL UVA^{eGFP} cells (bone marrow stem cell line), observed to be tightly packed in clusters in this study, were cultured with MDA-MB-231^{dsRed} cells (breast cancer cell line), forming only loose clusters [213]. Before assembly of the coculture, separate levitation characteristics height, assembly and morphology were observed for

D1 ORL UVA^{eGFP} and MDA-MB-231^{dsRed} cells induced with 100 mM Gd-BT-DO3A (Figure 3.14a, b). Levitation heights of D1 ORL UVA^{eGFP} and MDA-MB-231^{dsRed} cells were similar (P=0.9345). During culturing, MDA-MB-231^{dsRed} cells similarly reached to stable morphology and position in 24 h (Figure 3.14c-i). However, compared to D1 cells MDA-MB-231 clusters assembled at 24 h of the levitation culture had higher area, perimeter, elongation and length values (4.5, 4.6, 4.5 and 4.8-fold, respectively), suggesting loosely formed structures.

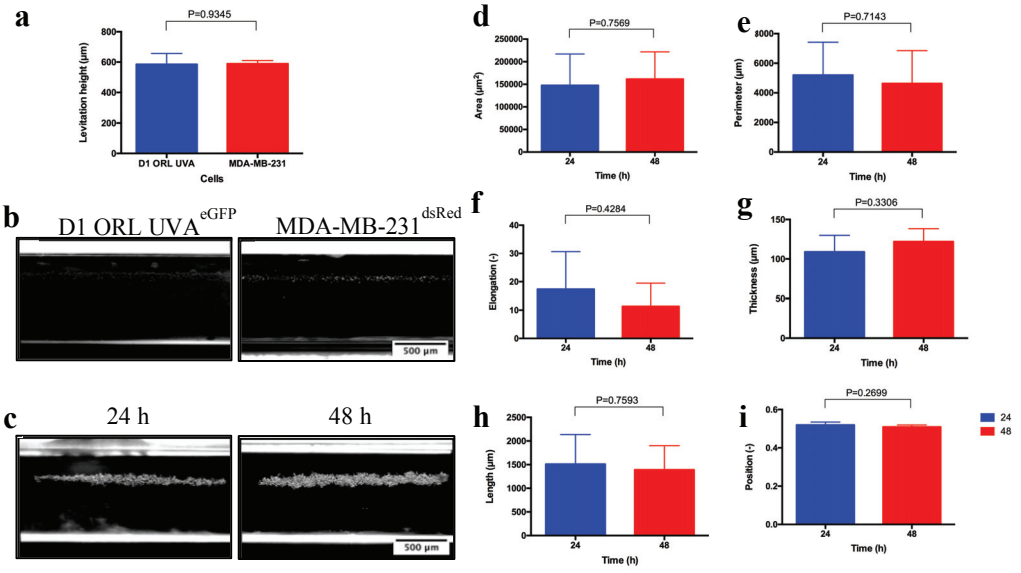

Figure 3.14. Levitation heights (from bottom surface of capillary) and (b) microscopy images of D1 ORL UVA^{eGFP} cells and MDA-MB-231^{dsRed} cells after time of equilibrium at 100 mM concentration of Gd-BT-DO3A (total 5000 cells). (c) Microscopy images of self-assembled MDA-MB- 231 clusters formed with magnetic levitation after 24 and 48 h of culture at 100 mM concentration of Gd-BT-DO3A (total 5000 cells). Scale bars: 500 µm. Quantitative description of MDA-MB-231^{dsRed} clusters formed for 24 or 48 h with magnetic levitation (100 mM Gd-BT-DO3A, total 5000 cells); (d) area, (e) perimeter, (f) elongation, (g) thickness and (h) length, and (i) position of the clusters between magnets (the top point of the bottom magnet:0, the bottom point of the top magnet:1). Data are plotted as mean of replicates with error bars (± SD). Groups were evaluated using the unpaired Student's t-test. Statistical significance was defined as $P<0.05$.

After examining separate assembly characteristics of both cell groups during weightlessness, biofabrication of biphasic assemblies was performed using different cell loading strategies with low and high cell density; **L1** (simultaneously loading of MDA

MB-231^{dsRed} and D1 ORL UVA^{eGFP} cells), **L2** (MDA-MB-231^{dsRed} cells onto D1 ORL UVA^{eGFP} self-assembled cluster) and **L3** (D1 ORL UVA^{eGFP} cells onto MDA-MB-231^{dsRed} clusters) (Figure 3.15). L1 assembly strategy produced assembled clusters with completely random positioning of cells (Figure 3.16). L2 loading strategy on the other hand resulted in sputtering of loose MDA-MB-231^{dsRed} cells on the surface of tightly formed D1 ORL UVA^{eGFP} cell clusters during weightlessness (Figure 3.17). Finally, L3 loading strategy caused periodic patterns showing D1 ORL UVA^{eGFP} integrating themselves into gaps within MDA-MB-231^{dsRed} clusters (Figure 3.18).

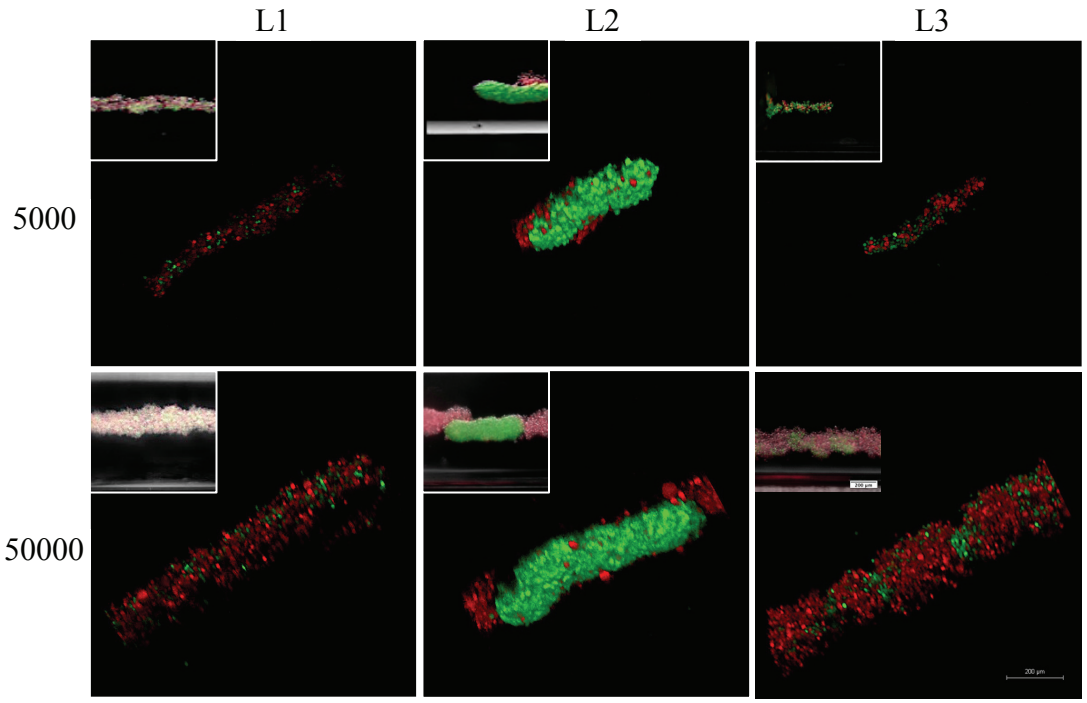

Figure 3.15. Levitation Cellular assembly of D1 ORL UVA^{eGFP} and MDA-MB-^{231dsRed} cells under microgravity. Confocal and conventional fluorescence microscopy (upper left) images showing self-assembled coculture clusters formed with magnetic levitation (100 mM Gd-BT-DO3A) and different cell loading strategies; L1: simultaneously loading of MDA-MB-231^{dsRed} and D1 ORL UVA^{eGFP} cells, L2: MDA-MB-231^{dsRed} cells onto D1 ORL UVA^{eGFP} clusters formed with magnetic levitation and L3: D1 ORL UVA^{eGFP} cells onto MDA-MB-231^{dsRed} clusters formed with magnetic levitation (total 5000 or 50000 cells). Scale bars: 200 µm.

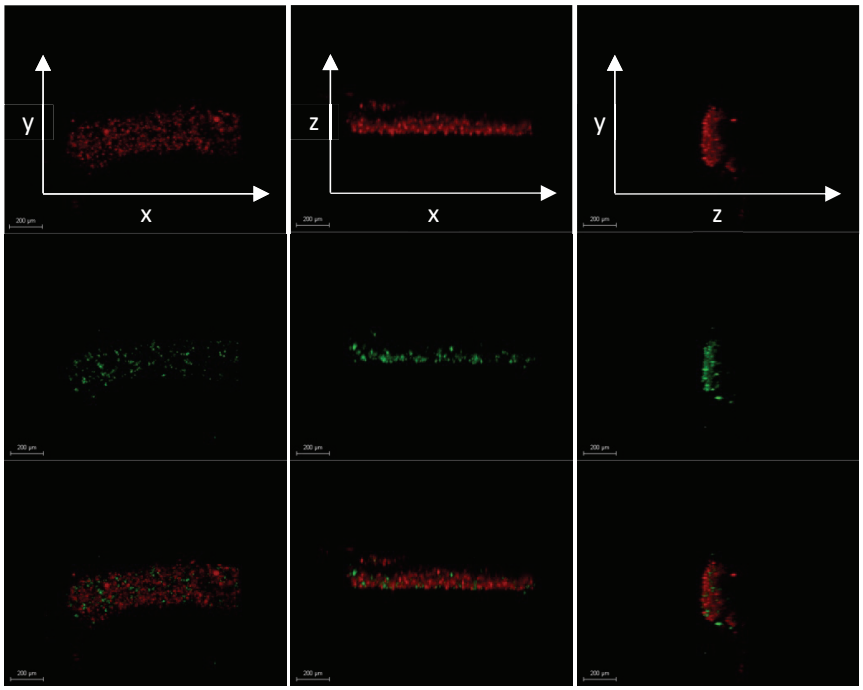

Figure 3.16. Micrographs showing cellular distribution of self-assembled clusters formed by L1 strategy. Green: D1 ORL UVA, Red: MDA-MB-231 (total 50000 cells with 1:1 cell ratio). Scale bar: 200 µm.

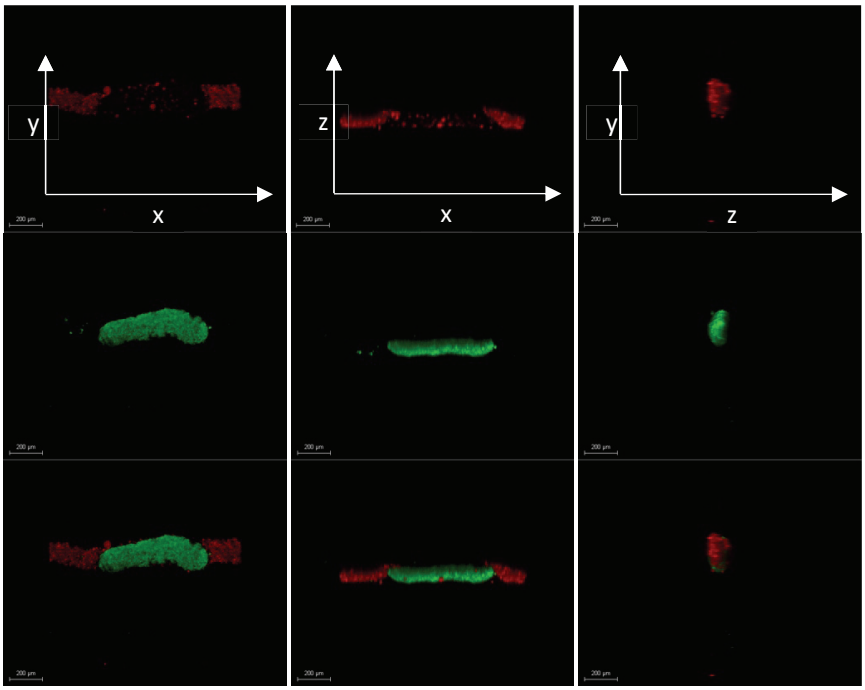

Figure 3.17. Micrographs showing cellular distribution of self-assembled clusters formed by L2 strategy. Green: D1 ORL UVA, Red: MDA-MB-231 (total 50000 cells with 1:1 cell ratio). Scale bar: 200 µm.

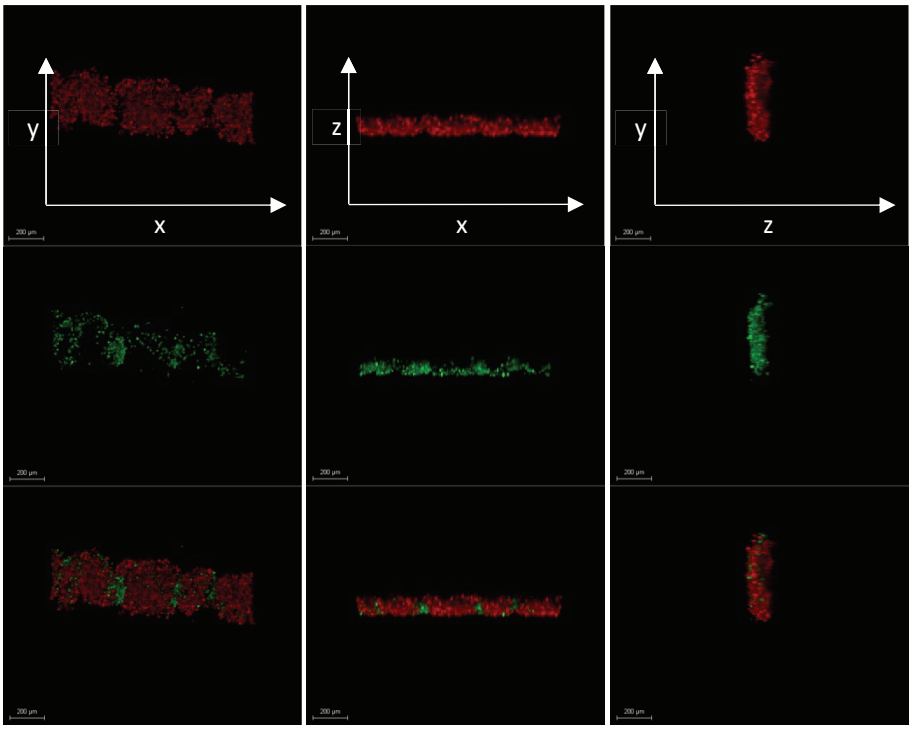

Figure 3.18. Micrographs showing cellular distribution of self-assembled clusters formed by L3 strategy. Green: D1 ORL UVA, Red: MDA-MB-231 (total 50000 cells with 1:1 cell ratio). Scale bar: 200 μm.

3.4. Discussion

We optimized a cellular magnetic levitation protocol by negative magnetophoresis suitable for long term cell culture and developed an *in situ* self-guided cellular assembly model during weightlessness. In summary, we first sought to determine commercially available chelate form and concentration of gadolinium that would be more appropriate to levitate and culture cells by considering viability and levitation position of the cells in the magnetic levitation system. Second, following the specification of the levitation protocol, we showed cellular dynamics and morphology of *in situ* assembly with varying cell numbers in the short and long term. Lastly, we directed biofabrication of various biphasic cellular organizations formed by coculturing cancer cells and stem cells in the levitation system. Provided that the Gd based magnetizing agent is quite stable [69] *in vitro* conditions, this strategy may be useful tool to study cellular and molecular level effects of microgravity on various models for future research.

Mechanical manipulation of cells in suspended culture via magnetic forces is relatively common in literature. By using magnetic beads, it is possible to manipulate cells through positive magnetophoresis [12, 214]. Cellular manipulation with positive magnetophoresis involves labeling cells with magnetic particles and then magnetizing these particles by applying an external magnetic field. This technology is enables the assembly of cells into 3D clusters scaffold free [215], and cells can even be organized into structures with a desired cellular pattern [216]. This approach is also useful in mechanobiology as it potentiates external application of mechanical forces on 3D cellular clusters in compressive [217] and tensile [218] modes. It is entirely possible to attach magnetic nanoparticles to extracellular area of the membrane to avoid toxicity [219]. However, magnetic levitation methodologies using positive magnetophoresis are not suitable to simulate exact weightlessness because of the heterogeneous force distribution on cellular structures. In contrast to these studies our aims to induce weightlessness on cells take advantage of the fact that cells and cellular sub-structures are diamagnetic in nature.

Diamagnetic properties of cells facilitate a repulsion by a force in the opposite direction of the applied magnetic field. This diamagnetic repulsive force on cells can be enhanced by suspending cells in a paramagnetic medium for a noticeable effect [29, 55]. In this study, we cultured cells in aqueous solutions containing Gd^{3+} with magnetic field gradient to create microgravity condition. However, free form of Gd^{3+} is toxic due to their size similar to Ca^{2+} which lead to competitive inhibition of cellular processes involving Ca^{2+} [65]. There are various commercially available forms of Gd^{3+} chelated with a ligand (linear or macrocyclic) to prevent direct toxicity of free ion. These contrast agents can be ionic or nonionic. We evaluated five different chelated form of gadolinium with regard to viability and levitation heights of cells. The results indicated that macrocyclic ligand containing agents (Gd-BT-DO3A and Gd-DOTA) provided higher cell viability compared to linear ligand containing ones, possibly due to their lower dissociation constants and higher chemical stability [68, 69]. Although the optimal chemical composition and concentration of Gd^{3+} have been established with regard to cell viability in this study, the presence of various cellular effects of Gd^{3+} depending on the concentration of Gd^{3+} and type of target cells [220, 221] appears to be a limitation of this strategy. Furthermore, we showed that Gd-based agents which do not dissociate into charged particles in solution caused higher levitation of cells and identified most appropriate paramagnetic medium composition to levitate D1 ORL UVA cells during long term culture. The Gd-BT-DO3A, determined to be most appropriate for magnetic levitation and long-term culture of cells

in this study, has also been preferred to magnetically manipulate cells in the other studies [17, 120, 211]. We have validated the method here by testing various chemical composition and concentration of Gd^{3+}. Another limitation to be taken into consideration is that the level of specific levitation to which cells are gathered may vary greatly for different cell types with different densities and the magnetic levitation strategy may not be suitable for each cell type combination when producing clusters comprising more than one cell type.

The principle of levitation through diamagnetophoresis with the use of Gd-based solutions, has previously been used for manipulation of cells [17, 211]. However, there is still an unmet need for the effect of Gd-based compositions on cell viability and levitation for long term culture. The effects of chemical composition and concentration of gadolinium ion-containing agents on cell viability and the levitation process, which have been investigated in the first part of this study, will be quite useful for further studies using the principle of levitation through diamagnetophoresis with paramagnetic solutions. Moreover, even though magnetic levitation principle has been used previously for the organization of suspended cells and previously clustered cellular blocks via a conventional method, separately [211], for the first time we showed that large cellular blocks (up to ≈2.68 cm in length) could be formed via magnetic levitation, and that cells were assembled to form first single cell type clusters and then to form coculture clusters in a single magnetic levitation device. Taken together, in this study a diamagnetic levitation strategy is presented as a fast and convenient method to simulate the microgravity condition and to examine its effects on 3D complex cellular organizations formed in the same device. The ground-based simulated microgravity strategy presents several advantages, such as: (1) more cost effective than other ground-based systems; (2) suitable for real-time imaging; (3) controllable cellular organization by changing magnetic field gradient pattern; (4) non-toxic to cells; and (5) easy to setup and use. The magnetic levitation-based multi-type cellular assembly strategy established here may allow for a wide range of biomedical studies that is not possible with space flight or other ground-based methodologies. This system is also suitable for automatization and operation-specific modification to be applied in several gravitational biology researches, particularly in mechanobiology.

CHAPTER 4

AXIAL-CIRCULAR MAGNETIC LEVITATION ASSISTED BIOFABRICATION AND MANIPULATION OF CELLULAR STRUCTURES

4.1. Background

4.1.1. Cell Magnetophoresis in Bioengineering Applications

Magnetic force-based manipulation of the living cells has emerged as a powerful tool for cellular and tissue level bioengineering applications [123, 222-224]. With the advances in technology and the improvements in design, magnetic manipulation systems with different complexity have been developed for various biotechnological goals including isolation and enrichment of rare cells [225, 226] and guiding cells into a particular spatial arrangement in 2 dimensional (2D) or 3 dimensional (3D) cultures [104, 106, 107]. Compared to the alternative operation principles such as electrical, optical and acoustic force-based techniques, magnetic manipulation offers various advantages such as minimal impact on cell viability, simple and low-cost design, and low sensitivity to environmental parameters such as ionic concentration and pH [227]. Cell magnetophoresis can be performed in two ways, either by manipulating the magnetic susceptibility of the cells or manipulating the magnetic susceptibility of the environment that cells are found [123, 222, 223]. Cells, that exhibit greater magnetic susceptibility than their surrounding buffer or medium due to labeling with magnetic particles or a rare intrinsic property of some cell types (i.e. paramagnetic hemoglobin containing blood cells and magnetotactic bacteria), move towards regions of the high magnetic field (positive magnetophoresis) [12]. However, most types of cells are intrinsically diamagnetic, and once placed into a surrounding environment with high magnetic susceptibility, they are repelled towards the minimal magnetic field in a magnetic field gradient (negative magnetophoresis, also referred to as diamagnetophoresis) [17, 70, 118, 159, 160, 167].

Stable cell trapping and self-assembly have been previously conducted by both positive and negative magnetophoresis to create viable 3D structures [128, 164, 228]. In positive magnetophoresis, it is possible to manipulate cells even with extremely small magnetic gradients using magnetic labels, allowing cell culture to reach high volume ratios up to several milliliters [156, 229]. However, this manipulation technique is challenging because magnetic labelling process is time-consuming and manually intensive [230] as well as prone to experimental variability based on variations in magnetic moments of beads [231] or cell labeling efficiency [232]. Thereby, there is an increasing demand for an alternative label-free technique.

4.1.2. Magnetic Levitation between Two Block Magnets

Negative magnetophoresis-based magnetic levitation of cells benefits from a label-free methodology. This approach was conventionally performed under a strong magnetic field generated by electromagnets due to the low magnetic susceptibility difference between the biological material and its surroundings [233]. As a simple and low-cost alternative, permanent magnets have been recently used to levitate diamagnetic objects in magnetic fluids that are paramagnetic salt solutions or ferrofluids under weak magnetic fields [125, 126, 223].

A magnetic levitation configuration was proposed to levitate diamagnetic objects based on their physical properties. This system levitates materials in paramagnetic solutions under a low magnetic field (<0.5 T) that is generated by two rectangular permanent magnets with the same poles facing each other [17, 64, 167]. However, this setup only allows biofabrication applications in microcapillaries, limiting working volumes for cells [128, 162, 164, 179]. Increasing the size of living structures is of prime importance for straightforward implementation of testing protocols by providing an adequate number of cells [234-236], and for the production of sizable tissue engineering constructs [237, 238].

A technique has been previously reported showing that large nonliving objects (9 mm in length) can be levitated between two square (5.0 x 5.0 x 2.5 cm) or disc (4.8 cm in diameter, 2.5 cm thick) permanent Neodymium (NdFeB) magnets larger than in microfluidic setups [239]. This technique has been then adapted to levitate millimeter-sized objects including living cell-laden beads and hydrogel units [120]. However, these

configurations require the assembly of 2 NdFeB magnet blocks that constantly exert opposing forces on the system that hinders the technological translation of these setups for long-term usage. Furthermore, opposing magnets constrains the physical boundaries of the setup, limiting the access to the media for proper cell manipulation.

4.1.3. Large-Scale Magnetic Levitation

Recently, a ring magnet-based magnetic levitation configuration has been demonstrated for the density-based characterization of nonliving objects [183]. This configuration is composed of a single ring magnet and a glass tube of a paramagnetic solution, that are placed coaxially to each other, to provide better visualization and manipulation than that of the two-magnet configurations. Further, levitation systems composed of a pair of ring magnets with the same-poles facing have been proposed to engineer a linear, axially symmetric magnetic field for levitation and density-based analysis of nonliving and living objects [240-242].

Another magnetic installation containing a glass cuvette placed on an axial hole of two upright ring-shaped neodymium magnets with like poles facing each other was used for magnetic levitation of pre-formed tissue spheroids in a paramagnetic medium [243]. Although these system designs allowed for a satisfying visualization of cell constructs, long-term culture of large living structures in a small culture volume, and performing routine cell culture operations such as media refreshment and recovery of samples, especially for mechanically unstable structures require additional considerations and remain untested.

Here, we showed the applicability of a one-step single ring magnet-based magnetic levitation design in formation and culture of 3D living structures. The system was shown to enable living cells to create large self-assembled 3D structures by preserving the cell viability and to allow mass transfers required for maintenance of the cell culture during magnetic levitation and combining biological units by levitation. We reported that the technique could be adapted for culture of several cell types and allowed transfer into intra-matrix culture. To the best of our knowledge, this is the first attempt to adapt a ring magnet-based magnetic levitation system for biofabrication of biological units and combining them.

4.2. Methods

4.2.1. Design of Magnetic Levitation System

Magnetic levitation system is composed of a ring high grade (N52) neodymium (NdFeB) magnet (1" od x 5/16" id x 1/4" thick, K&J Magnetics) and a cell culture tube positioned in hole of the magnet (Figure 1). The bottom of the cell culture chamber is attached to the hole of the ring magnet with glue pads or the chamber is fixed on the magnet with a scaled photoreactive resin piece (Clear v2 FLGPCL02) printed using 3D printer (Formlabs Form 2).

In the magnetic levitation system, gadolinium (Gd^{3+}) in the surrounding medium creates a difference ($\Delta_\chi = X_c - X_m$) between magnetic susceptibility of the medium (X_m) and cells' (X_c) to provide the levitation of cells where the magnetic force (F_{mag}) acting on cells and the force of gravity (F_g) balance each other. The magnetic forces directed to the centerline in the x-direction enables the cells to focus on the center for cellular aggregation.

4.2.2. Magnetic Levitation of Polymeric Beads

Polymer beads with densities of 1.02 g/mL (size: 10–20 μm) and 1.09 g/mL (size: 20–27 μm) (Cospheric LLC., ABD), were suspended in the cell culture medium containing 0, 100 and 200 mM Gd^{3+} (Gadavist®, Bayer). Polymer bead suspension was loaded to a micro-capillary channel (1 mm × 1 mm square cross-section, 50-mm length, Vitrocom) and the channel was positioned on surface of the ring magnet by passing it over the hole of the magnet. That is to say the surface plane of the ring magnet serves as a ground for the levitation process. Movement of the beads in the magnetic field gradient was visualized under a stereo microscope (Soif Optical Instruments).

4.2.3. Cell Culture

D1 ORL UVA (bone marrow stem cell line, American Type Culture Collection (ATCC)) and MDA-MB-231 (breast cancer cell line, ATCC) cells were cultured in DMEM (Gibco) supplemented with 10% fetal bovine serum (FBS) and 1% penicillin/streptomycin. 7F2 (mouse osteoblasts, ATCC) were cultured in alpha modified essential medium (αMEM) supplemented with 10% FBS and 1% penicillin/streptomycin. The cells were grown in a humidified 37°C incubator with 5% CO_2. The growth medium was refreshed every other day and the cells were passaged every four to six days.

For adipogenic induction, 7F2 cells were exposed to induction medium composed of 5 µg/mL insulin, 10 nM dexamethasone and 50 mM indomethacin for 7 days. The induction medium was refreshed every other day. The cells were observed under an inverted microscope (Olympus IX-83).

4.2.4. Levitation of Living Cells

The cells were detached with 0.25% trypsin-EDTA when the culture reached near confluency. Following centrifugation and removal of the supernatant, the cells were resuspended to 10^6 cells/mL in the culture medium with various Gd^{3+} concentrations (50 mM, 100 mM, 150 mM, and 200 mM). 200 µL of cell suspension was loaded into the cell culture tube unless otherwise noted, and the culture tube was placed in the hole of the ring magnet.

The cells were levitated in the magnetic levitation system for 24 h and imaged by a mobile phone equipped with a 15X micro focal length lens (Baseus) for short distance focusing. Horizontal diameter, vertical diameter, area and perimeter of the self-assembled clusters were measured with the ImageJ Fiji software.

4.2.5. Visualization of Trapping Region for Cellular Cluster in the Magnetic Levitation System

D1 ORL UVA cells were resuspended to 10^6 cells/mL in the culture medium with 200 mM Gd^{3+} and 100 µL of cell suspension was loaded into the cell culture chamber. Self-assembled cellular cluster after 48 h of levitation was moved upward and downward with the culture chamber to visualize cell trapping region in the vertical plane. For visualization of trapping region in the horizontal plane, the cell culture chamber was positioned horizontally on the ring magnet and moved parallel to the magnet surface until it passed the region where the movement of the cellular cluster was restricted. The motion of the cellular cluster was recorded by a mobile phone equipped with a 15X micro focal length lens.

4.2.6. Modification of the Medium and Magnetic Field

Ficoll® PM 400 (Sigma-Aldrich) was added to the culture medium to adjust the density of the medium to 1.02 and 1.04 g/mL. D1 ORL UVA cells (10^6 cells/mL) were suspended in the denser culture media with 0 or 100 mM Gd^{3+}. Levitation of cells in 200 µL were observed after 24 h of culture.

In order to further increase the magnetic susceptibility of the medium and thus the magnetic force on cells, levitation culture of D1 ORL UVA cells (10^6 cells/mL) was performed with increasing concentrations of Gd^{3+}; 0, 200, 350 and 500 mM. Levitation and aggregation of cells were observed within 5 h.

Two magnets have been attached with their opposite poles facing to strengthen the magnetic field in the levitation system. D1 ORL UVA cells were suspended in paramagnetic medium (150 or 200 mM Gd^{3+}) at a concentration of 10^6 cells/mL and levitated on holes of 1 ring magnet or 2 ring magnets whose opposite poles attached to each other. 200 µL of suspension was placed on levitation systems and cultures were observed after 2, 24 and 48 h.

4.2.7. Transfer of Cellular Cluster and Culture Medium in Magnetic Levitation System

D1 ORL UVA cells were suspended in paramagnetic medium at a final concentration of 10^6 cells/mL and 200 µL of cell suspension was cultured in magnetic levitation system for 48 h. To refresh the medium, old medium was removed with a pipette and fresh paramagnetic medium was slowly added to the culture.

To show the transfer of the resultant 3D culture, self-assembled compact clusters were harvested from the levitation culture without dispersion with a 1000 µL pipette tip. Harvested clusters were transferred to another levitation culture without dispersion with a 1000 µL pipette tip. All of the operations were recorded by a mobile phone equipped with a 15X micro focal length lens.

For culture maintenance of cellular cluster formed with magnetic levitation system in culture dish, D1 ORL UVA cells (10^6 cells/mL) were levitated in 200 mM Gd^{3+} containing paramagnetic medium for 48 h and transferred to a culture dish with Gd-free medium. The culture was maintained for 24 h for observation.

4.2.8. Live/Dead Assay

D1 ORL UVA cells were suspended in 200 mM Gd^{3+} containing paramagnetic medium and assembled in the magnetic levitation system. The levitation culture was maintained for 48 h before cell viability test. For viability test of the adipogenesis induced 3D structures, adipogenesis induced 7F2 cell were assembled in the magnetic levitation system for 24 h, then transferred to a culture plate and cultured for another 24 h. The viability of cells was assessed using live/dead assay (calcein-AM/propidium iodide, Sigma Aldrich) according to the manufacturer's protocol. The cells were stained for 15 min at 37°C. Images were acquired using a fluorescence microscope (Olympus IX-83). The cells were both investigated as 3D cluster form and as dissociated single cells.

4.2.9. Co-levitation Culture

D1 ORL UVA cells were assembled and maintained during levitation by ring magnet-based magnetic levitation system for 48 h. The self-assembled spheres were transferred one by one to the ring magnet-based magnetic levitation system to a medium containing 200 mM Gd^{3+} in magnetic levitation system using a micropipette for co-levitation culture. Transfer of the clusters into the co-levitation culture was recorded by a mobile phone. For the co-levitation of 3D clusters consisting of lipid accumulated 7F2 cells, adipogenesis-induced cells were levitated in Gd^{3+}-containing media at increasing concentrations (100, 150 and 200 mM) for 24 h, and the clusters were co-levitated in the same Gd-content medium in duplicate. Following a 24-h co-levitation cultures, the 3D structures were transferred to the cell culture petri dish and observed under an inverted microscope (Olympus IX-83). Merged areas of each pair of spheres (%) were measured with ImageJ Fiji software by thresholding, followed by, shape completion and particle analysis.

4.2.10. Embedding the 3D Structures within the Gel Matrix

D1 ORL UVA cells were suspended in 200 mM Gd^{3+} containing medium and assembled in the magnetic levitation system for 24 h. At the end of the 24 h of the culture, the medium was aspirated until only 20 µL remained in the culture dish for maintenance of the levitation. Matrigel (BD Biosciences) with five times the volume of the remaining medium, was slowly added to the culture at +4°C and the culture was kept in a humidified 37°C incubator for 3 h. After the Matrigel polymerized, the 3D cell structure in the gel was transferred to a culture plate with the help of a pipette tip, which was cut on one side and turned into a micro spoon. Embedding the 3D structures within Matrigel and transfer of the clusters in Matrigel were recorded by a mobile phone. The medium was added onto the 3D structure embedded in Matrigel in culture dish and cultured for 4 days.

4.2.11. Statistical Analysis

All experiments were repeated at least three times. Results are reported as mean ± standard deviation (SD). Statistical analyses were performed using Student's t-test (two-tail) or two-way analysis of variance (ANOVA) with Sidak post hoc correction, with GraphPad Prism version 6.0 (GraphPad Software). A p-value of < 5% was considered significant.

4.3. Results

4.3.1. Self-assembly of Living Cells in Ring Magnet-Based Magnetic Levitation

A magnetic levitation system composed of a NdFeB (grade N52) ring magnet and a cell culture chamber was designed for levitation and self-assembly of cells (Figure 4.1a-e). In the system, it is expected that the cells are pushed towards the magnetic field minima formed on the hole of the ring magnet, and the levitated cells in this region form cellular clusters by self-assembly of the cells over time. First, we demonstrated that the system enabled levitation for the density range of the cells, 1.02-1.9 g / mL, and that the cells were localized at 0.3-1.7 mm distance from the magnet surface that was inversely proportional to their density based on the computational simulation (Figure 4.1e).

In order to demonstrate the applicability of the ring magnet system for the levitation of living cells, polymeric beads with a density of 1.02 and 1.09 g/mL, representing the density of less dense and dense living cells [17, 118], respectively were suspended in paramagnetic solution containing Gd^{3+} (100 and 200 mM), and their movements on the ring magnet were monitored (Figure 4.2). Polymeric beads with a density of 1.02 g/mL were levitated in paramagnetic media containing both 100 and 200 mM Gd^{3+}, while denser particles (1.09 g/mL) were levitated in the medium containing 200 mM Gd^{3+}, as they showed sedimentation at 100 mM Gd^{3+} concentration.

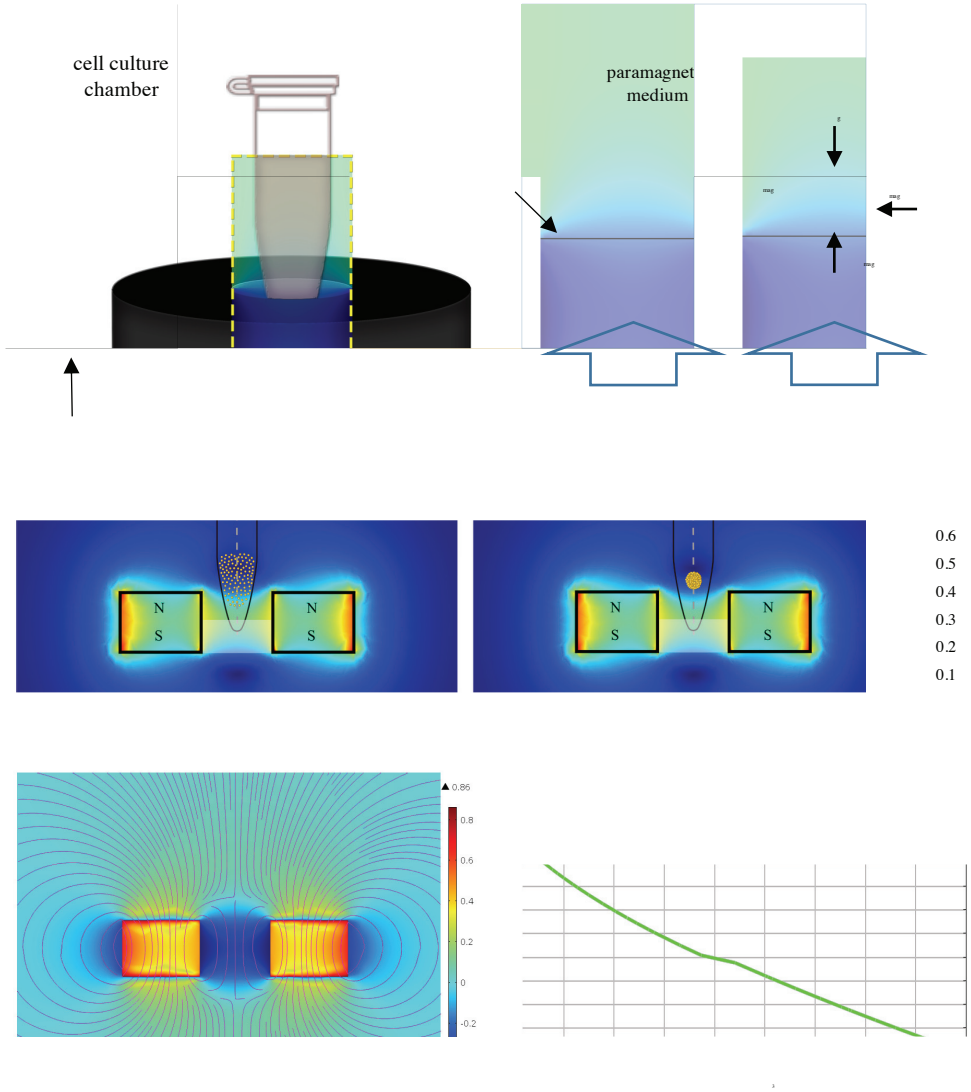

Figure 4.1. Magnetic force guided levitation and self-assembly. (a) Illustration of magnetic levitation system. Cell culture chamber is positioned on the ring magnet with bottom of the chamber attached to hole of the magnet. (b) Schematic representation of the cellular aggregation. The block arrows in the illustration represent upward magnetic induction. (c) Cellular aggregation represented on the simulation of magnetic flux density norm around the ring magnet. (d) Simulation of z component (B_z) of magnetic flux density around the ring magnet via Finite Element Methodology. Total magnetic induction (B_z+B_x) is presented as streamlines. (e) Modeled relationship between the cell density and levitation heights for 200 mM concentration of Gd^{3+} based on the computational model. Level of the magnet surface is considered as z = 0. Density of cells as a function of their lipid content determines levitation height, and while less dense adipocytes are positioned at a higher level denser cells are positioned lower.

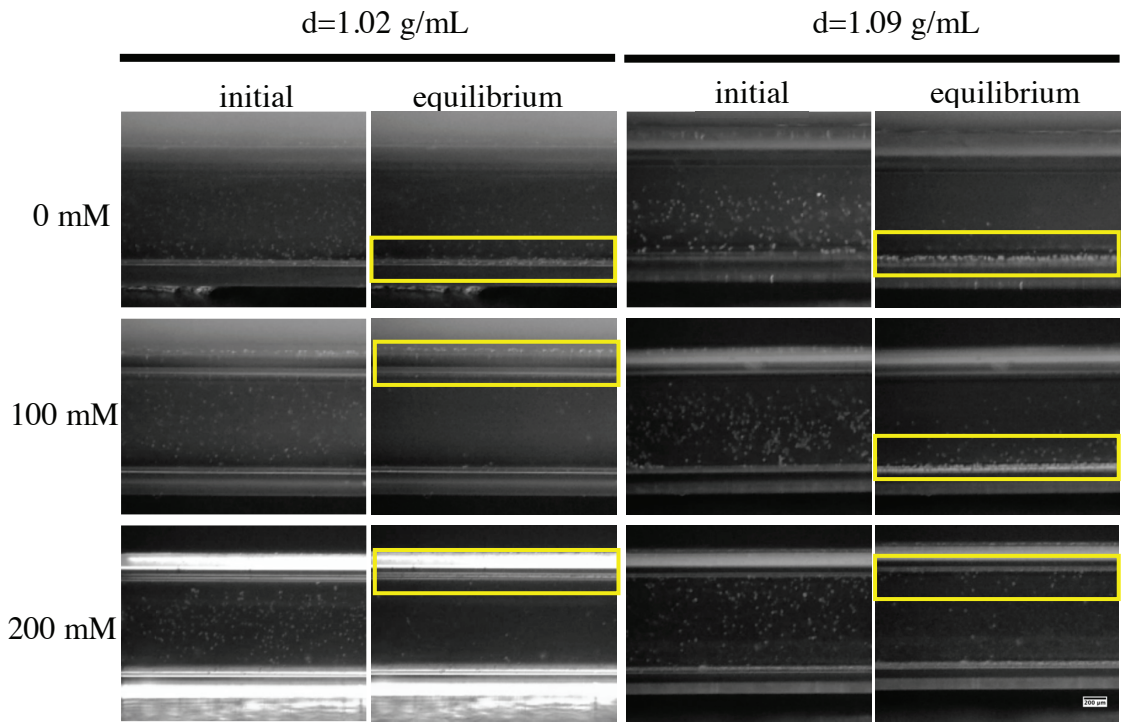

Figure 4.2. Micrographs of polymeric beads with density of 1.02 and 1.09 g/mL suspended in the culture medium with various Gd^{3+} concentrations (0, 100 and 200 mM) on the hole of ring magnet. The first micrographs were recorded at the beginning of the levitation process, and the second micrographs were recorded when the beads reached equilibrium position in the system (within 7 min). Yellow rectangles show the region where the cells were collected. Scale bar: 200 µm.

After demonstrating that the system was able to provide levitation of particles with a density close to that of living cells, D1 ORL UVA cells were suspended in medium with increased concentrations of Gd^{3+} (0, 50, 100 and 200 mM) and cultured in the levitation system for 24 h (Figure 4.3). In the control group without Gd^{3+} all of the cells settled on the floor of the chamber without levitation. In the paramagnetic medium containing 50 mM Gd^{3+}, no cellular aggregates were formed. During the first 2 h of culture, the beginning of the cell clustering process in the paramagnetic medium with 100 and 200 mM Gd^{3+} concentrations were observable above the hole of the ring magnet, towards the center of the hole with the naked eye as cloudy aggregation of cells, and after 24 h, compact 3D structures were formed in these groups. While the majority of cells suspended in 100 mM could not be levitated in the system and sedimented to the bottom, cells suspended in 200 mM formed large 3D self-assembled clusters with levitation (Figure 4.3a red circles). The average horizontal diameter of cell clusters formed in

medium with 200 mM Gd^{3+} was 867.33 ± 94.93 µm and approximately 1.7 times its vertical diameter. Cross-sectional area and perimeter of these clusters were measured as 0.39 ± 0.05 mm^2 and 3.52 ± 0.36 mm, respectively (Figure 4.3b).

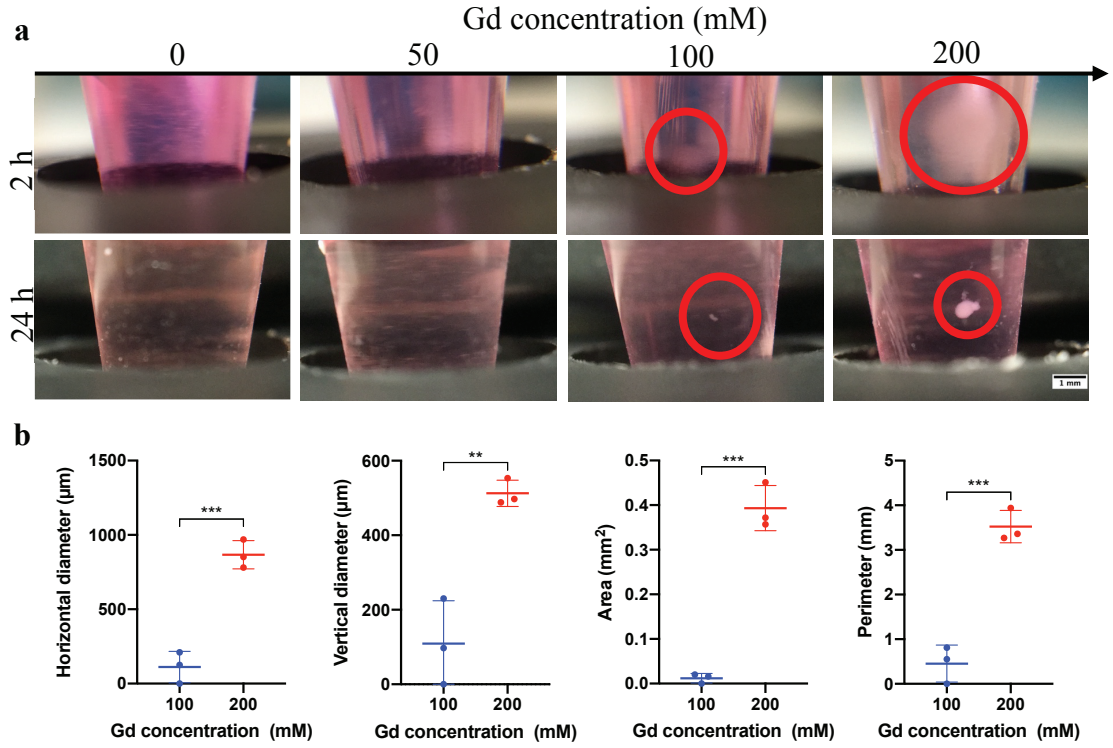

Figure 4.3. Self-assembly of D1 ORL UVA cells in ring magnet-based magnetic levitation system. (a) Micrographs of D1 ORL UVA cells cultured with ring magnet-based magnetic levitation (0, 50, 100 and 200 mM Gd^{3+}, 10^6 cells/mL, 100 µL) after 2 or 24 h of culture. Scale bar: 1 mm. (b) Size of the cellular clusters formed for 24 h with magnetic levitation (100 and 200 mM Gd^{3+}, 10^6 cells/mL, 100 µL); horizontal diameter, vertical diameter, area and perimeter. Data are plotted as mean of replicates with error bars (±SD) and statistical significance was determined by Student's t-test (two-tail). **: $p < 0.01$; ***: $p < 0.001$.

Next, magnetic levitation culture was performed by manipulating the culture medium properties and the magnetic field. In order to reduce the gravitational force acting on the cells and therefore to reduce the magnetic susceptibility required to provide levitation of cells, the density of the medium was increased by adding Ficoll to the culture medium, and D1 ORL UVA cells were levitated in these denser media (Figure 4.4). When the density of the culture medium was increased to 1.02 g/mL, the medium containing

100 mM Gd^{3+} concentration levitated most cells, unlike 1 g/mL medium (control group). Measured horizontal diameter, vertical diameter, area and perimeter of cellular structures formed in medium with 1.02 g/mL density were 1005.33 ± 123.29 µm, 712 ± 54.03 µm, 0.70 ± 0.13 mm^2 and 4.15 ± 1.09 mm, respectively. Moreover, horizontal diameter ($p = 0.73$), vertical diameter ($p = 0.67$), area ($p = 0.24$) and perimeter ($p = 0.82$) of cellular structures formed in medium with 1.02 g/mL density were statistically similar to structures observed with 1 g/mL medium with 200 mM Gd^{3+} concentration. Further increase in the medium density to 1.04 g/mL did not result in observable cluster formation.

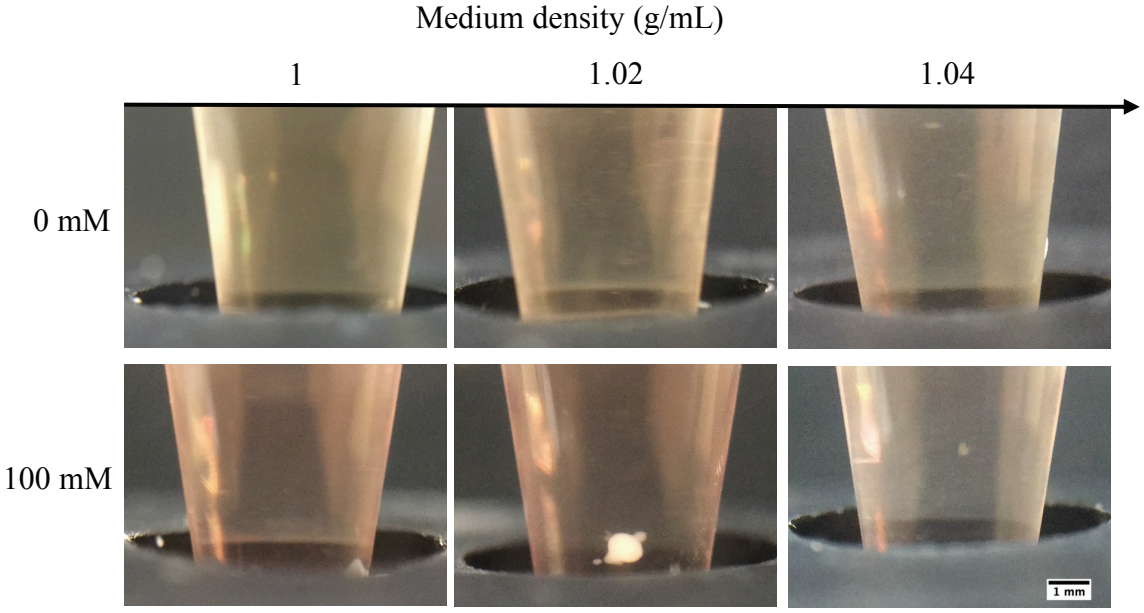

Figure 4.4. Micrographs of D1 ORL UVA cells levitated in culture medium with densities of 1 (without Ficoll), 1.02 and 1.04 g/mL with ring magnet-based magnetic levitation (0 and 100 Gd^{3+}) after 24 h of culture. Scale bar: 1 mm.

To test whether rising the magnetic susceptibility of the medium increased the formation rate of cell clusters, we applied 350 and 500 mM Gd^{3+} concentrations, however no compact 3D structure was formed in any group within 5-h levitation as in the media containing 200 mM Gd^{3+}. (Figure 4.5).

Finally, we tested whether changing the strength of magnetic field by increasing lateral magnet area two-fold would affect the size of D1 ORL UVA cell clusters (Figure 4.6a-e). However, biofabricated structures did not have a significant size difference in horizontal diameter ($p = 0.62$ and 0.74, respectively), vertical diameter ($p = 0.50$ and

0.56), area (p = 0.26 and 0.22) and perimeter (p = 0.99 and p = 0.57) in the medium containing 150 mM and 200 mM Gd^{3+}. Computational simulation for magnet thickness implied that the system achieved a tighter focusing of cells with increased magnet thickness (Figure 4.6f).

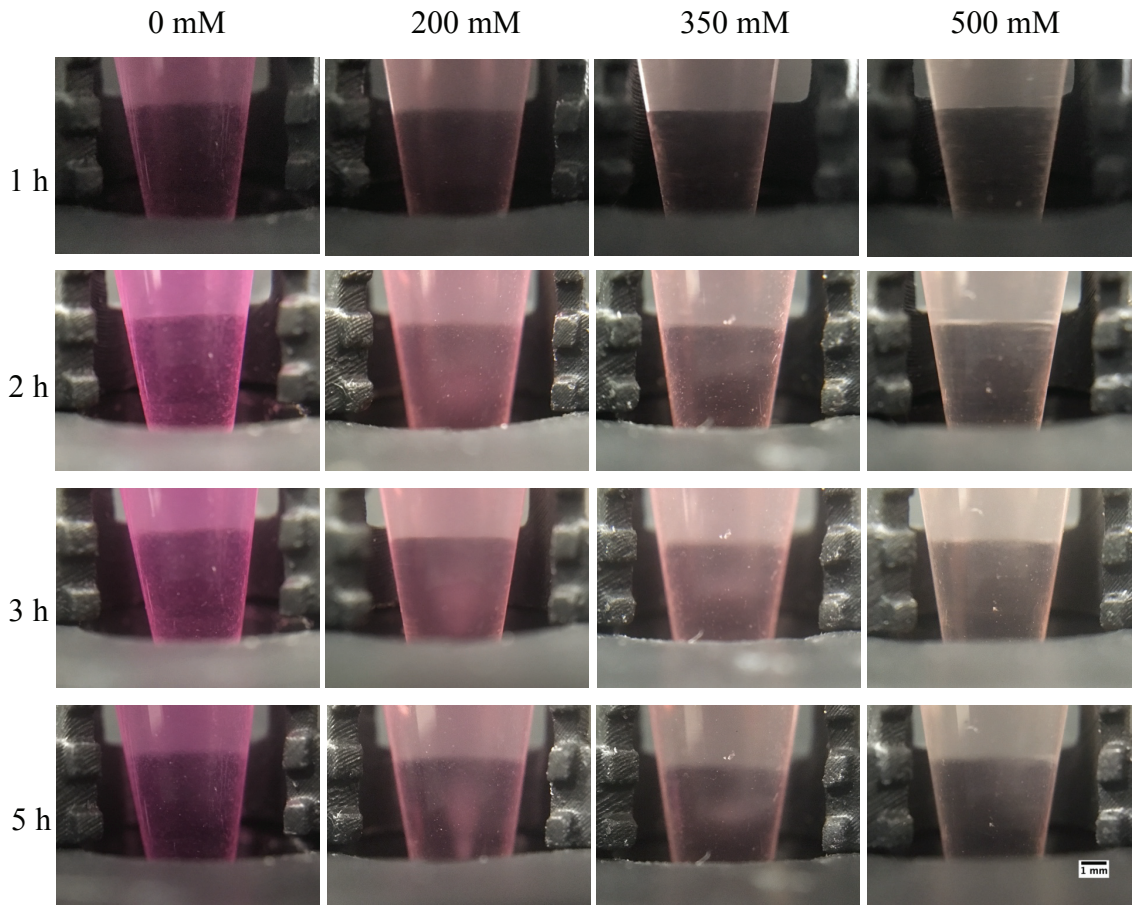

Figure 4.5. Micrographs of D1 ORL UVA cells cultured with increasing concentrations of Gd^{+3} (0, 200, 350 and 500 mM) in the ring magnet-based magnetic levitation platform within 5 h of culture. Each vertical unit on the 3D printed scaled piece: 1mm. Scale bar: 1 mm.

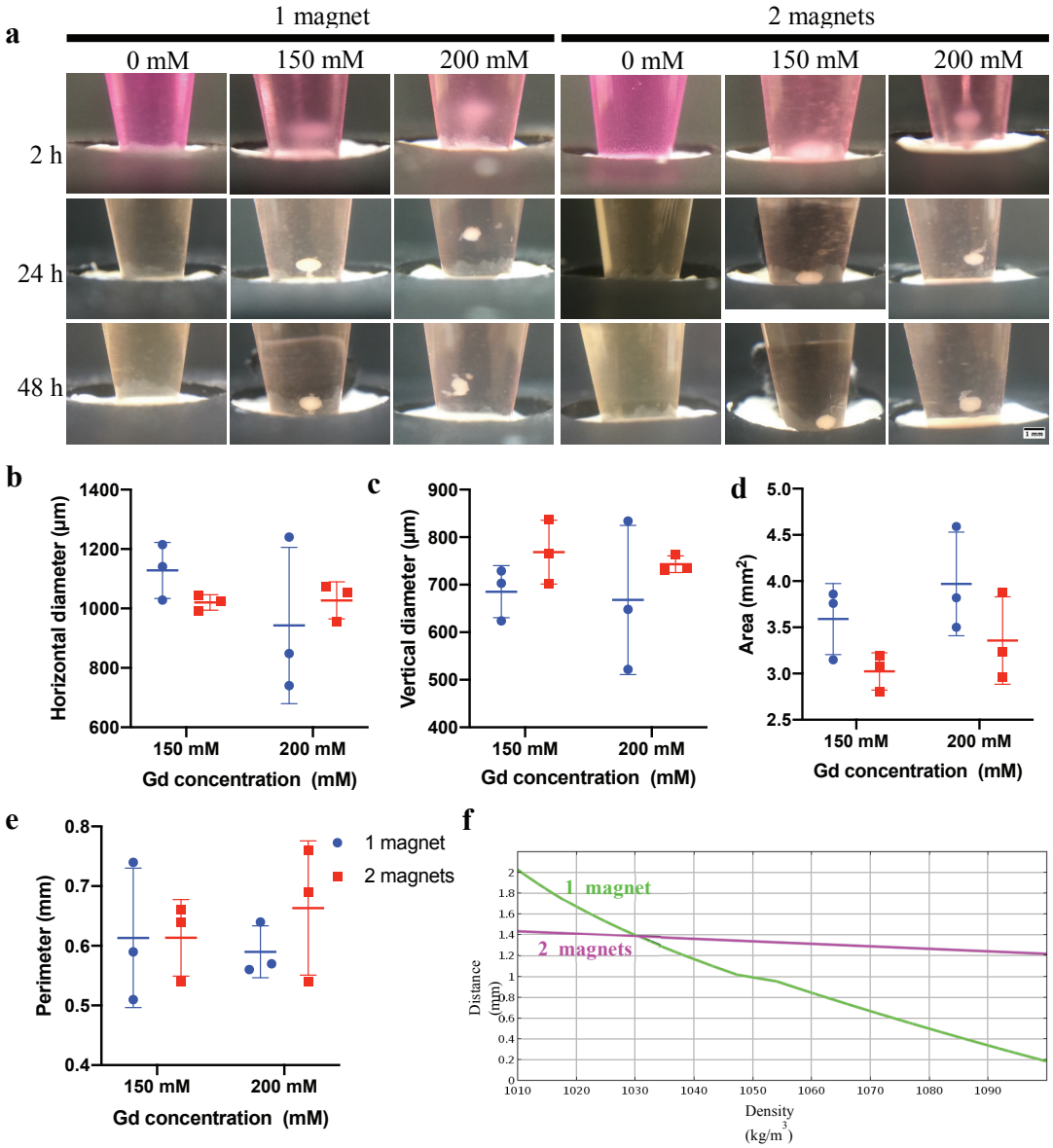

Figure 4.6. (a) Micrographs of D1 ORL UVA cells cultured in the ring magnet-based magnetic levitation platforms (0, 150, 200 mM Gd^{+3}) composed of 1 ring magnet or 2 ring magnets whose opposite poles attached to each other after 2, 24 and 48 h of culture. Scale bar: 1 mm. (b-e) Size of the cellular clusters formed for 24 h in the ring magnet-based magnetic levitation platforms (150, 200 mM Gd^{+3}) composed of 1 ring magnet or 2 ring magnets; horizontal diameter, vertical diameter, area and perimeter. Data are plotted as mean of replicates with error bars (±SD) and statistical significance was determined by two-way ANOVA with Sidak post hoc correction. (f) Modeled relationship between the cell density and levitation heights in the ring magnet-based magnetic levitation platforms (200 mM Gd^{+3}) composed of 1 ring magnet or 2 ring magnets based on the computational model. Level of the magnet surface is considered as z = 0.

4.3.2. Mass Manipulation in 3D Culture with Ring Magnet-Based Magnetic Levitation

We next investigated the suitability of ring magnet-based magnetic levitation setup for mass manipulations in cell culture with magnetic levitation. In order to visualize cell focusing region in ring magnet-based magnetic levitation in the vertical plane, D1 ORL UVA cluster that was assembled with magnetic levitation was moved vertically with the culture chamber (Figure 4.7a). Equilibrium position was robustly kept by the cell cluster during the movement of the system in both directions. Next, to observe cell focusing region on the horizontal plane, D1 ORL UVA cluster formed by magnetic levitation culture was moved from the center of the magnet to the outside, parallel to the surface of the ring magnet with the culture chamber (Figure 4.7b). When the cellular structure reached the boundary of the area above the hole of the magnet, it was moved back towards the center of the magnet due to the high magnetic field on the magnet surface.

Applicability of the medium refreshment, which is an essential factor for long term maintenance in cell culture, was tested during levitation. Medium refreshment of D1 ORL UVA cells that were self-assembled in the magnetic levitation system and cultured by levitation for 48 h was tested (Figure 4.7c). Fresh medium was also rendered as paramagnetic with adding Gd^{3+} prior to use to maintain the levitation of the cellular cluster. The ring magnet-based magnetic levitation system was found to be suitable for removing and replacing up to 80% of 200 µL total media volume with fresh medium, without causing the cellular cluster to settle. Gentle transfer of the medium using a micropipette ensured that the 3D structure in the system was not damaged.

We followed this test of liquid phase transfer by viable cell cluster transfer. 3D structures formed of 2×10^5 D1 ORL UVA cells were also gently collected from the levitation culture without being disturbed using a 1000 µL pipette tip (Figure 4.7d), and the clusters that were harvested from a levitation culture were found to be transferred to another levitation culture without any disturbance (Figure 4.7e).

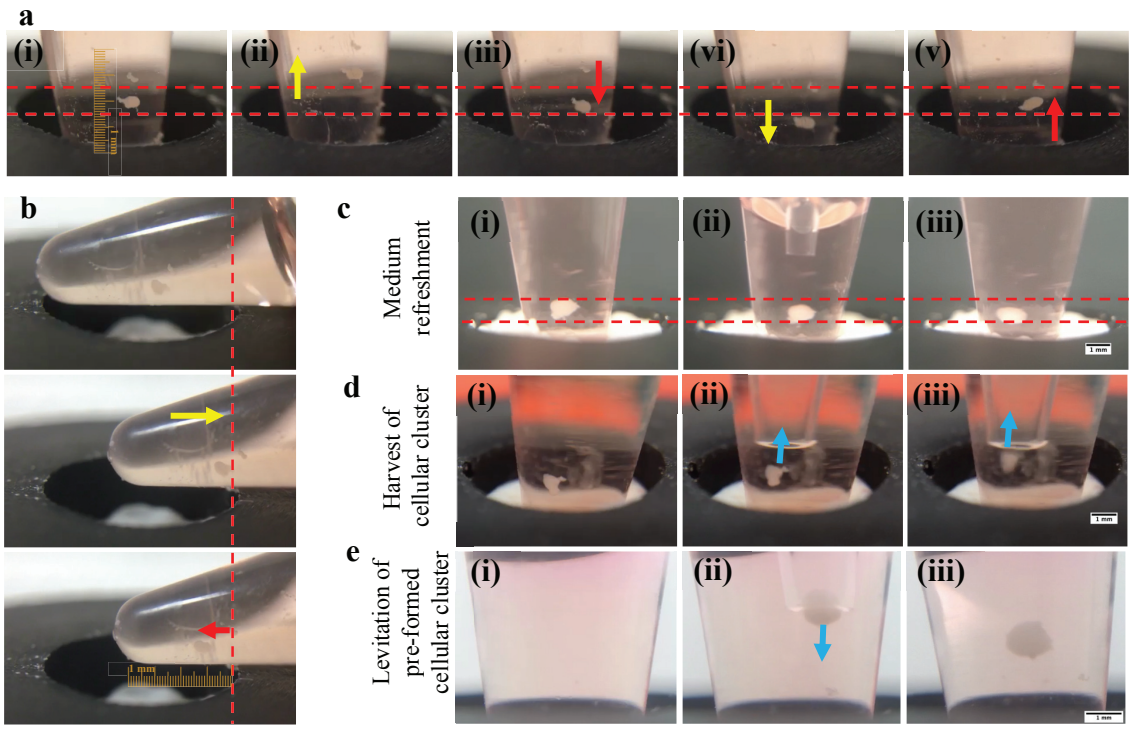

Figure 4.7. Mass manipulation in 3D culture with ring magnet-based magnetic levitation. (a) Trapping region of self-assembled D1 ORL UVA cluster (200 mM Gd^{3+}, 10^6 cells/mL, 100 µL) in the magnetic levitation system; (a) in the vertical plane, (b) in the horizontal plane. When the cellular cluster at equilibrium position (i) was moved upward with the culture chamber (ii), the cluster fell down into the equilibrium position (iii). When the cellular cluster was moved downward with the culture chamber (iv), the cluster rose back to its equilibrium position (v). Between the red dashed lines indicate the region in which the cellular cluster tends to be balanced in figure a. The red dashed line indicates the limit of the region in which the cellular cluster remains in the horizontal plane in figure b. Yellow arrows show the direction which the cellular cluster is moved with the culture chamber as an external force, and the red arrows show the direction which the cellular cluster inherently moves. (c) Refreshing culture medium of 3D cellular cluster formed in the magnetic levitation system (200 mM Gd^{3+}, 10^6 cells/mL, 200 µL) at the equilibrium position (i); removal of old medium (ii) and addition of fresh medium (iii). (d) Harvest of a 3D cellular cluster formed in the magnetic levitation system at the equilibrium position (i) by gently aspirating it with a pipette (ii, iii). (e) Transfer of 3D cellular cluster formed in the magnetic levitation system into another magnetic levitation device with a pipette. Scale bars: 1 mm.

4.3.3. Long Term Levitation Culture

Here, it is aimed to test the health of 3D cellular structures created by magnetic levitation culture and the ability to merge separately formed structures with levitation. Effects of the levitation culture on the health of D1 ORL UVA cells were tested by transferring 3D cellular spheres that were formed during 24 h of levitation culture to a standard culture dish for maintenance of culture (Figure 4.8a and Figure 4.9). We observed that the cells spread adherently at the edges of the 3D cellular cluster to ~43% of the cluster's diameter for the sphere with a diameter of about 713 ± 3 μm. In order to determine the viability of the 3D structures formed in the magnetic levitation system, we performed a live/dead assay to both an intact 3D cluster (Figure 4.8b) as well as to a dissociated form as a single-cell suspension (Figure 4.8c). Visual inspection of the live/dead fluorescence microscopy images showed that most of the cells were viable as apparent from the green calcein-AM signal in both 3D form and the single cell suspension.

The potential of the ring magnet-based magnetic levitation system to biofabricate complex structures consisting of multiple 3D living units was demonstrated by successful co-levitation of homocellular spheroids that were levitation cultured and transferred from a prior levitation culture (Figure 4.8d-g). The 3D spheres formed as a result of magnetic levitation of D1 ORL UVA cells were gently transferred into the medium containing 200 mM Gd^{3+} in the levitation system (Figure 4.8e). Co-levitation cultures formed by transferring two or four of them to the device were maintained for another 24 h to allow cell–cell attachment between spheroids and to form multi-unit 3D structures. We observed that the cellular spheres were fused after 24 h of co-levitation and they were successfully transferred to a different culture dish without deterioration for a better display of the inter-cluster contact zones in 3D structures (Figure 4.10). A 24 h co-levitation resulted in 1.07 ± 0.35% merging of the spheres in area and no statistical difference was observed between percentage fusion in bilateral and quadruple co-levitation cultures ($p=0.87$) (Figure 4.8h and Figure 4.11).

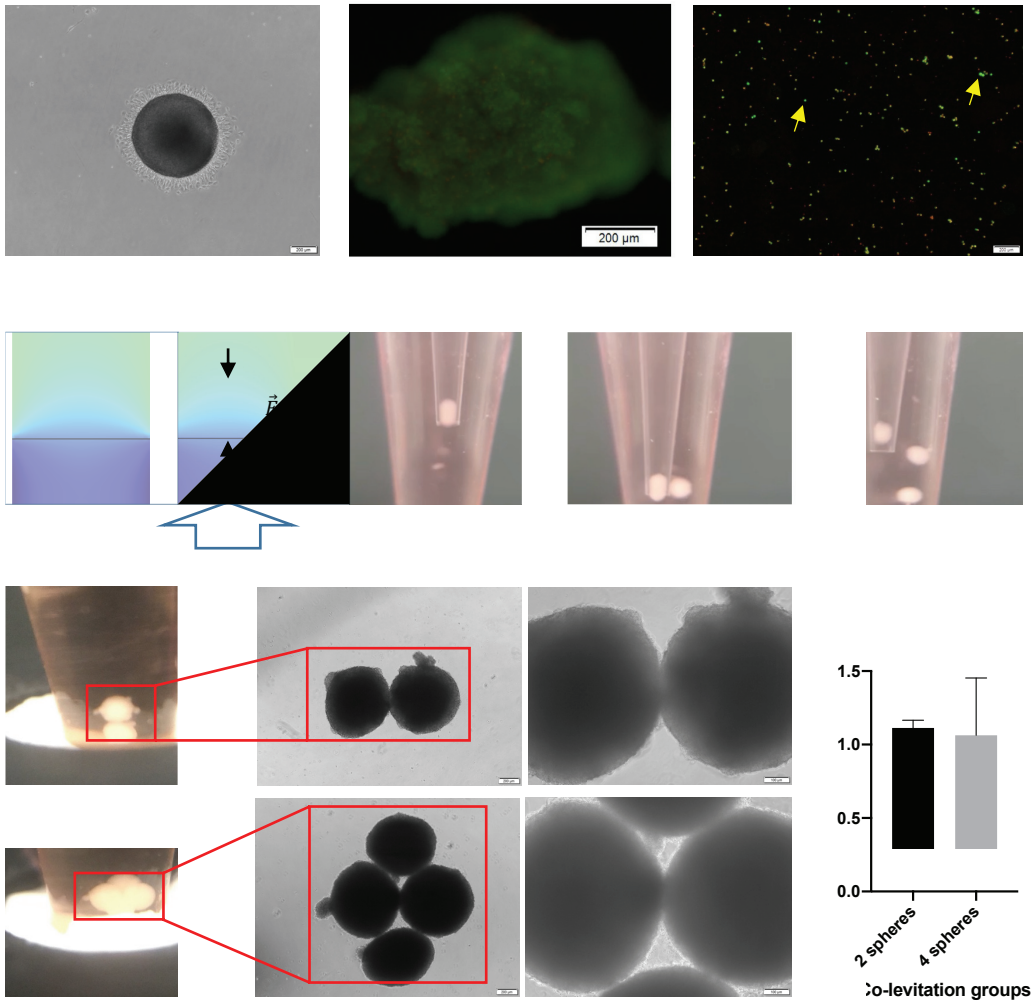

Figure 4.8. Post-operations on spheres formed by ring magnet-based levitation. (a) Micrograph of a self-assembled D1 ORL UVA 3D structure cultured with magnetic levitation (200 mM Gd3+, 106 cells/mL, 200 µL) for 48 h and then cultured for 24 h in the 2D culture dish. Fluorescent microscopy images of D1 ORL UVA (b) 3D structures formed with magnetic levitation and (c) cells dissociated from the 3D structures. (live: green, dead: red). Cell viability was visualized by live-dead staining (Calcein/PI). Yellow arrows denote some of alive cells. Scale bar: 200 µm. (d) Schematic representation of the co-levitation of self-assembled cellular clusters. (e) One-by-one transfer of D1 ORL UVA cellular clusters that were individually self-assembled and cultured for 48 h in ring magnet-based magnetic levitation system to the medium containing 200 mM Gd3+ in magnetic levitation system for co-levitation culture. Co-levitation culture of preformed (f) two and (g) four D1 ORL UVA cellular clusters in medium containing 200 mM Gd3+ in the magnetic levitation system for 24 h. Scale bars: 1 mm for culture chamber images, 200 and 100 µm for middle and right images, respectively, in f and g. (h) Merged area of spheres (%) co-levitated in a medium containing 200 mM Gd3+ for 24 h. Data are plotted as mean of replicates with error bars (±SD) and evaluated using the unpaired Student's t-test.

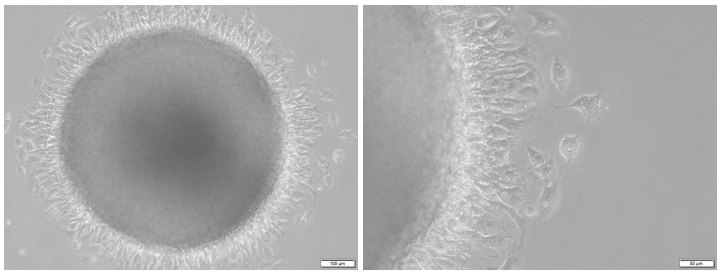

Figure 4.9. Micrograph of a self-assembled D1 ORL UVA 3D structure cultured with magnetic levitation (200 mM Gd^{3+}, 10^6 cells/mL, 200 µL) for 48 h and then cultured for 24 h in the culture dish. Scale bars: 100 and 50 µm, respectively.

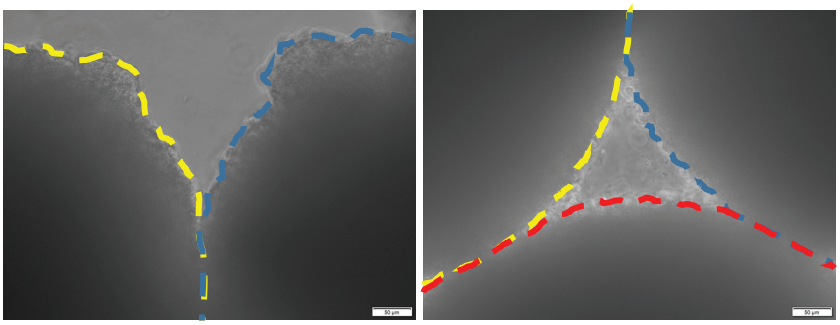

Figure 4.10. Zoomed-in view of the inter-cluster contact zones in 3D structures formed by 24-h co-levitation of two and four D1 ORL UVA cellular clusters in medium containing 200 mM Gd^{3+}. Dashed lines indicate the boundaries of the spheroids. Scale bar: 50 µm.

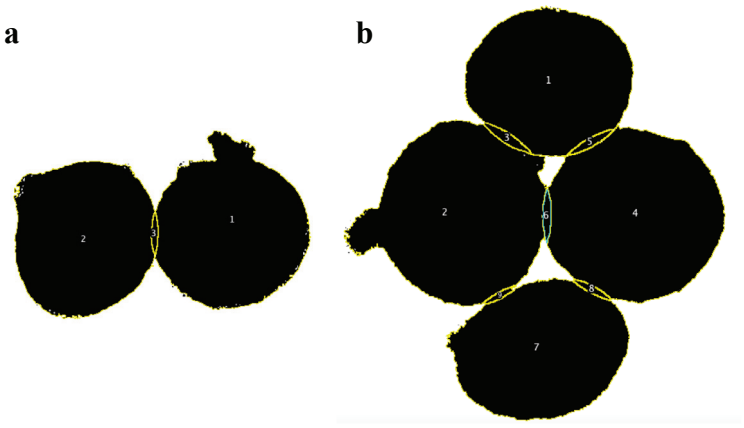

Figure 4.11. Images obtained for calculation of the merged areas (%) represented in figure 4.8h by an image processing for co-levitation culture of preformed (a) two and (b) four cellular clusters.

4.3.4. Magnetically Guided Self-Assembly of Cells with Different Single Cell Densities

Since one of the features determining the final position of the cells in the magnetic levitation principle is the inherent single cell densities, the levitation-based 3D culture protocol of low-density cells in the system was defined using adipocytes with low density due to cellular lipid accumulation [118]. Adipogenesis of 7F2 cells were induced for 7 days to obtain lipid accumulated cells (Figure 4.12). Following the observation of lipid accumulation, the cells were suspended in the paramagnetic medium containing increasing Gd^{3+} concentrations (0, 100, 150 and 200 mM) and levitation cultured over 24 h in the ring magnet-based magnetic levitation system (Figure 4.13a). We observed that the cells started to accumulate on the magnet towards the center in all paramagnetic medium containing Gd^{3+} between 100 and 200 mM at the 2nd h of the culture, and these stably levitated cells formed 3D structures at the 24th h of the culture. The spheres formed in 100 mM Gd^{3+} containing medium were 1.95 and 2.95 times larger in area (~ 5.8 mm^2), and 1.51 and 1.58 times larger in perimeter (~ 10.72 mm) than those formed in the medium containing 150 and 200 mM Gd^{3+}, respectively (Figure 4.13b). There was no statistically significant difference between the areas ($p=0.06$) and perimeters ($p=0.78$) of the clusters formed in the medium containing 150 and 200 mM Gd^{3+}. When the cells were assembled in the medium containing 100 mM Gd^{3+}, the shapes of the clusters were skewed in the direction of the vertical diameter rather than horizontal diameter compared to the clusters formed in paramagnetic medium containing higher Gd^{3+}. Closer inspection of the graph showed that the vertical diameter of the cellular clusters formed in the medium containing 100 mM Gd^{3+} was 3917 ± 622.55 μm and it was 2.38 and 2.72 times higher than the clusters formed at 150 mM and 200 mM Gd^{3+} concentrations, respectively.

In order to maintain culture of the adipogenesis induced 3D structures, which were formed as a result of 24-h levitation, spheroids were transferred to a culture plate and cultured for another 24 h (Figure 4.14). We observed that the transferred 3D structures were loose and many adipocytes dissociated from the edges of the 3D clusters in all paramagnetic medium groups after the transfer. While most of the cells separated from the main cluster were in suspended form, some lipid-containing cells were observed to spread over the culture surface.

Testing the viability of cells at the end of the culture by live/dead staining showed that most cells in the 3D cluster were alive (Figure 4.13c and Figure 4.15). It was observed that the cells were stained with calcein at the end of the culture at all Gd^{3+} concentrations applied in the levitation of cells.

We also carried out co-levitation of 3D adipogenesis-induced cell clusters formed separately in the medium containing same concentration of Gd^{3+} for 24 h (Figure 4.16). Although the clusters appeared together with the assistance of magnetic force in the levitation system at the 24th h of levitation, we observed that there was still no fusion between the clusters when transferred to the culture vessel and the clusters were dispersed with the transfer.

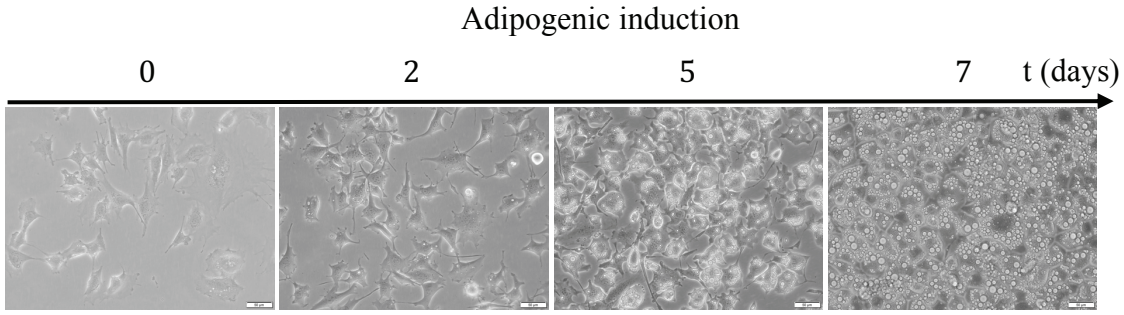

Figure 4.12. Micrographs of adipogenesis induced 7F2 cells over 7 days. Scale bar: 50 μm.

The ring magnet-based magnetic levitation system was also tested for biofabrication of 3D structures of MDA-MB-231 breast cancer cells levitation cultured for 24 h in medium containing 150 and 200 mM Gd^{3+} (Figure 4.13d). In the 2nd h of the culture, cell clustering began with a nebulous appearance in the paramagnetic medium and levitated tight 3D clusters with an area of 1.37 ± 0.17 mm^2 were observed at 24th h (Figure 4.13e). The horizontal diameter of the 3D structures formed in the media containing 150 mM Gd^{3+} was ~39% higher and the perimeter was ~22% higher than those formed in the medium containing 200 mM Gd^{3+}.

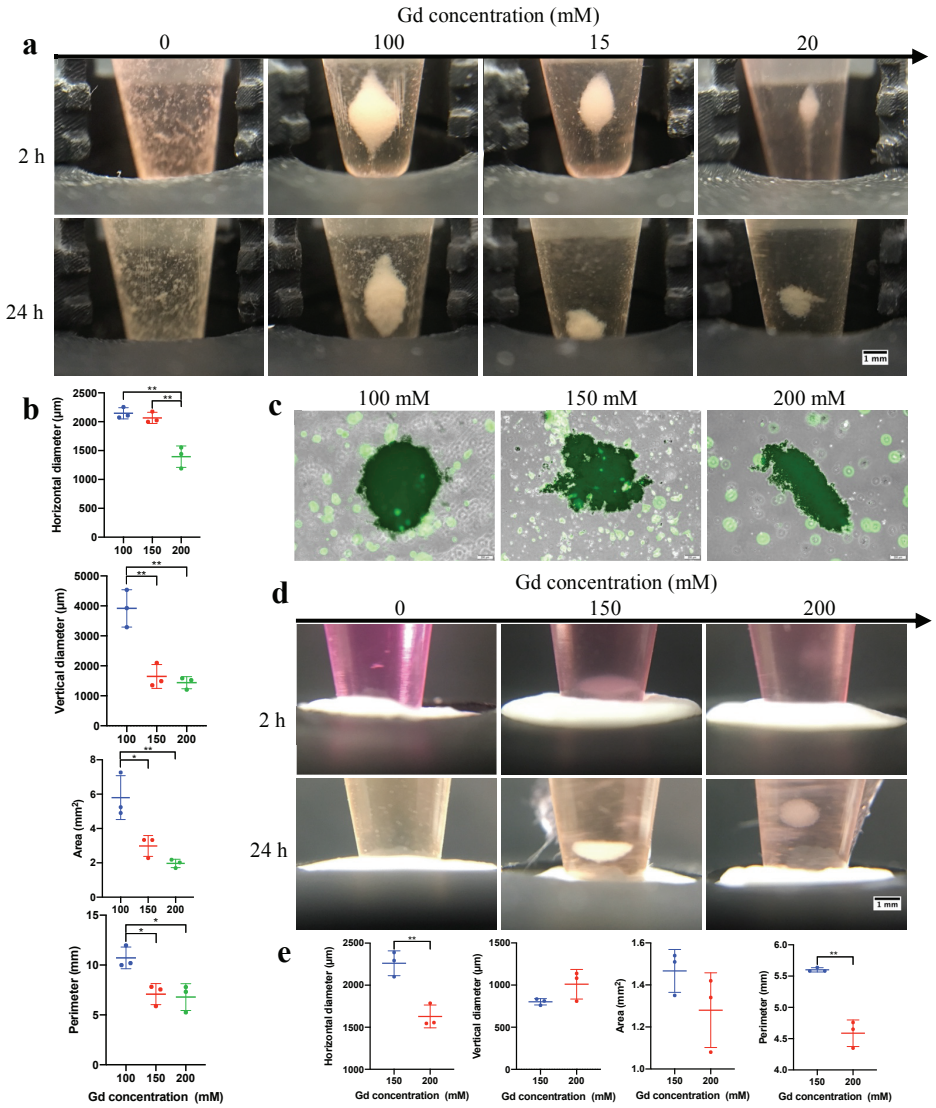

Figure 4.13. Levitation based 3D culture of different cell types. (a) Micrographs of adipogenesis induced 7F2 cells cultured with ring magnet-based magnetic levitation (0, 100, 150 and 200 mM Gd3+, 106 cells/mL, 200 µL) after 2 or 24 h of culture. Each vertical unit on the 3D printed scaled piece: 1mm. Scale bar: 1 mm. (b) Size of the adipogenesis induced 7F2 cellular clusters formed for 24 h with magnetic levitation; horizontal diameter, vertical diameter, area and perimeter. (c) Fluorescent microscopy images of adipogenesis induced 7F2 3D structures formed with magnetic levitation. Cell viability was visualized by live staining (Calcein-AM). Scale bar: 200 µm. (d) Micrographs of MDA-MB-231 cells cultured with ring magnet-based magnetic levitation (0, 150 and 200 mM Gd3+, 106 cells/mL, 200 µL) after 2 or 24 h of culture. Scale bar: 1 mm. (e) Size of the MDA-MB-231 cellular clusters formed for 24 h with magnetic levitation; horizontal diameter, vertical diameter, area and perimeter. Data are plotted as mean of replicates with error bars (±SD) and statistical significance was determined by Student's t-test (two-tail). *: $p < 0.05$; **: $p < 0.01$.

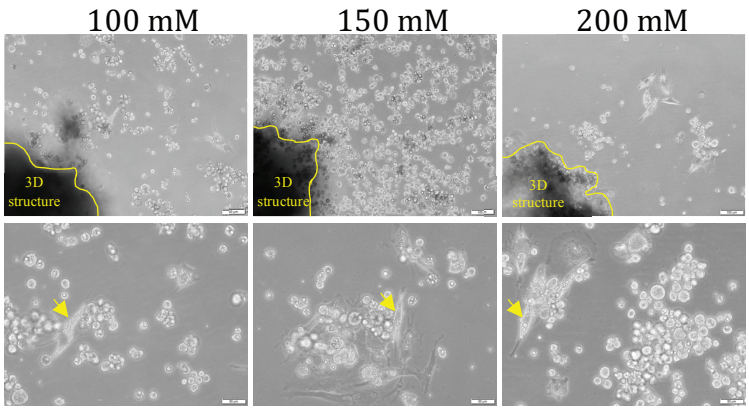

Figure 4.14. Micrographs of the adipogenesis induced 3D structures, which were formed as a result of 24-h levitation (100, 150 and 200 mM Gd^{3+}, 10^6 cells/mL, 200 µL) and then cultured for another 24 h on a culture plate. The edges of the 3D structure in the image are roughly drawn with yellow lines. Arrows show examples of lipid-accumulated cells spread on the culture surface. Scale bars: 100 µm for the upper images and 50 µm for the lower images.

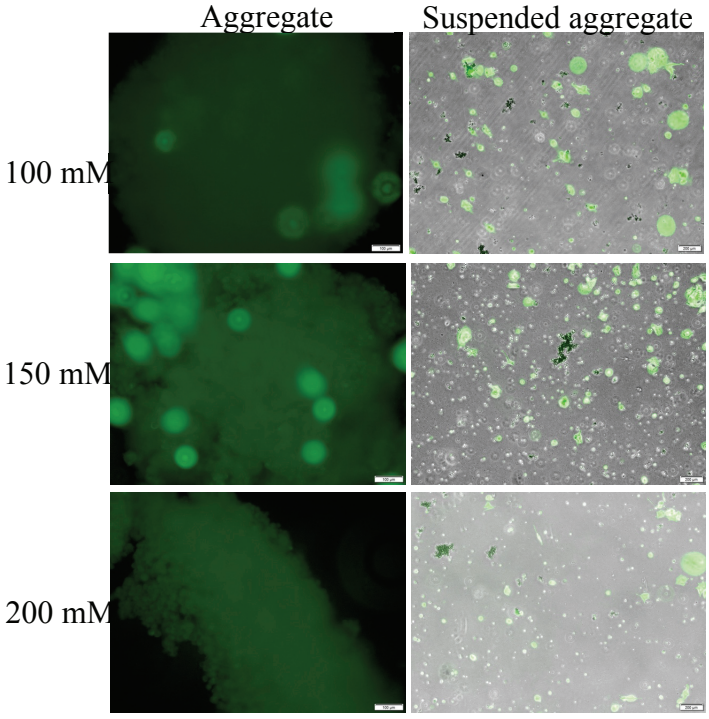

Figure 4.15. Micrographs Fluorescent microscopy images of adipogenesis induced 7F2 3D structures formed with magnetic levitation and cells dissociated from the 3D structures. Cell viability was visualized by live staining (Calcein-AM). Scale bars: 100 µm for the left images and 200 µm for the right images.

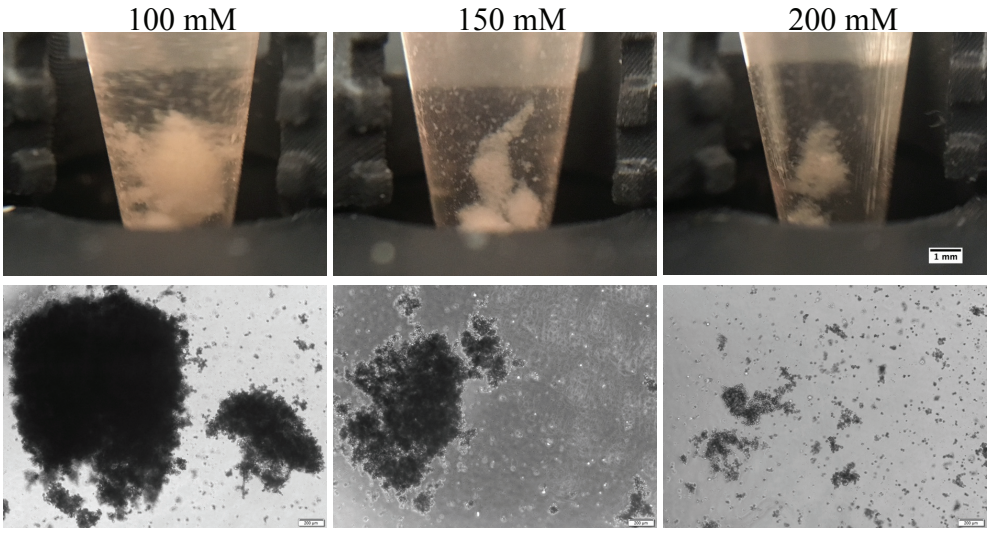

Figure 4.16. Co-levitation culture of preformed two adipogenesis induced 7F2 3D structures in medium containing 100, 150 and 200 mM Gd^{3+} in the magnetic levitation system for 24 h. The micrographs in the bottom row show these co-levitation products after transfer to the 2D culture dish. Each vertical unit on the 3D printed scaled piece: 1mm. Scale bars: 1 mm for culture chamber images, 200 µm for microscope images.

4.3.5. In-gel Culture of Self-assembled 3D Structures

In order to demonstrate the transferability and the sustainability of self-assembled 3D structures created with magnetic levitation into an in-gel culture, D1 ORL UVA cells were levitation cultured for 24 h and at the end of the culture self-assembled 3D structures were embedded in Matrigel (Figure 4.17a, b). After aspirating most of the levitation medium leaving enough to sustain the levitation of the 3D structure (~20 µL) we slowly added Matrigel to the levitation system. We transferred the Matrigel in a slow rate to the point that the Matrigel volume was five times the volume of the remaining medium. Matrix was added at +4°C that keep it in liquid form and polymerization was achieved by temperature change. It was shown that the levitated cellular structures could be successfully trapped within the Matrigel without any observable deformation. We then transferred the cellular structure within the gel matrix to a separate culture (Figure 4.17c-e). On the 4^{th} day of the culture, we observed that the 3D cellular structure consisted of viable cells spreading in the gel matrix (Figure 4.17f, Figure 4.18).

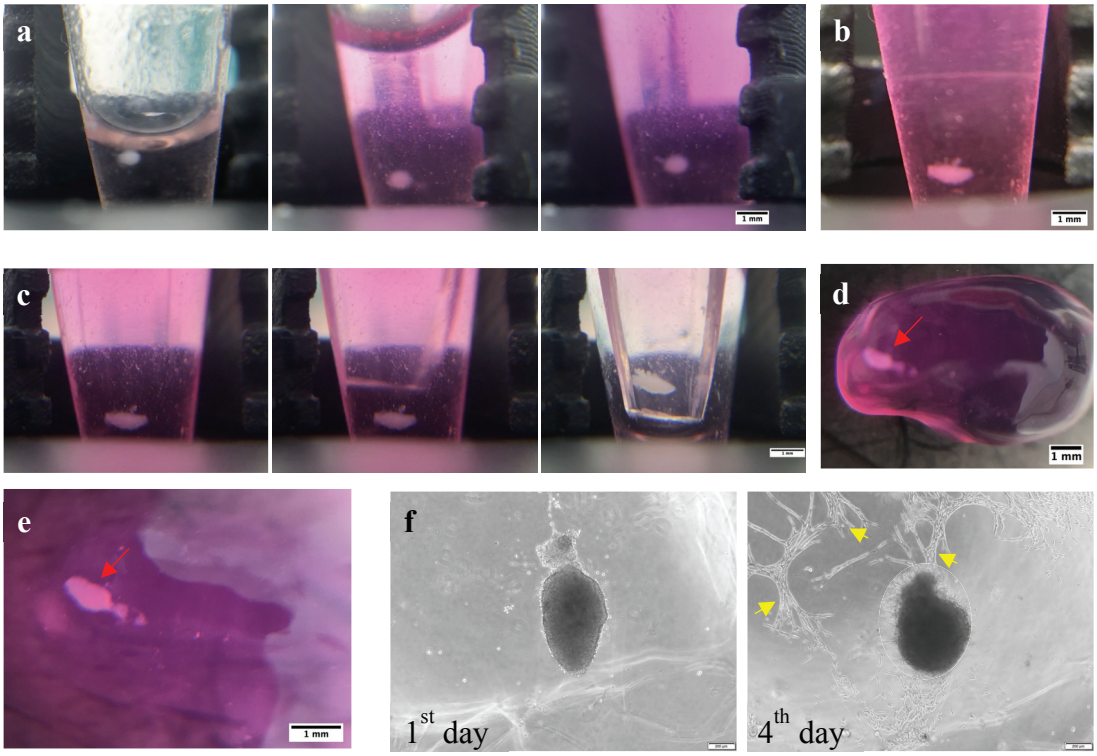

Figure 4.17. In-gel culture of self-assembled D1 ORL UVA 3D structures. (a) Embedding a 3D cellular structure assembled by magnetic levitation within Matrigel. (b) Cellular cluster in Matrigel at 3rd h of culture. (c) Harvest of gel-embedded 3D cluster using a pipette tip, which was cut into a micro-spoon. Matrigel-embedded 3D cluster that was transferred into a culture plate. (d) Before and (e) after medium addition on gel-embedded culture. Red arrows show the 3D clusters in the gel matrix. Each vertical unit on the 3D printed scaled piece: 1mm. Scale bar: 1 mm (f) Micrographs of the Matrigel-embedded 3D cluster after 1 and 4 days of culture. Yellow arrows indicate some of the cells spreading in the gel matrix. Scale bar: 200 µm.

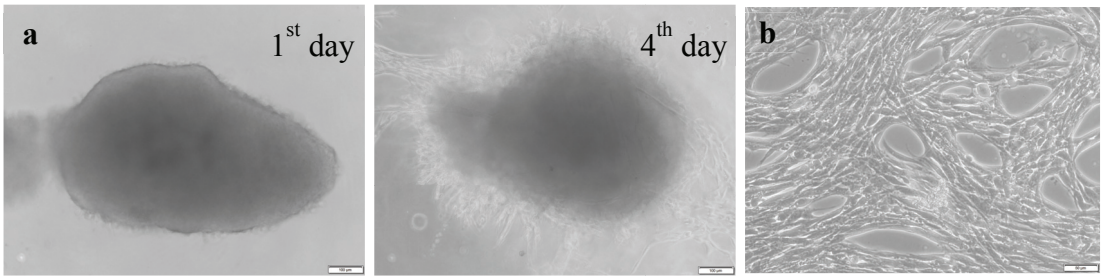

Figure 4.18. Micrographs of (a) the Matrigel-embedded 3D cluster after 1 and 4 days of culture, and (b) cells spread in Matrigel after 4 days. Scale bars: 100 µm for (a) and 50 µm for (b).

4.4. Discussion

Magnetic force-assisted cell manipulation provides a broadly applicable guidance tool in many fields such as biological or clinical research and tissue engineering. The availability of label-free protocols has recently led to a greater focus of research on these techniques due to both lowering required cost, time and labor, and enhancing compatibility of the technique for living cells. Some microcapillary based magnetic levitation systems, that were initially applied to detect and sort cells of interest according to their physical intrinsic properties [17, 118, 127, 244, 245], were later adapted for biofabrication [128, 164, 175]. While great progress has been made in the field, tissue engineering applications and biological testing protocols require manufacture of sizable living constructs to provide an adequate number of cells. Systems that allow cell culture applications on-site and offer low-cost applications with permanent magnets are essential to render the production easy to install and operate, and to enable on-site intervention to production process.

The standard diamagnetic levitation devices using capillary tubes (1 mm × 1 mm square cross-section) physically sandwiched between two block permanent magnets are able to create large cellular blocks (up to ~2.68 cm in length) [128]. Although these elongated living structures created in such systems are advantageous in terms of efficient mass transfer between cluster and its surrounding, they are not mechanically resistant to transfer processes due to their low thickness (up to ~280 μm) with low homogeneity towards the capillary ends, limiting their applications in bottom-up tissue engineering. Another magnetic levitation setup design was shown to increase the working volume by positioning larger block magnets (poles on 2 inch x 2 inch surfaces) further apart with a gap set to 2.5 cm [120]. This system allows remote 3D manipulation of millimeter-sized living objects. Such systems still contain opposing magnets occupying the top and bottom of the culture chamber to provide magnetic field gradient required for levitation, and this configuration limits operations on the culture during levitation process such as medium refreshment and transfer of the cellular structures. Ring magnet-based magnetic levitation system proposed here removes the upper physical barrier, hence providing an easy access to the levitating biological structures and to its surrounding medium. Furthermore, this setup eliminates the limit for the height of the cell culture chamber and thus enables levitation in great height culture containers. We showed that single step axial-circular

magnetic levitation made addition and removing of liquid or solid phases straightforward without removing the culture chamber from the magnetic field owing to a large and open operational space on the culture container. The ability to be processed during levitation also provided the opportunity to fully embed the levitated structures in another phase such as a gel matrix. The sustainability of the culture within a gel matrix ensures that the system can be applied effectively in broad studies including drug response, cell movement and stromal effects.

Mammalian cells exhibit different characteristics for densities depending on their type; e.g. ~1.044 g/mL for breast cancer cells, ~1.062 g/mL for lung cancer cells [17], ~1.084 g/mL for bone marrow originated stem cells [118]. Here we have shown that ring magnet-based magnetic levitation system is able to levitate objects with a density ranging from 1.02-1.09 g/mL by levitation of particles with known density. Considering the variability of density depending on cellular condition such as type of cell, pathological conditions and differentiation [246], the wide range of applicability of the system has been demonstrated. As models representing levitation of cells with different densities, stem cells, breast cancer cells and adipocytes were self-assembled into 3D structures with preserving cell viability in our system. It was shown that tight and intact 3D cellular units were produced with bone marrow originated stem cells and breast cancer cells and the magnetic levitation system could provide the fusion of biological units composed of stem cells. However, 3D adipocyte clusters were mechanically too unstable for transfer and fusion operations. As the system relies on cell-cell interaction independent of an external mechanical support, the technique is not suitable for natural self-assembly of each cell type. These loose structures may be modified and strengthened by using binary cell mixtures including fibroblasts [247] and stem cells [164] to act as an adhesive that promotes intercellular interactions.

The process of creating 3D cellular structures by magnetic guidance involves first focusing the single cells homogeneously distributed in the suspension by magnetic force and then gaining a stable architecture of the structure with cell-cell interactions in the focusing region. 3D stable structure formation on the ring magnet-based magnetic levitation system presented herein took more than 10 hours regardless of cell type. In order to shorten this period into couple hours, the magnetic force applied on the cells was increased by modifying the paramagnetic media, however the formation process could not be accelerated. Previously a magnetic manipulation method has been described to print 3D cellular structures within 6 hours [248]. Unlike our system, this method enabled

individual cells to focus on the culture surface rather than levitational assembly. In order to accelerate cellular aggregation in the ring magnet-based levitation system, the cell focusing process may be accelerated by the physical confinement of the cells in the region close to the low magnetic field (e.g. increasing magnet thickness) or by using binary cell mixtures as an adhesive.

Mini-tissue block fabrication shows great promise in formation of complex and large 3D anatomical structures. Tissue blocks, which create their own matrix and architecture, show a potential as building blocks for scale-up tissue fabrication. The absence of an external material allows biomaterial-based concerns such as material-induced toxicity and host inflammatory responses to be overcome [249-252]. However, while scaffolding provides void volume for passive diffusion of nutrients, gasses and wastes into the scaffolds to keep the cells alive [253], scaffold-free approaches lack this advantage. Our axial-circular magnetic levitation system may be equipped with a flow system that the bulk liquid phase is continuously refreshed to improve the diffusion between the sphere surface and the liquid phase without disturbing the levitation. In the case of increased spherical size and extended culture periods, the protocol should be tested for the health of cells in the central region prior to fabrication.

CHAPTER 5

CONCLUSION

In this doctoral thesis, magnetic levitation setups with two different configurations that provide label-free manipulation of cells were fabricated, and comprehensive procedures were described for the biofabrication of scaffold-free 3D cellular structures and their culture under levitation. In the first part of the study, a magnetic levitation configuration, that provides levitation between two block magnets and was previously used for density-based analysis, was successfully applied for the first time to form complex 3D structures in situ. In the second part of the study, a magnetic levitation platform that provides levitation on a single ring magnet was produced to expand the operational space in the levitation system between two magnets and to create sizeable and symmetrical structures. The system was applied for the first time to form, maintain and merge 3D cellular structures.

Previous studies have reported that the system that provides levitation between two magnets is suitable for the detection and separation of both non-living and living objects based on their density. In this study, effects of the operation on bone marrow-derived stem cells were investigated, since the device that provides levitation between two magnets is aimed to be applied for long-term culture of these cells. Among the various chelate forms of gadolinium, gadobutrol was found to be the most suitable composition in terms of both its effect on cell viability and the levitation height. Demonstrating that the gadobutrol concentration required for levitation can be applied safely in long-term culture of cells has enabled to add biofabrication and subsequent cell culture to the application areas of the system. The system enabled cells to focus in a low magnetic field region in less than 10 min and self-assembly of cells in less than a day, thus formation of scaffold-free 3D living structures under real-time observation. This system allows cells to be free of mechanical support, to ensure complete remote manipulation, and provide biofabrication by the self-assembly ability of cells. Taking advantage of this nature of the system, it has been shown that 3D structures with different cellular arrangements can be formed with different cell loading strategies into the system. This offers the opportunity of the system to be used in various bioengineering applications

for the production of biological models that require complex cellular arrangements involving horizontal or vertical cellular layers.

The axial-circular magnetic levitation device, which is another system produced here, has been successfully applied for the production and fusion of various living building blocks as an alternative to the previous method. This magnetic levitation device offers various advantages: (1) This system, that provides levitation on a single ring magnet, eliminates the upper physical limit and thus allows the formation of sizeable cellular blocks due to its high compatibility with different sizes of culture chambers. (2) Since the method offers an open operational area, it allows in situ interventions in the levitation chamber and makes straightforward transfer of materials such as cellular structures and medium. (3) In the previous system, increasing size of the cellular structure results in an increase in the horizontal direction due to the magnetic field gradient and the formation of elongated mechanically unstable structures. Although the number of cells is greatly increased in this system, the cellular structures maintain their spherical-like shape that facilitates their use as building blocks in bottom-up applications.

The magnetic levitation configurations presented here provide the magnetic field gradient with permanent magnets, allowing a low-cost production and operation as it is independent of electrical power. Providing a label-free application eliminates the variables and additional processes associated with magnetic cell labeling. This nozzle-free biofabrication method also prevents the creation of mechanical stress on the cells. These systems that are easy to set up and implement, cost-effective, and compatible with living cells have a great potential for the production and maintenance of cellular structures with controlled size and complexity. These magnetic levitation devices may be improved by integrating perfusion systems and automation, and offers broad applications in many areas such as bottom-up tissue engineering, cancer research, weightlessness research and drug testing with batch or continuous operations.

REFERENCES

1. Cardarelli, F., Magnetic Materials. *Materials Handbook: A Concise Desktop Reference* 2008, 487-517.

2. Getzlaff, M., Solid State Magnetism. In *Fundamentals of Magnetism*, Springer: 2008; pp 1-6.

3. Sun, C.; Lee, J. S. H.; Zhang, M., Magnetic nanoparticles in MR imaging and drug delivery. *Advanced Drug Delivery Reviews* 2008, *60* (11), 1252-1265.

4. Kolhatkar, A. G.; Jamison, A. C.; Litvinov, D.; Willson, R. C.; Lee, T. R., *Tuning the magnetic properties of nanoparticles*. 2013; Vol. 14, p 15977-16009.

5. Pankhurst, Q. A.; Connolly, J.; Jones, S.; Dobson, J., Applications of magnetic nanoparticles in biomedicine. *Journal of physics D: Applied physics* 2003, *36* (13), R167.

6. Issa, B.; Obaidat, I. M.; Albiss, B. A.; Haik, Y., Magnetic nanoparticles: Surface effects and properties related to biomedicine applications. *International Journal of Molecular Sciences* 2013, *14* (11), 21266-21305.

7. Gijs, M. A. M., Magnetic bead handling on-chip: New opportunities for analytical applications. *Microfluidics and Nanofluidics* 2004, *1* (1), 22-40.

8. Oldenburg, C. M.; Borglin, S. E.; Moridis, G. J., Numerical simulation of ferrofluid flow for subsurface environmental engineering applications. *Transport in Porous Media* 2000, *38* (3), 319-344.

9. Patton, J. A., MR imaging instrumentation and image artifacts. *Radiographics* 1994, *14* (5), 1083-1096.

10. Zborowski, M.; Chalmers, J. J., Magnetophoresis: Fundamentals and applications. *Wiley Encyclopedia of Electrical and Electronics Engineering* 1999, 1-23.

11. Weston, M. C.; Gerner, M. D.; Fritsch, I., Magnetic Fields for Fluid Motion. *Analytical Chemistry* 2010, *82* (9), 3411-3418.

12. Pamme, N., Magnetism and microfluidics. *Lab on a Chip* 2006, *6* (1), 24-38.

13. Gijs, M. A. M.; Lacharme, F. d. r.; Lehmann, U., Microfluidic applications of magnetic particles for biological analysis and catalysis. *Chemical Reviews* 2010, *110* (3), 1518-1563.

14. Bhuvanendran Nair Gourikutty, S.; Chang, C. P.; Puiu, P. D., Microfluidic immunomagnetic cell separation from whole blood. *Journal of chromatography. B, Analytical technologies in the biomedical and life sciences* 2016, *1011*, 77-88.

15. Hejazian, M.; Li, W.; Nguyen, N.-T., Lab on a chip for continuous-flow magnetic cell separation. *Lab on a Chip* 2015, *15* (4), 959-970.

16. Gerber, R.; Takayasu, M.; Friedlaender, F. J., *Generalization of HGMS Theory: The Capture of Ultra-fine Particles*. 1983; Vol. 19, p 2115-2117.

17. Durmus, N. G.; Tekin, H. C.; Guven, S.; Sridhar, K.; Yildiz, A. A.; Calibasi, G.; Ghiran, I.; Davis, R. W.; Steinmetz, L. M.; Demirci, U., Magnetic levitation of single cells. *Proceedings of the National Academy of Sciences* 2015, *112* (28), E3661-E3668.

18. Spring, S.; Bazylinski, D. A., Magnetotactic bacteria. *Prokaryotes* 2006, *2*, 842-862.

19. Melville, D.; Paul, F.; Roath, S., Direct magnetic separation of red cells from whole blood. *Nature* 1975, *255* (5511), 706-706.

20. Han, K.-H.; Frazier, A. B., Paramagnetic capture mode magnetophoretic microseparator for high efficiency blood cell separations. *Lab on a Chip* 2006, *6* (2), 265-273.

21. Hirota, N.; Kurashige, M.; Iwasaka, M.; Ikehata, M.; Uetake, H.; Takayama, T.; Nakamura, H.; Ikezoe, Y.; Ueno, S.; Kitazawa, K., Magneto-Archimedes separation and its application to the separation of biological materials. *Physica B: Condensed Matter* 2004, *346*, 267-271.

22. Zborowski, M.; Chalmers, J. J.; Lowrie, W. G., Magnetic Cell Manipulation and Sorting. In *Microtechnology for Cell Manipulation and Sorting*, Springer: 2017; pp 15-55.

23. Newman, J., *Physics of the life sciences*. Springer Science & Business Media: 2010.

24. Beaugnon, E.; Tournier, R., Levitation of organic materials. *Nature* 1991, *349* (6309).

25. Berry, M. V.; Geim, A. K., Of flying frogs and levitrons. *European Journal of Physics* 1997, *18* (4), 307.

26. Valles, J.; Lin, K.; Denegre, J. M.; Mowry, K. L., Stable magnetic field gradient levitation of Xenopus laevis: toward low-gravity simulation. *Biophysical Journal* 1997, *73* (2), 1130-1133.

27. Liu, Y.; Zhu, D.-M.; Strayer, D. M.; Israelsson, U. E., Magnetic levitation of large water droplets and mice. *Advances in Space Research* 2010, *45* (1), 208-213.

28. Herranz, R.; Larkin, O. J.; Dijkstra, C. E.; Hill, R. J.; Anthony, P.; Davey, M. R.; Eaves, L.; van Loon, J. J.; Medina, F. J.; Marco, R., Microgravity simulation by diamagnetic levitation: effects of a strong gradient magnetic field on the transcriptional profile of Drosophila melanogaster. *BMC genomics* 2012, *13* (1), 52.

29. Rodríguez-Villarreal, A. I.; Tarn, M. D.; Madden, L. A.; Lutz, J. B.; Greenman, J.; Samitier, J.; Pamme, N., Flow focussing of particles and cells based on their intrinsic properties using a simple diamagnetic repulsion setup. *Lab on a Chip* 2011, *11* (7), 1240-1248.

30. Peyman, S. A.; Kwan, E. Y.; Margarson, O.; Iles, A.; Pamme, N., Diamagnetic repulsion—a versatile tool for label-free particle handling in microfluidic devices. *Journal of Chromatography A* 2009, *1216* (52), 9055-9062.

31. Watarai, H.; Namba, M., Capillary magnetophoresis of human blood cells and their magnetophoretic trapping in a flow system. *Journal of chromatography A* 2002, *961* (1), 3-8.

32. Plouffe, B. D.; Lewis, L. H.; Murthy, S. K., Computational design optimization for microfluidic magnetophoresis. *Biomicrofluidics* 2011, *5* (1), 013413.

33. Ramadan, Q.; Poenar, D. P.; Yu, C., Customized trapping of magnetic particles. *Microfluidics and nanofluidics* 2009, *6* (1), 53-62.

34. Kim, S.; Han, S.-I.; Park, M.-J.; Jeon, C.-W.; Joo, Y.-D.; Choi, I.-H.; Han, K.-H., Circulating tumor cell microseparator based on lateral magnetophoresis and immunomagnetic nanobeads. *Analytical chemistry* 2013, *85* (5), 2779-2786.

35. Zhang, L.; Wang, J.; Wang, H.; Wang, W.; Li, Z.; Liu, J.; Yang, X.; Ji, X.; Luo, Y.; Hu, C., Moderate and strong static magnetic fields directly affect EGFR kinase domain orientation to inhibit cancer cell proliferation. *Oncotarget* 2016, *7* (27), 41527.

36. Zhang, J.; Ding, C.; Shang, P., Alterations of mineral elements in osteoblast during differentiation under hypo, moderate and high static magnetic fields. *Biological trace element research* 2014, *162* (1-3), 153-157.

37. Zhang, X.; Yarema, K.; Xu, A., Parameters of Magnetic Fields and Their Differential Biological Effects. In *Biological Effects of Static Magnetic Fields*, Springer: 2017; pp 3-25.

38. Sullivan, K.; Balin, A. K.; Allen, R. G., Effects of static magnetic fields on the growth of various types of human cells. *Bioelectromagnetics* 2011, *32* (2), 140-147.

39. Zhang, L.; Ji, X.; Yang, X.; Zhang, X., Cell type-and density-dependent effect of 1 T static magnetic field on cell proliferation. *Oncotarget* 2017, *8* (8), 13126.

40. Nam, J.; Huang, H.; Lim, H.; Lim, C.; Shin, S., Magnetic separation of malaria-infected red blood cells in various developmental stages. *Analytical chemistry* 2013, *85* (15), 7316-7323.

41. Lin, C.-Y.; Wei, P.-L.; Chang, W.-J.; Huang, Y.-K.; Feng, S.-W.; Lin, C.-T.; Lee, S.-Y.; Huang, H.-M., Slow freezing coupled static magnetic field exposure enhances cryopreservative efficiency—A study on human erythrocytes. *PloS one* 2013, *8* (3), e58988.

42. Chionna, A.; Tenuzzo, B.; Panzarini, E.; Dwikat, M. B.; Abbro, L.; Dini, L., Time dependent modifications of Hep G2 cells during exposure to static magnetic fields. *Bioelectromagnetics* 2005, *26* (4), 275-286.

43. Mo, W.-c.; Zhang, Z.-j.; Liu, Y.; Bartlett, P. F.; He, R.-q., Magnetic shielding accelerates the proliferation of human neuroblastoma cell by promoting G1-phase progression. *PloS one* 2013, *8* (1), e54775.

44. Wang, J.; Xiang, B.; Deng, J.; Freed, D. H.; Arora, R. C.; Tian, G., Inhibition of viability, proliferation, cytokines secretion, surface antigen expression, and adipogenic and osteogenic differentiation of adipose-derived stem cells by seven-day exposure to 0.5 T static magnetic fields. *Stem cells international* 2016, *2016*.

45. Marędziak, M.; Tomaszewski, K.; Polinceusz, P.; Lewandowski, D.; Marycz, K., Static magnetic field enhances the viability and proliferation rate of adipose tissue-derived mesenchymal stem cells potentially through activation of the phosphoinositide 3-kinase/Akt (PI3K/Akt) pathway. *Electromagnetic biology and medicine* 2017, *36* (1), 45-54.

46. Kim, S.; Im, W.-S.; Kang, L.; Lee, S.-T.; Chu, K.; Kim, B. I., The application of magnets directs the orientation of neurite outgrowth in cultured human neuronal cells. *Journal of neuroscience methods* 2008, *174* (1), 91-96.

47. Mo, W.-C.; Zhang, Z.-J.; Wang, D.-L.; Liu, Y.; Bartlett, P. F.; He, R.-Q., Shielding of the geomagnetic field alters actin assembly and inhibits cell motility in human neuroblastoma cells. *Scientific reports* 2016, *6*, 22624.

48. Glade, N.; Tabony, J., Brief exposure to high magnetic fields determines microtubule self-organisation by reaction–diffusion processes. *Biophysical chemistry* 2005, *115* (1), 29-35.

49. Zhang, L.; Hou, Y.; Li, Z.; Ji, X.; Wang, Z.; Wang, H.; Tian, X.; Yu, F.; Yang, Z.; Pi, L., 27 T ultra-high static magnetic field changes orientation and morphology of mitotic spindles in human cells. *elife* 2017, *6*, e22911.

50. Kose, A. R.; Fischer, B.; Mao, L.; Koser, H., Label-free cellular manipulation and sorting via biocompatible ferrofluids. *Proceedings of the National Academy of Sciences* 2009, *106* (51), 21478-21483.

51. Zhu, T.; Marrero, F.; Mao, L., Continuous separation of non-magnetic particles inside ferrofluids. *Microfluidics and nanofluidics* 2010, *9* (4-5), 1003-1009.

52. Zhu, T.; Cheng, R.; Lee, S. A.; Rajaraman, E.; Eiteman, M. A.; Querec, T. D.; Unger, E. R.; Mao, L., Continuous-flow ferrohydrodynamic sorting of particles and cells in microfluidic devices. *Microfluidics and nanofluidics* 2012, *13* (4), 645-654.

53. Winkleman, A.; Perez-Castillejos, R.; Gudiksen, K. L.; Phillips, S. T.; Prentiss, M.; Whitesides, G. M., Density-based diamagnetic separation: devices for detecting binding events and for collecting unlabeled diamagnetic particles in paramagnetic solutions. *Analytical chemistry* 2007, *79* (17), 6542-6550.

54. Shen, F.; Hwang, H.; Hahn, Y. K.; Park, J.-K., Label-free cell separation using a tunable magnetophoretic repulsion force. *Analytical chemistry* 2012, *84* (7), 3075-3081.

55. Abdel Fattah, A. R.; Meleca, E.; Mishriki, S.; Lelic, A.; Geng, F.; Sahu, R. P.; Ghosh, S.; Puri, I. K., In Situ 3D Label-Free Contactless Bioprinting of Cells through Diamagnetophoresis. *ACS Biomaterials Science & Engineering* 2016, *2* (12), 2133-2138.

56. Knowlton, S.; Sencan, I.; Aytar, Y.; Khoory, J.; Heeney, M.; Ghiran, I.; Tasoglu, S., Sickle cell detection using a smartphone. *Scientific reports* 2015, *5*.

57. Akiyama, Y.; Morishima, K. In *Label-free ultrarapid spheroid formation in microfluidic chip using magneto-Archimedes effect*, Micro Electro Mechanical Systems (MEMS), 2012 IEEE 25th International Conference on, 2012; IEEE: 2012; pp 116-119.

58. Rosensweig, R. E., *Ferrohydrodynamics*. Courier Corporation: 2013.

59. Zhao, W.; Cheng, R.; Lim, S. H.; Miller, J. R.; Zhang, W.; Tang, W.; Xie, J.; Mao, L., Biocompatible and Label-Free Separation of Cancer Cells of Cell Culture Lines from White Blood Cells in Ferrofluids. *Lab on a Chip* 2017.

60. Zhao, W.; Zhu, T.; Cheng, R.; Liu, Y.; He, J.; Qiu, H.; Wang, L.; Nagy, T.; Querec, T. D.; Unger, E. R., Label-Free and Continuous-Flow

Ferrohydrodynamic Separation of HeLa Cells and Blood Cells in Biocompatible Ferrofluids. *Advanced functional materials* 2015, *26* (22), 3990-3998.

61. Krebs, M. D.; Erb, R. M.; Yellen, B. B.; Samanta, B.; Bajaj, A.; Rotello, V. M.; Alsberg, E., Formation of ordered cellular structures in suspension via label-free negative magnetophoresis. *Nano letters* 2009, *9* (5), 1812-1817.

62. Tarn, M. D.; Hirota, N.; Iles, A.; Pamme, N., On-chip diamagnetic repulsion in continuous flow. *Science and technology of advanced materials* 2009, *10* (1), 014611.

63. Vojtíšek, M.; Tarn, M. D.; Hirota, N.; Pamme, N., Microfluidic devices in superconducting magnets: on-chip free-flow diamagnetophoresis of polymer particles and bubbles. *Microfluidics and nanofluidics* 2012, *13* (4), 625-635.

64. Mirica, K. A.; Shevkoplyas, S. S.; Phillips, S. T.; Gupta, M.; Whitesides, G. M., Measuring densities of solids and liquids using magnetic levitation: fundamentals. *Journal of the American Chemical Society* 2009, *131* (29), 10049-10058.

65. Sherry, A. D.; Caravan, P.; Lenkinski, R. E., Primer on gadolinium chemistry. *Journal of Magnetic Resonance Imaging* 2009, *30* (6), 1240-1248.

66. Idée, J. M.; Port, M.; Raynal, I.; Schaefer, M.; Le Greneur, S.; Corot, C., Clinical and biological consequences of transmetallation induced by contrast agents for magnetic resonance imaging: a review. *Fundamental & clinical pharmacology* 2006, *20* (6), 563-576.

67. Heinrich, M. C.; Kuhlmann, M. K.; Kohlbacher, S.; Scheer, M.; Grgic, A.; Heckmann, M. B.; Uder, M., Cytotoxicity of iodinated and gadolinium-based contrast agents in renal tubular cells at angiographic concentrations: in vitro study. *Radiology* 2007, *242* (2), 425-434.

68. Kauffmann, P.; Ith, A.; O'Brien, D.; Gaude, V.; Boué, F.; Combe, S.; Bruckert, F.; Schaack, B.; Dempsey, N. M.; Haguet, V., Diamagnetically trapped arrays of living cells above micromagnets. *Lab on a Chip* 2011, *11* (18), 3153-3161.

69. Schmitt-Willich, H., Stability of linear and macrocyclic gadolinium based contrast agents. *The British journal of radiology* 2007, *80* (955), 581-582.

70. Winkleman, A.; Gudiksen, K. L.; Ryan, D.; Whitesides, G. M.; Greenfield, D.; Prentiss, M., A magnetic trap for living cells suspended in a paramagnetic buffer. *Applied physics letters* 2004, *85* (12), 2411-2413.

71. Tocchio, A.; Durmus, N. G.; Sridhar, K.; Mani, V.; Coskun, B.; El Assal, R.; Demirci, U., Magnetically Guided Self-Assembly and Coding of 3D Living Architectures. *Advanced Materials* 2017.

72. Zeng, J.; Chen, C.; Vedantam, P.; Brown, V.; Tzeng, T.-R. J.; Xuan, X., Three-dimensional magnetic focusing of particles and cells in ferrofluid flow through a straight microchannel. *Journal of Micromechanics and Microengineering* 2012, *22* (10), 105018.

73. Zhao, W.; Cheng, R.; Jenkins, B. D.; Zhu, T.; Okonkwo, N. E.; Jones, C. E.; Davis, M. B.; Kavuri, S. K.; Hao, Z.; Schroeder, C., Label-free Ferrohydrodynamic Cell Separation of Circulating Tumor Cells. *Lab on a Chip* 2017.

74. Ji, H. M.; Samper, V.; Chen, Y.; Heng, C. K.; Lim, T. M.; Yobas, L., Silicon-based microfilters for whole blood cell separation. *Biomedical Microdevices* 2008, *10* (2), 251-257.

75. Huang, S.-B.; Wu, M.-H.; Lin, Y.-H.; Hsieh, C.-H.; Yang, C.-L.; Lin, H.-C.; Tseng, C.-P.; Lee, G.-B., High-purity and label-free isolation of circulating tumor cells (CTCs) in a microfluidic platform by using optically-induced-dielectrophoretic (ODEP) force. *Lab on a Chip* 2013, *13* (7), 1371-1383.

76. Karabacak, N. M.; Spuhler, P. S.; Fachin, F.; Lim, E. J.; Pai, V.; Ozkumur, E.; Martel, J. M.; Kojic, N.; Smith, K.; Chen, P.-i., Microfluidic, marker-free isolation of circulating tumor cells from blood samples. *Nature protocols* 2014, *9* (3), 694-694.

77. Ho, P.-L., Magnetic nanoparticles for pathogen detection. *Pathology* 2014, *46*, S45.

78. Huang, G.; Huang, Q.; Xie, L.; Xiang, G.; Wang, L.; Xu, H.; Ma, L.; Luo, X.; Xin, J.; Zhou, X.; Jin, X.; Zhang, L., A rapid, low-cost, and microfluidic chip-based system for parallel identification of multiple pathogens related to clinical pneumonia. *Scientific Reports* 2017, *7* (1), 6441.

79. Cheng, X.; Irimia, D.; Dixon, M.; Ziperstein, J. C.; Demirci, U.; Zamir, L.; Tompkins, R. G.; Toner, M.; Rodriguez, W. R., A microchip approach for practical label-free CD4+ T-cell counting of HIV-infected subjects in resource-poor settings. *JAIDS Journal of Acquired Immune Deficiency Syndromes* 2007, *45* (3), 257-261.

80. Boyle, D. S.; Hawkins, K. R.; Steele, M. S.; Singhal, M.; Cheng, X., Emerging technologies for point-of-care CD4 T-lymphocyte counting. *Trends in Biotechnology* 2012, *30* (1), 45-54.

81. Stephens, M.; Talary, M. S.; Pethig, R.; Burnett, A. K.; Mills, K. I., The dielectrophoresis enrichment of CD34+ cells from peripheral blood stem cell harvests. *Bone marrow transplantation* 1996, *18* (4), 777-782.

82. Muslimov, A. R.; Timin, A. S.; Petrova, A. V.; Epifanovskaya, O. S.; Shakirova, A. I.; Lepik, K. V.; Gorshkov, A.; Il'Inskaja, E. V.; Vasin, A. V.; Afanasyev, B. V.; Fehse, B.; Sukhorukov, G. B., Mesenchymal Stem Cells Engineering: Microcapsules-Assisted Gene Transfection and Magnetic Cell Separation. *ACS Biomaterials Science and Engineering* 2017, *3* (10), 2314-2324.

83. Ger, T.-R.; Huang, C.-Y.; Lai, M.-F., Cell culture arrangement using ferromagnetic diamond-shaped thin films. *IEEE Transactions on Magnetics* 2013, *49* (7), 3453-3455.

84. Tseng, H.; Balaoing, L. R.; Grigoryan, B.; Raphael, R. M.; Killian, T.; Souza, G. R.; Grande-Allen, K. J., A three-dimensional co-culture model of the aortic valve using magnetic levitation. *Acta biomaterialia* 2014, *10* (1), 173-182.

85. Fuhr, G.; Glasser, H.; Müller, T.; Schnelle, T., Cell manipulation and cultivation under a.c. electric field influence in highly conductive culture media. *Biochimica et Biophysica Acta (BBA) - General Subjects* 1994, *1201* (3), 353-360.

86. Voldman, J., Electrical forces for microscale cell manipulation. *Annual review of biomedical engineering* 2006, *8*, 425-454.

87. Čemažar, J.; Douglas, T. A.; Schmelz, E. M.; Davalos, R. V., Enhanced contactless dielectrophoresis enrichment and isolation platform via cell-scale microstructures. *Biomicrofluidics* 2016, *10* (1), 14109-14109.

88. Chronis, N.; Lee, L. P., Electrothermally activated SU-8 microgripper for single cell manipulation in solution. *Journal of Microelectromechanical systems* 2005, *14* (4), 857-863.

89. Kim, S. M.; Lee, S. H.; Suh, K. Y., Cell research with physically modified microfluidic channels: A review. *Lab on a Chip* 2008, *8* (7), 1015-1023.

90. Lo, C.-M.; Wang, H.-B.; Dembo, M.; Wang, Y.-l., Cell movement is guided by the rigidity of the substrate. *Biophysical journal* 2000, *79* (1), 144-152.

91. Jin, A.; Ozawa, T.; Tajiri, K.; Obata, T.; Kondo, S.; Kinoshita, K.; Kadowaki, S.; Takahashi, K.; Sugiyama, T.; Kishi, H., A rapid and efficient single-cell manipulation method for screening antigen-specific antibody–secreting cells from human peripheral blood. *Nature medicine* 2009, *15* (9), 1088-1092.

92. Coakley, W. T.; Bardsley, D. W.; Grundy, M. A.; Zamani, F.; Clarke, D. J., Cell manipulation in ultrasonic standing wave fields. *Journal of Chemical Technology and Biotechnology* 1989, *44* (1), 43-62.

93. Laurell, T.; Petersson, F.; Nilsson, A., Chip integrated strategies for acoustic separation and manipulation of cells and particles. *Chemical Society Reviews* 2007, *36* (3), 492-506.

94. Lenshof, A.; Johannesson, C.; Evander, M.; Nilsson, J.; Laurell, T., Acoustic Cell Manipulation BT - Microtechnology for Cell Manipulation and Sorting. Lee, W.; Tseng, P.; Di Carlo, D., Eds. Springer International Publishing: Cham, 2017; pp 129-173.

95. Ashkin, A.; Dziedzic, J. M.; Yamane, T., Optical trapping and manipulation of single cells using infrared laser beams. *Nature* 1987, *330* (6150), 769-771.

96. Cheng, J.; Rahman, M. A.; Ohta, A. T., Optical Manipulation of Cells BT - Microtechnology for Cell Manipulation and Sorting. Lee, W.; Tseng, P.; Di Carlo, D., Eds. Springer International Publishing: Cham, 2017; pp 93-128.

97. Grier, D. G., A revolution in optical manipulation. *Nature* 2003, *424* (6950), 810-816.

98. Pamme, N.; Manz, A., On-Chip Free-Flow Magnetophoresis: Continuous Flow Separation of Magnetic Particles and Agglomerates. *Analytical Chemistry* 2004, *76* (24), 7250-7256.

99. Zhao, W.; Cheng, R.; Miller, J. R.; Mao, L., Label-Free Microfluidic Manipulation of Particles and Cells in Magnetic Liquids. *Advanced Functional Materials* 2016, *26* (22), 3916-3932.

100. Wiklund, M.; Günther, C.; Lemor, R.; Jäger, M.; Fuhr, G.; Hertz, H. M., Ultrasonic standing wave manipulation technology integrated into a dielectrophoretic chip. *Lab on a Chip* 2006, *6* (12), 1537-1544.

101. Morais, P. C.; Santos, R. L.; Pimenta, A. C. M.; Azevedo, R. B.; Lima, E. C. D., Preparation and characterization of ultra-stable biocompatible magnetic fluids using citrate-coated cobalt ferrite nanoparticles. *Thin solid films* 2006, *515* (1), 266-270.

102. Zeng, J.; Deng, Y.; Vedantam, P.; Tzeng, T. R.; Xuan, X., Magnetic separation of particles and cells in ferrofluid flow through a straight microchannel using two offset magnets. *Journal of Magnetism and Magnetic Materials* 2013, *346*, 118-123.

103. Nguyen, N. T., Micro-magnetofluidics: Interactions between magnetism and fluid flow on the microscale. *Microfluidics and Nanofluidics* 2012, *12* (1-4), 1-16.

104. Mattix, B.; Olsen, T. R.; Gu, Y.; Casco, M.; Herbst, A.; Simionescu, D. T.; Visconti, R. P.; Kornev, K. G.; Alexis, F., Biological magnetic cellular spheroids as building blocks for tissue engineering. *Acta biomaterialia* 2014, *10* (2), 623-629.

105. Parfenov, V. A.; Koudan, E. V.; Bulanova, E. A.; Karalkin, P. A.; Pereira, F. D.; Norkin, N. E.; Knyazeva, A. D.; Gryadunova, A. A.; Petrov, O. F.; Vasiliev,

M., Scaffold-free, label-free and nozzle-free biofabrication technology using magnetic levitational assembly. *Biofabrication* 2018.

106. Ino, K.; Okochi, M.; Honda, H., Application of magnetic force-based cell patterning for controlling cell–cell interactions in angiogenesis. *Biotechnology and bioengineering* 2009, *102* (3), 882-890.

107. Whatley, B. R.; Li, X.; Zhang, N.; Wen, X., Magnetic-directed patterning of cell spheroids. *Journal of biomedical materials research Part A* 2014, *102* (5), 1537-1547.

108. Ito, A.; Takizawa, Y.; Honda, H.; Hata, K.-i.; Kagami, H.; Ueda, M.; Kobayashi, T., Tissue engineering using magnetite nanoparticles and magnetic force: heterotypic layers of cocultured hepatocytes and endothelial cells. *Tissue engineering* 2004, *10* (5-6), 833-840.

109. Ishii, M.; Shibata, R.; Shimizu, Y.; Yamamoto, T.; Kondo, K.; Inoue, Y.; Ouchi, N.; Tanigawa, T.; Kanemura, N.; Ito, A., Multilayered adipose-derived regenerative cell sheets created by a novel magnetite tissue engineering method for myocardial infarction. *International journal of cardiology* 2014, *175* (3), 545-553.

110. Thevenot, P.; Sohaebuddin, S.; Poudyal, N.; Liu, J. P.; Tang, L. In *Magnetic nanoparticles to enhance cell seeding and distribution in tissue engineering scaffolds*, Nanotechnology, 2008. NANO'08. 8th IEEE Conference on, IEEE: 2008; pp 646-649.

111. Küstermann, E.; Himmelreich, U.; Kandal, K.; Geelen, T.; Ketkar, A.; Wiedermann, D.; Strecker, C.; Esser, J.; Arnhold, S.; Hoehn, M., Efficient stem cell labeling for MRI studies. *Contrast media & molecular imaging* 2008, *3* (1), 27-37.

112. Wildgruber, M.; Lee, H.; Chudnovskiy, A.; Yoon, T.-J.; Etzrodt, M.; Pittet, M. J.; Nahrendorf, M.; Croce, K.; Libby, P.; Weissleder, R., Monocyte subset dynamics in human atherosclerosis can be profiled with magnetic nano-sensors. *PloS one* 2009, *4* (5), e5663.

113. Chen, C.-C. V.; Ku, M.-C.; Jayaseema, D.; Lai, J.-S.; Hueng, D.-Y.; Chang, C., Simple SPION incubation as an efficient intracellular labeling method for tracking neural progenitor cells using MRI. *PloS one* 2013, *8* (2), e56125.

114. Calero, M.; Gutiérrez, L.; Salas, G.; Luengo, Y.; Lázaro, A.; Acedo, P.; Morales, M. P.; Miranda, R.; Villanueva, A., Efficient and safe internalization of magnetic iron oxide nanoparticles: two fundamental requirements for biomedical applications. *Nanomedicine: Nanotechnology, Biology and Medicine* 2014, *10* (4), 733-743.

115. Kostura, L.; Kraitchman, D. L.; Mackay, A. M.; Pittenger, M. F.; Bulte, J. W., Feridex labeling of mesenchymal stem cells inhibits chondrogenesis but not adipogenesis or osteogenesis. *NMR in Biomedicine* 2004, *17* (7), 513-517.

116. Kedziorek, D. A.; Muja, N.; Walczak, P.; Ruiz-Cabello, J.; Gilad, A. A.; Jie, C. C.; Bulte, J. W., Gene expression profiling reveals early cellular responses to intracellular magnetic labeling with superparamagnetic iron oxide nanoparticles. *Magnetic resonance in medicine* 2010, *63* (4), 1031-1043.

117. Wang, Z. M.; Wu, R. G.; Wang, Z. P.; Ramanujan, R. V., Magnetic Trapping of Bacteria at Low Magnetic Fields. *Scientific Reports* 2016, *6*, 26945-26945.

118. Sarigil, O.; Anil-Inevi, M.; Yilmaz, E.; Mese, G.; Tekin, H. C.; Ozcivici, E., Label-free density-based detection of adipocytes of bone marrow origin using magnetic levitation. *Analyst* 2019, *144* (9), 2942-2953.

119. Akiyama, Y.; Morishima, K., Label-free cell aggregate formation based on the magneto-Archimedes effect. *Applied Physics Letters* 2011, *98* (16), 163702.

120. Tasoglu, S.; Yu, C. H.; Liaudanskaya, V.; Guven, S.; Migliaresi, C.; Demirci, U., Magnetic levitational assembly for living material fabrication. *Advanced healthcare materials* 2015, *4* (10), 1469-1476.

121. Qian, A.; Yin, D.; Yang, P.; Lv, Y.; Tian, Z.; Shang, P., Application of diamagnetic levitation technology in biological sciences research. *IEEE Transactions on Applied Superconductivity* 2013, *23* (1), 3600305-3600305.

122. Rivron, N. C.; Rouwkema, J.; Truckenmüller, R.; Karperien, M.; De Boer, J.; Van Blitterswijk, C. A., Tissue assembly and organization: developmental mechanisms in microfabricated tissues. *Biomaterials* 2009, *30* (28), 4851-4858.

123. Yaman, S.; Anil-Inevi, M.; Ozcivici, E.; Tekin, H. C., Magnetic force-based microfluidic techniques for cellular and tissue bioengineering. *Frontiers in bioengineering and biotechnology* 2018, *6*, 192.

124. Akiyama, Y.; Morishima, K. In *Spheroid array formation by non-label cell manipulation using magneto-Archimedes effect*, Micro-NanoMechatronics and Human Science (MHS), 2011 International Symposium on, IEEE: 2011; pp 45-50.

125. Mirica, K. A.; Phillips, S. T.; Mace, C. R.; Whitesides, G. M., Magnetic levitation in the analysis of foods and water. *Journal of agricultural and food chemistry* 2010, *58* (11), 6565-6569.

126. Mirica, K. A.; Ilievski, F.; Ellerbee, A. K.; Shevkoplyas, S. S.; Whitesides, G. M., Using Magnetic Levitation for Three Dimensional Self-Assembly. *Advanced Materials* 2011, *23* (36), 4134-4140.

127. Tasoglu, S.; Khoory, J. A.; Tekin, H. C.; Thomas, C.; Karnoub, A. E.; Ghiran, I. C.; Demirci, U., Levitational image cytometry with temporal resolution. *Advanced Materials* 2015, *27* (26), 3901-3908.

128. Anil-Inevi, M.; Yaman, S.; Yildiz, A. A.; Mese, G.; Yalcin-Ozuysal, O.; Tekin, H. C.; Ozcivici, E., Biofabrication of in situ self assembled 3D cell cultures in a weightlessness environment generated using magnetic levitation. *Scientific reports* 2018, *8* (1), 7239.

129. Anil-Inevi, M.; Delikoyun, K.; Mese, G.; Tekin, H. C.; Ozcivici, E., Axial-circular magnetic levitation assisted biofabrication and manipulation of cellular structures. *bioRxiv* 2021.

130. Garrett-Bakelman, F. E.; Darshi, M.; Green, S. J.; Gur, R. C.; Lin, L.; Macias, B. R.; McKenna, M. J.; Meydan, C.; Mishra, T.; Nasrini, J., The NASA Twins Study: A multidimensional analysis of a year-long human spaceflight. *Science* 2019, *364* (6436), eaau8650.

131. Buravkova, L.; Rykova, M.; Grigorieva, V.; Antropova, E., Cell interactions in microgravity: cytotoxic effects of natural killer cells in vitro. *Journal of gravitational physiology: a journal of the International Society for Gravitational Physiology* 2004, *11* (2), P177-80.

132. Kacena, M. A.; Todd, P.; Landis, W. J., Osteoblasts subjected to spaceflight and simulated space shuttle launch conditions. *In Vitro Cellular & Developmental Biology-Animal* 2003, *39* (10), 454-459.

133. Buravkova, L.; Romanov, Y. A.; Konstantinova, N.; Buravkov, S.; Gershovich, Y. G.; Grivennikov, I., Cultured stem cells are sensitive to gravity changes. *Acta astronautica* 2008, *63* (5-6), 603-608.

134. Ozcivici, E.; Luu, Y. K.; Adler, B.; Qin, Y.-X.; Rubin, J.; Judex, S.; Rubin, C. T., Mechanical signals as anabolic agents in bone. *Nature Reviews Rheumatology* 2010, *6* (1), 50.

135. Benjamin, M.; Hillen, B., Mechanical influences on cells, tissues and organs-'Mechanical Morphogenesis'. *European journal of morphology* 2003, *41* (1), 3-7.

136. Fitts, R. H.; Riley, D. R.; Widrick, J. J., Functional and structural adaptations of skeletal muscle to microgravity. *Journal of Experimental Biology* 2001, *204* (18), 3201-3208.

137. Vico, L.; Collet, P.; Guignandon, A.; Lafage-Proust, M.-H.; Thomas, T.; Rehailia, M.; Alexandre, C., Effects of long-term microgravity exposure on cancellous and cortical weight-bearing bones of cosmonauts. *The Lancet* 2000, *355* (9215), 1607-1611.

138. Crucian, B. E.; Stowe, R. P.; Pierson, D. L.; Sams, C. F., Immune system dysregulation following short-vs long-duration spaceflight. *Aviation, space, and environmental medicine* 2008, *79* (9), 835-843.

139. Aubert, A. E.; Beckers, F.; Verheyden, B., Cardiovascular function and basics of physiology in microgravity. *Acta cardiologica* 2005, *60* (2), 129-151.

140. Tamma, R.; Colaianni, G.; Camerino, C.; Di Benedetto, A.; Greco, G.; Strippoli, M.; Vergari, R.; Grano, A.; Mancini, L.; Mori, G., Microgravity during spaceflight directly affects in vitro osteoclastogenesis and bone resorption. *The FASEB Journal* 2009, *23* (8), 2549-2554.

141. Sandonà, D.; Desaphy, J.-F.; Camerino, G. M.; Bianchini, E.; Ciciliot, S.; Danieli-Betto, D.; Dobrowolny, G.; Furlan, S.; Germinario, E.; Goto, K., Adaptation of mouse skeletal muscle to long-term microgravity in the MDS mission. *PloS one* 2012, *7* (3), e33232.

142. Delikoyun, K.; Cine, E.; Anil-Inevi, M.; Ozuysal, M.; Ozcivici, E.; Tekin, H. C. In *Lensless Digital in-Line Holographic Microscopy for Space Biotechnology Applications*, 2019 9th International Conference on Recent Advances in Space Technologies (RAST), IEEE: 2019; pp 937-940.

143. Anken, R., Simulation of microgravity for studies in gravitational biology: principles, devices and applications. *Current Biotechnology* 2013, *2* (3), 192-200.

144. Wagner, E. B.; Granzella, N. P.; Saito, H.; Newman, D. J.; Young, L. R.; Bouxsein, M. L., Partial weight suspension: a novel murine model for investigating adaptation to reduced musculoskeletal loading. *Journal of applied physiology* 2010, *109* (2), 350-357.

145. Ozcivici, E.; Garman, R.; Judex, S., High-frequency oscillatory motions enhance the simulated mechanical properties of non-weight bearing trabecular bone. *Journal of biomechanics* 2007, *40* (15), 3404-3411.

146. Ozcivici, E.; Judex, S., Trabecular bone recovers from mechanical unloading primarily by restoring its mechanical function rather than its morphology. *Bone* 2014, *67*, 122-129.

147. Ozcivici, E.; Zhang, W.; Donahue, L. R.; Judex, S., Quantitative trait loci that modulate trabecular bone's risk of failure during unloading and reloading. *Bone* 2014, *64*, 25-32.

148. Judex, S.; Zhang, W.; Donahue, L. R.; Ozcivici, E., Genetic loci that control the loss and regain of trabecular bone during unloading and reambulation. *Journal of Bone and Mineral Research* 2013, *28* (7), 1537-1549.

149. Judex, S.; Zhang, W.; Donahue, L. R.; Ozcivici, E., Genetic and tissue level muscle-bone interactions during unloading and reambulation. *Journal of musculoskeletal & neuronal interactions* 2016, *16* (3), 174.

150. Morey-Holton, E. R.; Globus, R. K., Hindlimb unloading rodent model: technical aspects. *Journal of applied physiology* 2002, *92* (4), 1367-1377.

151. Rucci, N.; Migliaccio, S.; Zani, B. M.; Taranta, A.; Teti, A., Characterization of the osteoblast-like cell phenotype under microgravity conditions in the NASA-approved rotating wall vessel bioreactor (RWV). *Journal of cellular biochemistry* 2002, *85* (1), 167-179.

152. Qian, A.; Li, D.; Han, J.; Gao, X.; Di, S.; Zhang, W.; Hu, L.; Shang, P., Fractal dimension as a measure of altered actin cytoskeleton in MC3T3-E1 cells under simulated microgravity using 3-D/2-D clinostats. *IEEE Transactions on Biomedical Engineering* 2012, *59* (5), 1374-1380.

153. Wuest, S. L.; Richard, S.; Kopp, S.; Grimm, D.; Egli, M., Simulated microgravity: critical review on the use of random positioning machines for mammalian cell culture. *BioMed research international* 2015, *2015*.

154. Pavalko, F. M.; Chen, N. X.; Turner, C. H.; Burr, D. B.; Atkinson, S.; Hsieh, Y.-F.; Qiu, J.; Duncan, R. L., Fluid shear-induced mechanical signaling in MC3T3-E1 osteoblasts requires cytoskeleton-integrin interactions. *American Journal of Physiology-Cell Physiology* 1998, *275* (6), C1591-C1601.

155. Kaysen, J.; Campbell, W.; Majewski, R.; Goda, F.; Navar, G.; Lewis, F.; Goodwin, T.; Hammond, T., Select de novo gene and protein expression during renal epithelial cell culture in rotating wall vessels is shear stress dependent. *Journal of Membrane Biology* 1999, *168* (1), 77-89.

156. Souza, G. R.; Molina, J. R.; Raphael, R. M.; Ozawa, M. G.; Stark, D. J.; Levin, C. S.; Bronk, L. F.; Ananta, J. S.; Mandelin, J.; Georgescu, M.-M., Three-dimensional tissue culture based on magnetic cell levitation. *Nature nanotechnology* 2010, *5* (4), 291-296.

157. Haisler, W. L.; Timm, D. M.; Gage, J. A.; Tseng, H.; Killian, T.; Souza, G. R., Three-dimensional cell culturing by magnetic levitation. *Nature protocols* 2013, *8* (10), 1940-1949.

158. Schenck, J. F., Health and physiological effects of human exposure to whole-body four-tesla magnetic fields during MRI. *Annals of the New York Academy of Sciences* 1992, *649* (1), 285-301.

159. Sarigil, O.; Anil-Inevi, M.; Yilmaz, E.; Cagan, M.; Mese, G.; Tekin, H. C.; Ozcivici, E. In *Application of Magnetic Levitation Induced Weightlessness to*

Detect Cell Lineage, 2019 9th International Conference on Recent Advances in Space Technologies (RAST), IEEE: 2019; pp 933-935.

160. Delikoyun, K.; Yaman, S.; Anil-Inevi, M.; Ozcivici, E.; Tekin, H. C. In *Cell Separation with Hybrid Magnetic Levitation-Based Lensless Holographic Microscopy Platform*, 2019 Medical Technologies Congress (TIPTEKNO), IEEE: 2019; pp 1-4.

161. Delikoyun, K.; Yaman, S.; Yilmaz, E.; Sarigil, O.; Anil-Inevi, M.; Ozcivici, E.; Tekin, H. C., HologLev: Hybrid Magnetic Levitation Platform Integrated with Lensless Holographic Microscopy for Density-Based Cell Analysis. *bioRxiv* 2020.

162. Anil-Inevi, M.; Yalcin-Ozuysal, O.; Sarigil, O.; Mese, G.; Ozcivici, E.; Yaman, S.; Tekin, H. C. In *Biofabrication of Cellular Structures Using Weightlessness as a Biotechnological Tool*, 2019 9th International Conference on Recent Advances in Space Technologies (RAST), IEEE: 2019; pp 929-931.

163. Anil-Inevi, M.; Sarigil, O.; Kizilkaya, M.; Mese, G.; Tekin, H. C.; Ozcivici, E., Stem Cell Culture Under Simulated Microgravity. *Cell Biology and Translational Medicine, Volume 10: Stem Cells in Tissue Regeneration* 2020, 105-132.

164. Sarigil, O.; Anil-Inevi, M.; Firatligil-Yildirir, B.; Unal, Y. C.; Yalcin-Ozuysal, O.; Mese, G.; Tekin, H. C.; Ozcivici, E., Scaffold-free biofabrication of adipocyte structures with magnetic levitation. *Biotechnology and bioengineering* 2021, *118* (3), 1127-1140.

165. Sarigil, O.; Anil-Inevi, M.; Yilmaz, E.; Ozcelik, O.; Mese, G.; Tekin, H. C.; Ozcivici, E. In *Magnetic levitation-based adipose tissue engineering using horizontal magnet deployment*, 2020 Medical Technologies Congress (TIPTEKNO), IEEE: 2020; pp 1-4.

166. Anil-Inevi, M.; Unal, Y. C.; Yaman, S.; Tekin, H. C.; Mese, G.; Ozcivici, E. In *Assessment of cell cycle and viability of magnetic levitation assembled cellular structures*, 2020 Medical Technologies Congress (TIPTEKNO), IEEE: 2020; pp 1-4.

167. Anil-Inevi, M.; Yilmaz, E.; Sarigil, O.; Tekin, H. C.; Ozcivici, E., Single cell densitometry and weightlessness culture of mesenchymal stem cells using magnetic levitation. In *Stem Cell Nanotechnology*, Springer: 2019; pp 15-25.

168. Kumar, A. A.; Patton, M. R.; Hennek, J. W.; Lee, S. Y. R.; D'Alesio-Spina, G.; Yang, X.; Kanter, J.; Shevkoplyas, S. S.; Brugnara, C.; Whitesides, G. M., Density-based separation in multiphase systems provides a simple method to identify sickle cell disease. *Proceedings of the National Academy of Sciences* 2014, *111* (41), 14864-14869.

169. Zhao, Y.; Lai, H. S. S.; Zhang, G.; Lee, G.-B.; Li, W. J., Rapid determination of cell mass and density using digitally controlled electric field in a microfluidic chip. *Lab on a Chip* 2014, *14* (22), 4426-4434.

170. Bryan, A. K.; Hecht, V. C.; Shen, W.; Payer, K.; Grover, W. H.; Manalis, S. R., Measuring single cell mass, volume, and density with dual suspended microchannel resonators. *Lab on a Chip* 2014, *14* (3), 569-576.

171. Kelland, D.; Hiresaki, Y.; Friedlaender, F.; Takayasu, M., Diamagnetic particle capture and mineral separation. *IEEE Transactions on Magnetics* 1981, *17* (6), 2813-2815.

172. Kendall, B.; Vollero, M.; Hinkle, L., Passive levitation of small particles in vacuum: Possible applications to vacuum gauging. *Journal of Vacuum Science & Technology A: Vacuum, Surfaces, and Films* 1987, *5* (4), 2458-2462.

173. Pardo, S. J.; Patel, M. J.; Sykes, M. C.; Platt, M. O.; Boyd, N. L.; Sorescu, G. P.; Xu, M.; van Loon, J. J.; Wang, M. D.; Jo, H., Simulated Microgravity Using the Random Positioning Machine Inhibits Differentiation and Alters Gene Expression Profiles of 2T3 Pre-osteoblasts. *American Journal of Physiology-Cell Physiology* 2005.

174. Qiu, Q.; Ducheyne, P.; Gao, H.; Ayyaswamy, P., Formation and differentiation of three-dimensional rat marrow stromal cell culture on microcarriers in a rotating-wall vessel. *Tissue engineering* 1998, *4* (1), 19-34.

175. Tocchio, A.; Durmus, N. G.; Sridhar, K.; Mani, V.; Coskun, B.; El Assal, R.; Demirci, U., Magnetically guided self-assembly and coding of 3D living architectures. *Advanced Materials* 2018, *30* (4), 1705034.

176. Knowlton, S. M.; Sencan, I.; Aytar, Y.; Khoory, J.; Heeney, M. M.; Ghiran, I. C.; Tasoglu, S., Sickle cell detection using a smartphone. *Sci Rep* 2015, *5*, 15022.

177. Knowlton, S.; Joshi, A.; Syrrist, P.; Coskun, A. F.; Tasoglu, S., 3D-printed smartphone-based point of care tool for fluorescence- and magnetophoresis-based cytometry. *Lab Chip* 2017, *17* (16), 2839-2851.

178. Moes, M. J.; Gielen, J. C.; Bleichrodt, R.-J.; van Loon, J. J.; Christianen, P. C.; Boonstra, J., Simulation of microgravity by magnetic levitation and random positioning: effect on human A431 cell morphology. *Microgravity Science and Technology* 2011, *23* (2), 249-261.

179. Türker, E.; Demirçak, N.; Arslan-Yildiz, A., Scaffold-free three-dimensional cell culturing using magnetic levitation. *Biomaterials Science* 2018, *6* (7), 1745-1753.

180. Baskan, O.; Mese, G.; Ozcivici, E., Low-intensity vibrations normalize adipogenesis-induced morphological and molecular changes of adult

mesenchymal stem cells. *Proceedings of the Institution of Mechanical Engineers, Part H: Journal of Engineering in Medicine* 2017, *231* (2), 160-168.

181. Sherry, A. D.; Caravan, P.; Lenkinski, R. E., Primer on gadolinium chemistry. *Journal of Magnetic Resonance Imaging: An Official Journal of the International Society for Magnetic Resonance in Medicine* 2009, *30* (6), 1240-1248.

182. Ge, S.; Wang, Y.; Deshler, N. J.; Preston, D. J.; Whitesides, G. M., High-throughput density measurement using magnetic levitation. *Journal of the American Chemical Society* 2018, *140* (24), 7510-7518.

183. Zhang, C.; Zhao, P.; Gu, F.; Xie, J.; Xia, N.; He, Y.; Fu, J., Single-ring magnetic levitation configuration for object manipulation and density-based measurement. *Analytical chemistry* 2018, *90* (15), 9226-9233.

184. Tamm, C.; Sabri, F.; Ceccatelli, S., Mitochondrial-mediated apoptosis in neural stem cells exposed to manganese. *Toxicological Sciences* 2007, *101* (2), 310-320.

185. Brady, R. T.; O'Brien, F. J.; Hoey, D. A., Mechanically stimulated bone cells secrete paracrine factors that regulate osteoprogenitor recruitment, proliferation, and differentiation. *Biochemical and biophysical research communications* 2015, *459* (1), 118-123.

186. Pathak, M. M.; Nourse, J. L.; Tran, T.; Hwe, J.; Arulmoli, J.; Dai Trang, T. L.; Bernardis, E.; Flanagan, L. A.; Tombola, F., Stretch-activated ion channel Piezo1 directs lineage choice in human neural stem cells. *Proceedings of the National Academy of Sciences* 2014, *111* (45), 16148-16153.

187. Ogawa, H.; Kozhemyakina, E.; Hung, H.-H.; Grodzinsky, A. J.; Lassar, A. B., Mechanical motion promotes expression of Prg4 in articular cartilage via multiple CREB-dependent, fluid flow shear stress-induced signaling pathways. *Genes & development* 2014, *28* (2), 127-139.

188. Ozcivici, E.; Luu, Y. K.; Adler, B.; Qin, Y.-X.; Rubin, J.; Judex, S.; Rubin, C. T., Mechanical signals as anabolic agents in bone. *Nature Reviews Rheumatology* 2010, *6* (1), 50-59.

189. Ingber, D. E., Mechanical control of tissue growth: function follows form. *Proceedings of the National Academy of Sciences of the United States of America* 2005, *102* (33), 11571-11572.

190. Orr, A. W.; Helmke, B. P.; Blackman, B. R.; Schwartz, M. A., Mechanisms of mechanotransduction. *Developmental cell* 2006, *10* (1), 11-20.

191. Grigoriev, A. I.; Egorov, A. D., General mechanisms of the effect of weightlessness on the human body. *Advances in space biology and medicine* 1992, *2*, 1-42.

192. Sibonga, J. D.; Evans, H. J.; Sung, H.; Spector, E.; Lang, T.; Oganov, V.; Bakulin, A.; Shackelford, L.; LeBlanc, A., Recovery of spaceflight-induced bone loss: bone mineral density after long-duration missions as fitted with an exponential function. *Bone* 2007, *41* (6), 973-978.

193. Smith, S.; Abrams, S.; Davis-Street, J.; Heer, M.; O'Brien, K.; Wastney, M.; Zwart, S., Fifty years of human space travel: implications for bone and calcium research. *Annual review of nutrition* 2014, *34*, 377-400.

194. Nagaraja, M. P.; Risin, D., The current state of bone loss research: data from spaceflight and microgravity simulators. *Journal of cellular biochemistry* 2013, *114* (5), 1001-1008.

195. Tesch, P. A.; Berg, H. E.; Bring, D.; Evans, H. J.; LeBlanc, A. D., Effects of 17-day spaceflight on knee extensor muscle function and size. *European journal of applied physiology* 2005, *93* (4), 463-468.

196. Ohira, T.; Kawano, F.; Ohira, T.; Goto, K.; Ohira, Y., Responses of skeletal muscles to gravitational unloading and/or reloading. *The Journal of Physiological Sciences* 2015, *65* (4), 293-310.

197. Aventaggiato, M.; Barreca, F.; Vernucci, E.; Bizzarri, M.; Ferretti, E.; Russo, M. A.; Tafani, M., Putative receptors for gravity sensing in mammalian cells: The effects of microgravity. *Applied Sciences* 2020, *10* (6), 2028.

198. Zayzafoon, M.; Gathings, W. E.; McDonald, J. M., Modeled microgravity inhibits osteogenic differentiation of human mesenchymal stem cells and increases adipogenesis. *Endocrinology* 2004, *145* (5), 2421-2432.

199. Zhang, C.; Li, L.; Jiang, Y.; Wang, C.; Geng, B.; Wang, Y.; Chen, J.; Liu, F.; Qiu, P.; Zhai, G., Space microgravity drives transdifferentiation of human bone marrow-derived mesenchymal stem cells from osteogenesis to adipogenesis. *The FASEB Journal* 2018, *32* (8), 4444-4458.

200. Luu, Y. K.; Capilla, E.; Rosen, C. J.; Gilsanz, V.; Pessin, J. E.; Judex, S.; Rubin, C. T., Mechanical stimulation of mesenchymal stem cell proliferation and differentiation promotes osteogenesis while preventing dietary-induced obesity. *Journal of Bone and Mineral Research* 2009, *24* (1), 50-61.

201. Paulsen, K.; Tauber, S.; Goelz, N.; Simmet, D. M.; Engeli, S.; Birlem, M.; Dumrese, C.; Karer, A.; Hunziker, S.; Biskup, J., Severe disruption of the cytoskeleton and immunologically relevant surface molecules in a human macrophageal cell line in microgravity—results of an in vitro experiment on board of the Shenzhou-8 space mission. *Acta Astronautica* 2014, *94* (1), 277-292.

202. Chatani, M.; Morimoto, H.; Takeyama, K.; Mantoku, A.; Tanigawa, N.; Kubota, K.; Suzuki, H.; Uchida, S.; Tanigaki, F.; Shirakawa, M., Acute

transcriptional up-regulation specific to osteoblasts/osteoclasts in medaka fish immediately after exposure to microgravity. *Scientific reports* 2016, *6*, 39545.

203. Gambara, G.; Salanova, M.; Ciciliot, S.; Furlan, S.; Gutsmann, M.; Schiffl, G.; Ungethuem, U.; Volpe, P.; Gunga, H.-C.; Blottner, D., Gene expression profiling in slow-type calf soleus muscle of 30 days space-flown mice. *PloS one* 2017, *12* (1), e0169314.

204. Herranz, R.; Anken, R.; Boonstra, J.; Braun, M.; Christianen, P. C.; de Geest, M.; Hauslage, J.; Hilbig, R.; Hill, R. J.; Lebert, M., Ground-based facilities for simulation of microgravity: organism-specific recommendations for their use, and recommended terminology. *Astrobiology* 2013, *13* (1), 1-17.

205. Begley, C. M.; Kleis, S. J., The fluid dynamic and shear environment in the NASA/JSC rotating-wall perfused-vessel bioreactor. *Biotechnology and bioengineering* 2000, *70* (1), 32-40.

206. Hammond, T.; Hammond, J., Optimized suspension culture: the rotating-wall vessel. *American Journal of Physiology-Renal Physiology* 2001, *281* (1), F12-F25.

207. Svejgaard, B.; Wehland, M.; Ma, X.; Kopp, S.; Sahana, J.; Warnke, E.; Aleshcheva, G.; Hemmersbach, R.; Hauslage, J.; Grosse, J., Common effects on cancer cells exerted by a random positioning machine and a 2d clinostat. *PLoS One* 2015, *10* (8), e0135157.

208. Hemmersbach, R.; Strauch, S. M.; Seibt, D.; Schuber, M., Comparative studies on gravisensitive protists on ground (2D and 3D clinostats) and in microgravity. *Microgravity Science and Technology* 2006, *18* (3), 257-259.

209. Pardo, S. J.; Patel, M. J.; Sykes, M. C.; Platt, M. O.; Boyd, N. L.; Sorescu, G. P.; Xu, M.; van Loon, J. J.; Wang, M. D.; Jo, H., Simulated microgravity using the Random Positioning Machine inhibits differentiation and alters gene expression profiles of 2T3 preosteoblasts. *American Journal of Physiology-Cell Physiology* 2005, *288* (6), C1211-C1221.

210. Beaugnon, E.; Tournier, R., Levitation of water and organic substances in high static magnetic fields. *Journal de Physique III* 1991, *1* (8), 1423-1428.

211. Tocchio, A.; Durmus, N. G.; Sridhar, K.; Mani, V.; Coskun, B.; El Assal, R.; Demirci, U., Magnetically Guided Self-Assembly and Coding of 3D Living Architectures. *Advanced Materials* 2017, *30* (4), 1705034.

212. Demiray, L.; Ozcivici, E., Bone marrow stem cells adapt to low-magnitude vibrations by altering their cytoskeleton during quiescence and osteogenesis. *Turkish Journal of Biology* 2015, *39* (1), 88-97.

213. Ivascu, A.; Kubbies, M., Rapid generation of single-tumor spheroids for high-throughput cell function and toxicity analysis. *Journal of biomolecular screening* 2006, *11* (8), 922-932.

214. Gijs, M. A.; Lacharme, F.; Lehmann, U., Microfluidic applications of magnetic particles for biological analysis and catalysis. *Chemical reviews* 2009, *110* (3), 1518-1563.

215. Ghosh, S.; Kumar, S.; Puri, I.; Elankumaran, S., Magnetic assembly of 3D cell clusters: visualizing the formation of an engineered tissue. *Cell proliferation* 2016, *49* (1), 134-144.

216. Grogan, S. P.; Pauli, C.; Chen, P.; Du, J.; Chung, C. B.; Kong, S. D.; Colwell Jr, C. W.; Lotz, M. K.; Jin, S.; D'Lima, D. D., In situ tissue engineering using magnetically guided three-dimensional cell patterning. *Tissue Engineering Part C: Methods* 2012, *18* (7), 496-506.

217. Mazuel, F.; Reffay, M.; Du, V.; Bacri, J.-C.; Rieu, J.-P.; Wilhelm, C., Magnetic flattening of stem-cell spheroids indicates a size-dependent elastocapillary transition. *Physical review letters* 2015, *114* (9), 098105.

218. Du, V.; Luciani, N.; Richard, S.; Mary, G.; Gay, C.; Mazuel, F.; Reffay, M.; Menasché, P.; Agbulut, O.; Wilhelm, C., A 3D magnetic tissue stretcher for remote mechanical control of embryonic stem cell differentiation. *Nature communications* 2017, *8* (1), 400.

219. Mattix, B. M.; Olsen, T. R.; Casco, M.; Reese, L.; Poole, J. T.; Zhang, J.; Visconti, R. P.; Simionescu, A.; Simionescu, D. T.; Alexis, F., Janus magnetic cellular spheroids for vascular tissue engineering. *Biomaterials* 2014, *35* (3), 949-960.

220. Lihua, Y.; Zhe, S.; Huixue, L.; Xiaoda, Y.; Kuiy, W., Gadolinium induced apoptosis of human embryo liver L02 cell line by ROS-mediated AIF pathway. *Journal of Rare Earths* 2011, *29* (2), 178-184.

221. Shen, L.; Yang, A.; Yao, P.; Sun, X.; Chen, C.; Mo, C.; Shi, L.; Chen, Y.; Liu, Q., Gadolinium promoted proliferation in mouse embryo fibroblast NIH3T3 cells through Rac and PI3K/Akt signaling pathways. *Biometals* 2014, *27* (4), 753-762.

222. Pan, Y.; Du, X.; Zhao, F.; Xu, B., Magnetic nanoparticles for the manipulation of proteins and cells. *Chemical Society Reviews* 2012, *41* (7), 2912-2942.

223. Zhao, W.; Cheng, R.; Miller, J. R.; Mao, L., Label-free microfluidic manipulation of particles and cells in magnetic liquids. *Advanced functional materials* 2016, *26* (22), 3916-3932.

224. Castro, E.; Mano, J. F., Magnetic force-based tissue engineering and regenerative medicine. 2013.

225. Chen, P.; Huang, Y.-Y.; Hoshino, K.; Zhang, J. X. J., Microscale Magnetic Field Modulation for Enhanced Capture and Distribution of Rare Circulating Tumor Cells. *Scientific Reports* 2015, *5* (1), 8745-8745.

226. Zeng, L.; Qiu, L.; Yang, X.-T.; Zhou, Y.-H.; Du, J.; Wang, H.-Y.; Sun, J.-H.; Yang, C.; Jiang, J.-X., Isolation of lung multipotent stem cells using a novel microfluidic magnetic activated cell sorting system. *Cell Biology International* 2015, *39* (11), 1348-1353.

227. Nam-Trung, N., Micro-magnetofluidics: interactions between magnetism and fluid flow on the microscale. *Microfluid Nanofluid* 2012, *12*, 1-16.

228. Haisler, W. L.; Timm, D. M.; Gage, J. A.; Tseng, H.; Killian, T.; Souza, G. R., Three-dimensional cell culturing by magnetic levitation. *Nature protocols* 2013, *8* (10), 1940.

229. Jeong, Y. G.; Lee, J. S.; Shim, J. K.; Hur, W., A scaffold-free surface culture of B16F10 murine melanoma cells based on magnetic levitation. *Cytotechnology* 2016, *68* (6), 2323-2334.

230. Robert, D.; Pamme, N.; Conjeaud, H.; Gazeau, F.; Iles, A.; Wilhelm, C., Cell sorting by endocytotic capacity in a microfluidic magnetophoresis device. *Lab on a chip* 2011, *11* (11), 1902-1910.

231. Tarn, M. D.; Peyman, S. A.; Robert, D.; Iles, A.; Wilhelm, C.; Pamme, N., The importance of particle type selection and temperature control for on-chip free-flow magnetophoresis. *Journal of magnetism and magnetic materials* 2009, *321* (24), 4115-4122.

232. Jing, Y.; Mal, N.; Williams, P. S.; Mayorga, M.; Penn, M. S.; Chalmers, J. J.; Zborowski, M., Quantitative intracellular magnetic nanoparticle uptake measured by live cell magnetophoresis. *The FASEB Journal* 2008, *22* (12), 4239-4247.

233. Simon, M.; Geim, A., Diamagnetic levitation: flying frogs and floating magnets. *Journal of applied physics* 2000, *87* (9), 6200-6204.

234. Menasche, B. L.; Crisman, L.; Gulbranson, D. R.; Davis, E. M.; Yu, H.; Shen, J., Fluorescence Activated Cell Sorting (FACS) in Genome-Wide Genetic Screening of Membrane Trafficking. *Current protocols in cell biology* 2019, *82* (1), e68.

235. Shen, Y.; Vignali, P.; Wang, R., Rapid profiling cell cycle by flow cytometry using concurrent staining of DNA and mitotic markers. *Bio Protoc* 2017, *7*, e2517.

236. Van Peer, G.; Mestdagh, P.; Vandesompele, J., Accurate RT-qPCR gene expression analysis on cell culture lysates. *Scientific reports* 2012, *2*, 222.

237. Morrison, W. A.; Marre, D.; Grinsell, D.; Batty, A.; Trost, N.; O'Connor, A. J., Creation of a large adipose tissue construct in humans using a tissue-engineering chamber: a step forward in the clinical application of soft tissue engineering. *EBioMedicine* 2016, *6*, 238-245.

238. Park, I. S.; Jin, R. L.; Oh, H. J.; Truong, M. D.; Choi, B. H.; Park, S. H.; Park, D. Y.; Min, B. H., Sizable Scaffold-Free Tissue-Engineered Articular Cartilage Construct for Cartilage Defect Repair. *Artificial organs* 2019, *43* (3), 278-287.

239. Subramaniam, A. B.; Yang, D.; Yu, H.-D.; Nemiroski, A.; Tricard, S.; Ellerbee, A. K.; Soh, S.; Whitesides, G. M., Noncontact orientation of objects in three-dimensional space using magnetic levitation. *Proceedings of the National Academy of Sciences* 2014, *111* (36), 12980-12985.

240. Ge, S.; Whitesides, G. M., "Axial" magnetic levitation using ring magnets enables simple density-based analysis, separation, and manipulation. *Analytical chemistry* 2018, *90* (20), 12239-12245.

241. Zhang, C.; Zhao, P.; Tang, D.; Xia, N.; Zhang, X.; Nie, J.; Gu, F.; Zhou, H.; Fu, J., Axial magnetic levitation: A high-sensitive and maneuverable density-based analysis device. *Sensors and Actuators B: Chemical* 2019, *304*, 127362.

242. Zhang, C.; Zhao, P.; Gu, F.; Zhang, X.; Xie, J.; He, Y.; Zhou, H.; Fu, J.; Turng, L.-S., Axial-Circular Magnetic Levitation: A Three-Dimensional Density Measurement and Manipulation Approach. *Analytical Chemistry* 2020.

243. Parfenov, V. A.; Koudan, E. V.; Bulanova, E. A.; Karalkin, P. A.; Pereira, F. D.; Norkin, N. E.; Knyazeva, A. D.; Gryadunova, A. A.; Petrov, O. F.; Vasiliev, M. M., Scaffold-free, label-free and nozzle-free biofabrication technology using magnetic levitational assembly. *Biofabrication* 2018, *10* (3), 034104.

244. Baday, M.; Ercal, O.; Sahan, A. Z.; Sahan, A.; Ercal, B.; Inan, H.; Demirci, U., Density Based Characterization of Mechanical Cues on Cancer Cells Using Magnetic Levitation. *Advanced healthcare materials* 2019, *8* (10), 1801517.

245. Delikoyun, K.; Yaman, S.; Yilmaz, E.; Sarigil, O.; Inevi, M. A.; Ozcivici, E.; Tekin, H. C., HologLev: Hybrid Magnetic Levitation Platform Integrated with Lensless Holographic Microscopy for Density-Based Cell Analysis. *bioRxiv* 2020.

246. Neurohr, G. E.; Amon, A., Relevance and Regulation of Cell Density. *Trends in Cell Biology* 2020, *30* (3), 213-225.

247. Mishriki, S.; Aithal, S.; Gupta, T.; Sahu, R. P.; Geng, F.; Puri, I. K., Fibroblasts Accelerate Formation and Improve Reproducibility of 3D Cellular Structures Printed with Magnetic Assistance. *Research* 2020, *2020*.

248. Mishriki, S.; Fattah, A. A.; Kammann, T.; Sahu, R.; Geng, F.; Puri, I., Rapid Magnetic 3D Printing of Cellular Structures with MCF-7 Cell Inks. *Research* 2019, *2019*, 9854593.

249. Norotte, C.; Marga, F. S.; Niklason, L. E.; Forgacs, G., Scaffold-free vascular tissue engineering using bioprinting. *Biomaterials* 2009, *30* (30), 5910-5917.

250. Murata, D.; Arai, K.; Nakayama, K., Scaffold-Free Bio-3D Printing Using Spheroids as "Bio-Inks" for Tissue (Re-) Construction and Drug Response Tests. *Advanced Healthcare Materials* 2020, 1901831.

251. Anil, M.; Ayyildiz-Tamis, D.; Tasdemir, S.; Sendemir-Urkmez, A.; Gulce-Iz, S., Bioinspired materials and biocompatibility. In *Emerging Research on Bioinspired Materials Engineering*, IGI Global: 2016; pp 294-322.

252. Anil-Inevi, M.; Sağlam-Metiner, P.; Kabak, E. C.; Gulce-Iz, S., Development and verification of a three-dimensional (3D) breast cancer tumor model composed of circulating tumor cell (CTC) subsets. *Molecular Biology Reports* 2020, *47* (1), 97-109.

253. Mekala, N. K.; Baadhe, R. R.; Potumarthi, R., Mass transfer aspects of 3D cell cultures in tissue engineering. *Asia-Pacific Journal of Chemical Engineering* 2014, *9* (3), 318-329.

VITA

MÜGE ANIL İNEVİ

Education:

Ph.D., Bioengineering (GPA: 4.00/4.00) | Izmir Institute of Technology | İzmir –Turkey, 2021, Thesis: "Magnetic levitation of cells from bone marrow origin"

MSc, Bioengineering (GPA: 3.85/4.00) | Ege University | İzmir –Turkey, 2014, Thesis: "Three-dimensional osteosarcoma model development with cancer stem cells on bacterial cellulose tissue engineering scaffold"

BSc, Bioengineering (GPA: 3.50/4.00) | Ege University | İzmir –Turkey, 2012

Professional & Research Experience and Scholarship

2016 – 2021 Research Assistant Bioengineering, Izmir Institute of Technology

2015 – 2021 TUBITAK, 2211/C National PhD Scholarship Program in the Priority Fields in Science and Technology

2013 - 2015 'Developing 3-Dimensional Vascularized Tumor Models Using Bacterial Cellulose as Scaffold *in vitro*' TUBITAK, Project no: **113M243**, scholarship student

2010 – 2011, Erasmus Scholarship, BSc Bologna University (Italy), Department of Chemical Engineering

List of selected publications:

Sarigil, O., **Anil-Inevi, M.**, Yilmaz, E., Mese, G., Tekin, H. C., & Ozcivici, E. (2019). Label-free density-based detection of adipocytes of bone marrow origin using magnetic levitation. ***Analyst***, *144*(9), 2942-2953.

Yaman, S., **Anil-Inevi, M.**, Ozcivici, E., & Tekin, H. C. (2018). Magnetic force-based microfluidic techniques for cellular and tissue bioengineering. ***Frontiers in bioengineering and biotechnology***, *6*, 192.

Anil-Inevi, M., Yaman, S., Yildiz, A. A., Mese, G., Yalcin-Ozuysal, O., Tekin, H. C., & Ozcivici, E. (2018). Biofabrication of in situ self assembled 3D cell cultures in a weightlessness environment generated using magnetic levitation. ***Scientific reports***, *8*(1), 1-10.